University of Massachusetts Amherst
ScholarWorks@UMass Amherst

Doctoral Dissertations | Dissertations and Theses

December 2020

FILAMENTS, FIBERS, AND FOLIATIONS IN FRUSTRATED SOFT MATERIALS

Daria Atkinson
University of Massachusetts Amherst

Follow this and additional works at: https://scholarworks.umass.edu/dissertations_2

 Part of the Geometry and Topology Commons, and the Statistical, Nonlinear, and Soft Matter Physics Commons

Recommended Citation

Atkinson, Daria, "FILAMENTS, FIBERS, AND FOLIATIONS IN FRUSTRATED SOFT MATERIALS" (2020). *Doctoral Dissertations*. 1990.
https://doi.org/10.7275/19165765 https://scholarworks.umass.edu/dissertations_2/1990

This Open Access Dissertation is brought to you for free and open access by the Dissertations and Theses at ScholarWorks@UMass Amherst. It has been accepted for inclusion in Doctoral Dissertations by an authorized administrator of ScholarWorks@UMass Amherst. For more information, please contact scholarworks@library.umass.edu.

FILAMENTS, FIBERS, AND FOLIATIONS IN FRUSTRATED SOFT MATERIALS

A Dissertation Presented

by

DARIA W. ATKINSON

Submitted to the Graduate School of the
University of Massachusetts Amherst in partial fulfillment
of the requirements for the degree of

DOCTOR OF PHILOSOPHY

September 2020

Physics

© Copyright Daria W. Atkinson 2020

All rights reserved

Released under CC BY-SA 4.0

FILAMENTS, FIBERS, AND FOLIATIONS IN FRUSTRATED SOFT MATERIALS

A Dissertation Presented

by

DARIA W. ATKINSON

Approved as to style and content by:

Gregory M. Grason, Co-chair

Christian D. Santangelo, Co-chair

Robert B. Kusner, Member

Shuang Zhou, Member

Narayanan Menon, Department Chair
Physics

to the dream of another possible future

ACKNOWLEDGMENTS

Viewed in this way, you can never again see a tree as a single entity, despite its visual dominance. It towers. It's impressive. But in the end, it's a fragile endeavor that can only stand thanks to the contributions of many. We celebrate the tree that stretches to the sky, but it is the ground we should ultimately thank.

To be taught, if fortunate
Becky Chambers

Science is a community endeavor, and this dissertation no less. Rob Kusner and participants of the "Packing of Continua" workshop at the Aspen Center for Physics (NSF PHY 1607611) were the source of countless helpful discussions for Chapter 2, on the geometry of equidistant curve packings, and Benny Davidovitch provided many helpful comments on the work presented in Chapter 3. I'm incredibly thankful to Mike Dimitriyev, Doug Hall, Alexa Kuenstler, M.E. Lee-Trimble, Jonathan Selinger, and Hao Wu for comments on drafts of this dissertation, and the manuscript of the paper [1] from which much of Ch. 2 follows. This work was supported by the National Science Foundation under grant Nos. DMR-1608862 and DMR-1507377.

I'm also incredibly grateful to Greg and Chris for their mentorship over the past five years; both of you have played a huge role in my growth as a scientist, and I've always counted myself extraordinarily lucky to have your support and advice, both on the work presented in this dissertation, and in all the extra stuff that's come up at the intersection of my personal and professional lives. I can't thank you both enough.

The Grason and Santangelo groups have also been essential in the completion of this dissertation work, especially Ishan Prasad, Doug Hall, Abhiram Reddy, Carlos

Duque, Michelle Berry, and Mary Elizabeth Lee-Trimble. Without your advice, comments, arguments, criticisms, revisions, friendship, and patience with my torturous and technical group meeting presentations, and general scientific community, this would be a much poorer dissertation than it is; and without your friendship, I would have missed at least one 5am flight, and I don't know that my PhD would've been completed at all, leaving me cursed to wander the halls of Conte and Hasbrouck for an eternity.

I'm also thankful to those in the broader scientific community with whom I haven't yet worked directly, but who have nonetheless encouraged and supported me along the way. Special thanks here go to Sabetta Matsumoto, Karen Daniels, and Shubha Tewari, for their mentorship and support; as well as Naryanon Menon, Shuang Zhou, Benny Davidovitch and the broader soft matter community at UMass, especially Alyssa, Alexa, and Sarah, without whom none of this would have been possible.

Other friends and colleagues have also been well tireless in their support, hyping me up; reminding me to go grocery shopping; talking me through the bad times; singing, crying, and shouting with me; and constantly sabotaging my plans to quit physics entirely and become an old-timey cattle rustler with an ice cream stand on the side. So thank you to Anne, Alex, Ivy, Leland, Becky, Lorelei, Nicole, Sarah, Violet, Fiona, Casey, Doug, and Nat; you all have a share of this as well, leaving me with what's looking more and more like three eighths of a PhD, at most. Friends far away (and even those nearby in the past couple of months) have been there by phone, skype, zoom, discord, and about once a year over the winter holidays, so thank you to Stephen Kuenstner, Melody Judilla, Mary McCreary, James Browning, and Laura Colbran, I would have been so lost without you.

And of course, I have to thank my family: my mom and dad, Anna, and Grandma for everything, and especially for being understanding when I go a month or so without texting or calling (sorry!).

ABSTRACT

FILAMENTS, FIBERS, AND FOLIATIONS IN FRUSTRATED SOFT MATERIALS

SEPTEMBER 2020

DARIA W. ATKINSON

B.A., CARLETON COLLEGE

Ph.D., UNIVERSITY OF MASSACHUSETTS AMHERST

Directed by: Professors Gregory M. Grason and Christian D. Santangelo

Assemblies of one-dimensional filaments appear in a wide range of physical systems: from biopolymer bundles, columnar liquid crystals, and superconductor vortex arrays; to familiar macroscopic materials, like ropes, cables, and textiles. Interactions between the constituent filaments in such systems are most sensitive to the *distance of closest approach* between the central curves which approximate their configuration, subjecting these distinct assemblies to common geometric constraints. Dual to strong dependence of inter-filament interactions on changes in the distance of closest approach is their relative insensitivity to *reptations*, translations along the filament backbone. In this dissertation, after briefly reviewing the mechanics and geometry of frustrated elastic materials relevant for the discussion of fiber geometry and elasticity in Chapter 1, we examine in detail the geometry associated with constant spacing between continuous filament fields, and the associated couplings between stretching of lengths between filaments, symmetries of multi-filament energies, and the shapes adopted by filament bundles.

In Chapter 2, we consider two distinct notions of constant spacing in multi-filament packings in three Euclidean dimensions, E^3: *equidistance*, where the distance of closest approach is constant along the length of filament pairs; and *isometry*, where the distances of closest approach between all neighboring filaments are constant and equal. We show that, although any smooth curve in E^3 permits one dimensional families of collinear equidistant curves belonging to a ruled surface, there are only two families of tangent fields with mutually equidistant integral curves in E^3. The relative shapes and configurations of curves in these families are highly constrained: they must be either (isometric) developable domains, which can bend, but not twist; or (non-isometric) constant-pitch helical bundles, which can twist, but not bend. Thus, filament textures that are simultaneously bent and twisted, such as twisted toroids of condensed DNA plasmids or wire ropes, are doubly frustrated: twist frustrates constant neighbor spacing in the cross-section, while non-equidistance requires additional longitudinal variations of spacing along the filaments. To illustrate the consequences of the failure of equidistance, we compare spacing in three "almost equidistant" ansatzes for twisted toroidal bundles and use our formulation of equidistance to construct upper bounds on the growth of longitudinal variations of spacing with bundle thickness.

In Chapter 3, we show that because the elastic response of non-equidistant filament bundles is frustrated, it cannot adequately be described by linearized, two-dimensional strains. To describe non-equidistant configurations, we derive a geometrically nonlinear, coordinate invariant, gauge-like theory for the elasticity of filamentous materials. For small strains, we derive the Euler-Lagrange equations for general, non-equidistant filament bundles, and show that, while force balance is qualitatively similar to that for 2D crystals, there are corrections which account for the non-integrability of twisted filament fields. Because of these corrections, force balance along the filament tangents couples to the convective flow tensor, which measures local deviations from equidis-

tance. Within this framework, we discuss the impact of filament texture on bundle elasticity, and extend the analysis of helical filament bundles to the large twist limit.

In Chapter 4, we finally turn our attention to longitudinally frustrated, non-equidistant bundles. Taking twisted toroidal filament bundles, which can be found in condensates of nucleic acids under confinement (e.g., inside a viral capsid), as a geometric prototype for the more general class of non-equidistant filament bundles, we derive the linearized force-balance equations in the limit of small central-filament curvature. While we make substantial progress towards a qualitative understanding of the behavior of non-equidistant filaments, the general solution to the Euler-Lagrange equations remains out of reach due to the presence of singularities at the outer boundary that emerge as a result of our perturbation scheme.

We conclude by discussing the progress made in this dissertation in understanding the physics of frustrated fibers, and speculating about the ramifications for more general soft-elastic materials.

TABLE OF CONTENTS

LIST OF TABLES

Table **Page**

LIST OF FIGURES

Figure **Page**

CHAPTER 1

BORN IN THE WRONG GEOMETRY: GEOMETRICALLY FRUSTRATED ELASTICITY IN FILAMENTOUS MATERIALS

We were a cabal... a flock of higher theorists

Flying
Kate Millett

1.1 Geometry and elasticity

The mechanical properties of materials are all tangled up with their shape and structure. From the influence of crystalline symmetries on materials' independent elastic moduli [2] and curvature coupling in cusps [3] and cracks [4–6] of thin elastic sheets to frustrated phases of chiral liquid crystals, [7, 8] the shape of things governs, and is in turn governed by, their equilibrium elastic properties. Not nearly narrow, a geometric perspective on materials instead explains both the intuitive and inexplicable, both the marvelous and the seemingly mundane. Across lengthscales—from the collective interactions of molecules microns or smaller to the mechanics of megastructures many meters large—and contexts—from pasta and pizza and flowers and fabrics to developing technologies in robotics and sensors—the language of geometry is essential for descriptions of soft materials. Geometric descriptions of soft materials are also, fortunately, fairly universal. While there are manifold manifestations of, for example, elastic sheets, from graphene and other atomically thin sheets to the more familiar fabrics and paper, all of these can, to a certain extent, be described with the same simple geometric picture, where stresses are given by changes in length

and curvature on embedding a surface into Euclidean three dimensional space. Indeed, this geometric perspective is so powerful that, with only slight modifications to the original picture, programmable, shape morphing materials, both artificial and biological, can be described.

The connection between geometry and elasticity is deep. Because changes in lengths and orientations are often suppressed by interactions between constituent atoms or molecules, effective descriptions of the reversible deformations of soft materials are often conveniently described in geometric language, whether discrete, as for mechanical metamaterials, or continuous and differentiable, as for rods, sheets, and many liquid crystalline systems. This geometric formulation of continuum elasticity helps draw immediate connections between geometric quantities, like curvatures, and the "bread and butter" elastic response of a medium, in terms of stresses and strains.

Also important for the observed behavior of elastic materials is that geometric features of the world we live in (which, ignoring relativistic contributions, is basically euclidean three space) can be readily observed in the complex emergent behavior of materials, governed by simple local rules which are, in some sense, incompatible with their embedding space [7, 9–12]. We call this *geometric frustration* of the elastic minima or ordered phases, and it means the material isn't really sure what to do, and so we get to see all sorts of cool new phases and responses, like the blue phases of chiral nematic liquid crystals and the twist grain boundary phases of chiral smectic liquid crystals. Geometric frustration can even be used to control material responses, programming the shape of elastic sheets [13, 14], the emergence of defects [4, 15], and the shape and size of meso-scale assemblies [11, 16].

Other contributions to the dazzling phenomenology of elastic materials, from buckling or coiling instabilities to pattern formation and the existence of soft deformations, can be attributed to *geometric nonlinearities*, which become important when materials undergo large deformations, even when the strain developed is small. Constraints

on displacement or orientation fields arising from purely geometrical considerations—like the Gauss-Codazzi-Mainardi equations for surfaces in E^3[17], or the unit director describing uniaxial nematic liquid crystals—add additional complexity to theories describing the large deformations of materials, and stabilize a variety of non-trivial configurations.

Geometric non-linearities and geometrical frustration are, of course, related. For example, out of plane height fluctuations are soft modes of thin-elastic sheets, and so a linear description would not capture, for example, the shape of draping fabrics, or the wrinkling of a sheet on a sphere [18]. And, while progress can be made for many materials by looking only at behavior away from boundaries, or other isolated regions, in frustrated materials geometric non-linearities are necessary for describing the super-extensive strains which accumulate in the bulk, and must be considered [12]. Since frustration is not only commonplace, but can have consequences both convenient [19] and catastrophic, the description and understanding of the accompanying geometric non-linearities remains an important and incomplete task in the study of materials in many disciplines. In this dissertation, we will explore geometric frustration, and the energetic non-linearities necessary to describe it, in one particular class of materials: bundles of filaments, fibers, and columnar liquid crystals.

1.2 Columnar and filamentous matter

Ordered arrangements of columns, fibers and filaments are a common geometrical motif; and such materials are found across a wide range of length-scales, from clumps of wet hair [20], carbon nanotube yarns [21, 22], biopolymer bundles [23], and discotic liquid crystals [24] to macroscopic multi-filament wires and cables [25, 26].

Because filament bundles are *liquid crystalline*, and have two solid-like directions and one fluid-like, uncorrelated direction, they exhibit characteristics of both 2d solids and bulk nematic liquid crystals. However, as a result of geometric coupling between

the elastic and orientational modes, they exhibit novel properties that result from the coupling of filament textures, which describe the local tangents to the filaments at each point in space, and inter-filament spacing. In order to facilitate the description of these couplings, it's useful to first describe individually the elasticity of thin sheets and nematic liquid crystals; we will also use this opportunity to introduce the notation we will use throughout for tensor calculus on Riemannian manifolds.

1.2.1 Thin elastic sheets

The geometric theory of thin elastic sheets dates back to the work of Föppl and von Kármán in the early 20th century [27, 28], but here we present a more geometrical framework which has been developed to account for the possibility of curvilinear coordinates [29] and non-Euclidean target metrics [30, 31]. As a brief note on notation: we will, in this discussion and throughout, use lower-case latin letters to index over the material (Lagrangian) coordinates for surfaces in E^3, upper case latin letters to index over the three material coordinates for filament bundles in E^3, and lower case greek letters to index over the space in material coordinates orthogonal to the local tangent vector. Throughout we adopt Einstein summation notation, so that repeated indices imply summation. To refer to points in the target (Eulerian) coordinates, we will throughout use boldface (e.g., $\mathbf{r}$ for the deformation map), and additionally assume that there is an embedding into Euclidean space, E^3.

The *Green-St. Venant strain tensor*, which measures the changes in lengths between two neighboring points, can be defined here in terms of the metric, g, of an embedding and a *target metric*, g^{tar} which is determined by the rest lengths between constituent molecules, by

$$\epsilon_{ij} = \tfrac{1}{2}(g_{ij} - g^{\text{tar}}_{ij}), \tag{1.1}$$

which corresponds to a linear measure of changes in lengths. The components of the metric g are related to a deformation field, $\mathbf{r}$, which points to the location in

Euclidean three space, by

$$g_{ij} = \partial_i \mathbf{r} \cdot \partial_j \mathbf{r}. \tag{1.2}$$

When the strains developed in the material are small, even when the accompanying deformations are large, we can neglect terms which are higher than quadratic order in the strain in the elastic energy, so that

$$\begin{aligned} E_{\text{strain}} &= \tfrac{1}{2} \int dV C^{ijkl} \epsilon_{ij} \epsilon_{kl} \\ &= \tfrac{1}{2} \int dV S^{ij} \epsilon_{ij}. \end{aligned} \tag{1.3}$$

The energetic cost for bending of the sheet can be expressed in terms of the *shape operator*,

$$L = -\nabla \hat{N}. \tag{1.4}$$

This tensor, whose action on the tangent vectors defines the curvatures of the surface at a point, can be used to measure the energetic cost of bending elasticity which accompany finite sheet thickness. Importantly for us, however, it also plays a role in the normal-force balance of sheets with vanishing thickness. If we were to work out the force balance equations from the variation of Eq. (1.3), we would find (see [30, 32, 33]) that

$$EL \cdot \hat{N} = S^{ij} L_{ij} = 0 \tag{1.5}$$

$$EL^j = \text{div}(S)^j = \partial_i S^{ij} + S^{ik} \Gamma^j_{ik} = 0, \tag{1.6}$$

where here $L_{ij} = g_{jk} L^k_i$, and Γ^j_{ik} is the Christoffel symbol associated with the usual covariant derivative of a surface in E^3 [17]. The take away here can be summarized briefly: in-plane force balance is driven by gradients in the stress tensor, S^{ij}, while normal force balance couples stresses to the curvatures of the surface at the midline, even in the absence of an energetic contribution from sheet bending.

1.2.2 Nematic liquid crystals

The elastic energy density of nematic liquid crystals deep in the ordered phase [34] can be expressed in terms of the averaged molecular orientation, $\mathbf{n}$, as:

$$f = \tfrac{1}{2}K_{11}[\nabla\cdot\mathbf{n}]^2+\tfrac{1}{2}K_{22}[\mathbf{n}\cdot(\nabla\times\mathbf{n})]^2+\tfrac{1}{2}K_{33}[(\mathbf{n}\cdot\nabla)\mathbf{n}]^2+K_{24}\nabla\cdot[(\mathbf{n}\cdot\nabla)\mathbf{n}-(\nabla\cdot\mathbf{n})\mathbf{n}], \quad (1.7)$$

where the K are independent elastic moduli, and are typically known as the splay (K_{11}), twist (K_{22}), bend (K_{33}), and saddle-splay (K_{24}).

The Frank free-energy can be rewritten slightly, in terms of the squares of 4 irreducible representations under rotations of the gradient tensor, $\nabla\mathbf{n}$, so that:

$$f = \tfrac{1}{2}(K_{11} - K_{24})S^2 + \tfrac{1}{2}(K_{22} - K_{24})T^2 + \tfrac{1}{2}K_{33}\|\mathbf{B}\|^2 + K_{24}\mathrm{tr}(\mathbf{\Gamma}^2), \quad (1.8)$$

where $S = \nabla \cdot \mathbf{n}$ is the splay, $T = \mathbf{n} \cdot (\nabla \times \mathbf{n})$ is the twist, and $\mathbf{B} = -(\mathbf{n} \cdot \nabla)\mathbf{n}$, as before, but here we have broken up the saddle splay term, with components which are independent of splay and twist now written in terms of the symmetric, traceless *biaxial splay* tensor [35, 36]

$$\mathbf{\Gamma}_{ij} = \tfrac{1}{2}\big[\nabla\mathbf{n} + (\nabla\mathbf{n})^T + \mathbf{n}\otimes\mathbf{b} + \mathbf{b}\otimes\mathbf{n} - S(I - \mathbf{n}\otimes\mathbf{n})\big], \quad (1.9)$$

where I is the Euclidean metric [1]. Notably, these four quadratic modes allow systematic investigation of the frustrated geometries of director fields in E^3 (and other geometries). In two dimensions, where only splay and bend are relevant, Niv and Efrati have derived an explicit connection between the two and the curvature of the

[1] Machon and Alexander, Selinger, and Virga [35–37] use $\mathbf{\Delta}$ to refer to the biaxial splay tensor, which for us risks confusion with the local distance of closest approach between two filaments; so here we use $\mathbf{\Gamma}$ for the biaxial splay tensor, and hope that distinct contexts (and different numbers of indices, when relevant) will help the reader differentiate it from the Christoffel symbols, Γ^i_{jk}.

embedding manifold [12]. In E^3, the more general decomposition has been used to show that the heliconical texture associated with twist bend nematics is the only *uniform* configuration, which has S, T, $\|\mathbf{B}\|$ and $\mathbf{\Gamma}$ constant in space [37].

1.2.3 Frustration in filamentous and columnar materials

Prior to these developments, work by Kléman and Bouligand [38, 39] showed that columnar liquid-crystalline textures which permit hexagonal packing between columns can be similarly expressed in terms of these liquid-crystalline modes, describing the developable domains, for which only the bend $\mathbf{b}$, does not vanish. These **isometric** packings of filaments and columns, which have an effective Euclidean metric to the quotient surface, and are readily observed in discotic liquid crystals [24]. With distances of closest approach between filaments restricted to the plane normal to their tangents, these ordered ground states are effectively two dimensional.

Early descriptions of the elasticity of filament bundles and columnar liquid crystals were inspired principally by the connection between these isometric packings and the elasticity of 2d crystals. Using a strain tensor which accounts only for in-plane deformations, so that

$$\epsilon_{\alpha\beta} = \partial_\alpha u_\beta + \partial_\beta u_\alpha + \partial_\alpha \mathbf{u} \cdot \partial_\beta \mathbf{u}, \tag{1.10}$$

where $\mathbf{u}$ is the in-plane displacement field, accurately accounts for the relatively small displacements associated with many bulk columnar phases [40, 41].

There are, however, problems with this relatively simple description: the strain tensor isn't invariant under global rotations of the filament bundle which fix the planar section. To see why (following [42]) imagine a bundle of filaments perpendicular to the $x-y$ plane, which are then uniformly rotated as in Fig. 1.1. The resulting deformation field is given by:

$$\mathbf{r} = \mathbf{x} + \big[x(1-\cos\alpha) + z\sin\alpha\big]\hat{x}, \tag{1.11}$$

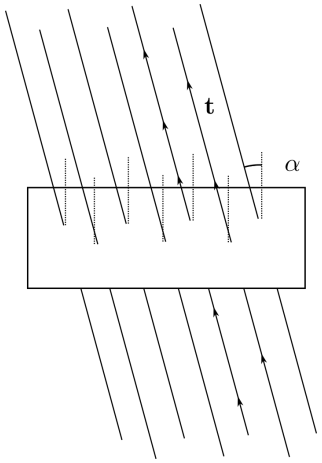

Figure 1.1: If a bundle of filaments, initially perpendicular to the $x-y$ plane, is rotated uniformly through an angle α, the strain tensor described Eq. (1.10) will develop a non-vanishing strain. To account for the rotation invariance of physical filament bundles, contributions from the tilt of the filament tangents, as in Eq. (1.13) are necessary.

and so the strain tensor in Eq. (1.10) is given by:

$$(\epsilon) = \begin{pmatrix} 1-\cos(\alpha) - \frac{1}{2}(1-\cos(\alpha))^2 & 0 \\ 0 & 0 \end{pmatrix}. \tag{1.12}$$

This is obviously unphysical, as we've done nothing more than change our coordinates. Minimal corrections to this planar model are necessary to ensure rotation invariance, and are given by the Selinger-Bruinsma strain tensor:

$$\epsilon_{ij} = \tfrac{1}{2}\big[\partial_i u_j + \partial_j u_i - \partial_i \mathbf{u}\cdot\partial_j \mathbf{u} - \partial_i u_z \partial_j u_z\big], \tag{1.13}$$

where i and j indices sum over a planar cross-section of the bundle. By recognizing that $\partial_i u_z \approx t_i$, we see that this strain tensor incorporates changes in distance associated with purely textural degrees of freedom. It turns out that this 2d strain can be made exact for the *equidistant* filament bundles described in Ch. 2. The Selinger-Bruinsma strain tensor can shed considerable light on the geometry [43] and elasticity

[44, 45] of the equidistant helical domains, and in the Föppl-von Kármán limit, where $\Omega R < 1$ (where R is the bundle radius and Ω is inversely proportional to the helical pitch) has been used to analyze the defect response and local deformation fields of twisted filament bundles [5, 46, 47].

The connection between twist and splay, on the one hand, and strain in the columnar order, on the other, gives rise to a wide array of phenomenology, from ordered arrays of defects in the tilt-grain boundary phase [40, 41, 48], to diverging moduli on approach to the columnar critical point [49]. For bundles of helices with constant pitch, Bruss and Grason [43] have shown that the competition between twist and hexagonal packing can be thought of in terms of an effective curvature, proportional to the twist squared [1, 43, 50] because the helical bundles are equidistant. This longitudinal symmetry allows a direct mapping from the bundle of filaments in E^3 to a two dimensional Riemannian manifold which has everywhere positive Gaussian curvature, and by taking the same, (no longer exact) two dimensional metric, some light can be shed on the coupling between textural and elastic degrees of freedom in frustrated filament bundles [47, 51].

In Ch. 2, we essentially complete this analysis, and show that all geometric constraints on *constant spacing* in filament bundles and columnar liquid crystals can be accounted for by a combination of the splay and biaxial-splay modes of the Frank free energy, which we call the *convective flow tensor*. By solving for bundles with vanishing convective flow tensor in a tubular neighborhood of a central curve, we show that there are only two families of equidistant filament bundles: the isometric developable domains, which have zero twist, but can bend freely; and the equidistant helical domains, which have uniform twist, but are constrained to lie along a straight line.

As a consequence of our proof in Ch. 2, we then show explicitly in Ch. 3 that the 2d Selinger-Bruinsma strain tensor fails to capture the longitudinal frustration associ-

ated with non-equidistance, for which a more comprehensive geometric description is needed. In Ch. 3, we derive the fully geometrically non-linear strain tensor necessary to account for non-equidistance by presenting a simple symmetry argument, inspired by classical gauge theories. After commenting on the connection between the resulting *covariant derivative* and the geometry of fiber bundles of a Riemannian manifold, we then use this non-linear theory to revisit the elasticity of helical filament bundles with large twist ($\Omega R > 1$), incorporating contributions from filament stretching and bending which are important for experimental systems [52, 53].

In Ch. 4, we finally address the role that longitudinal frustration plays in the elastic response of weakly curved twisted-toroidal filaments. We begin by calculating the linearized force-balance equations for weakly curved twisted-toroidal filament bundles by introducing perturbations to the helical bundle fixed point. After showing that a simple Fourier analysis allows the force balance equations to be decomposed into orthogonal modes in the Eulerian polar coordinate, $\tilde{\phi} = \phi + \Omega s$, we show that the resulting system of inhomogeneous differential equations is singular on both boundaries. By analyzing the behavior of a power series ansatz at the boundaries, we also show that the resultant singular boundary value problem (BVP) cannot be described by a simple power series ansatz, and discuss several possibilities for working around the singular behavior.

We conclude in Ch. 5 by summarizing the progress made in this dissertation to the study of geometrically frustrated elasticity and the physics of filament bundles, and then outline several possible directions for future work.

CHAPTER 2

CONSTANT SPACING IN FILAMENT BUNDLES

Besides: there's nothing so rejuvenating as a new proof, eloquently laid out in clear language. It's better than tea.

The Lady's Guide to Celestial Mechanics
Olivia Waite

2.1 Introduction

Constant spacing between subunits governs a wide range of self-organized and manufactured pattern-forming assemblies [54]. At the smallest size scales, such assemblies arise generically as the ground states of a large family of interaction potentials. Whether or not inter-element spacing is constant is fundamental to the behavior of materials, from the underlying processes of their formation, to their defects and distortions, and, ultimately, to their macroscopic responses[1] (e.g. mechanical, optical).

The geometry of constant spacing and its implications for physical models of matter have been extensively studied for point-like (e.g. close-packings of spheres [54, 55]) and surface-like (e.g. smectic liquid crystals [56]) subunits in three dimensions. In comparison, the constant spacing of curve-like, quasi one-dimensional subunits, remains poorly understood.

Perhaps the best studied regime of filament packings, motivated in part by physical models of protein and the packing of nucleic acids, arise from the close packing of a

[1]This chapter adapted from material presented in [1]

small number (typically, $N = 1$ or 2) of plied or knotted flexible tubes [57–62]. In contrast, numerous physical scenarios – from clumps of wet hair [20], carbon nanotube yarns [21, 22] and biopolymer bundles [23] to macroscopic multi-filament wires and cables [25, 26] – motivate the consideration of structures composed of an arbitrarily large number of filaments $N \gg 1$. In 2D, the constraints on the constant spacing of $N \gg 1$ curves have been studied in the context of ordered stripe assemblies on variable shape surfaces [63, 64]. Comparatively, packing $N \gg 1$ curves in a finite of volume of Euclidean three-space, E^3, which is most relevant to the structure of molecular fibers or macroscopic cables, introduces additional complexity due to two interrelated, but inequivalent notions of *constant spacing*. In this chapter, we call *equidistant* families of curves for which the shortest distance between curves is constant along their length. We then call *isometric* those equidistant families that permit uniform spacing between neighbors in their cross-section (see Figs. 2.1a–c). At a pairwise level, equidistance is equivalent to constant surface contact between uniform diameter flexible tubes, and as such, is a natural way to describe optimal packings of cohesive filaments.

In this chapter, we present several results concerning the existence of families of equidistant curves in E^3. We begin with a general introduction to ordered filament packings, outlining the differences between regular arrangements of filaments in two and three dimensions. We show that, for any sufficiently smooth curve in E^3, there exist families of non-parallel equidistant curves which envelop a ruled surface, a natural generalization of the planar, parallel result. We then show that, for two such equidistant curves, it is always possible to place a third curve, which is equidistant to—but does not lie on the ruled surface spanned by—the first two curves. Then, in order to understand the generic constraints of equidistance for $N \gg 1$ non-collinear curves, we consider a continuum, vector field description of equidistant filament textures, which unlike the ruled surface families "occupy" a finite 3D volume. Solving explicitly for all unit-vector fields with sufficiently differentiable (C^3) equidistant in-

tegral curves, we show that equidistance imposes constraints on the first derivatives of the curves' tangents characterized by the vanishing of a two-component symmetric matrix, $\mathbf{H}$, of directional derivatives perpendicular to the local tangent. Remarkably, and in stark contrast to the unconstrained equidistant triplets, there exist only two families of equidistant integral curves: the *developable domains*, which can be bent, but not twisted [39, 65], (Fig. 2.1d); and *helical domains* with constant pitch [43], which can be uniformly twisted, but not bent (Fig. 2.1e). We summarize the distinct features of these two families, outlining their compatibility with isometric packing and the constraints each family imposes on the relative shapes of curves in the packing.

In the remainder of the chapter, we explore the consequences and limitations of this central result by numerically probing a simple family of "almost equidistant" filament bundles with both bend and twist: twisted toroidal bundles (Fig. 2.1f). Such structures, are experimentally realized in systems of biopolymer condensates [66–68], and have recently gained interest as characterizing of a new class of topological soliton "hopfion" textures in liquid crystals [69–71] and magnets [72–74]. we show that twisted toroids are a natural test bed for the structure of non-equidistant bundles, as the textures can continuously approach equidistance in the two asymptotic limits of *either* infinite major radius and finite twist (helical domain) *or* infinite helical pitch and finite curvature (developable domain). Because we expect the ground states of even complex, frustrated filament assemblies to minimize their deviations from uniform spacing, we approach this problem by comparing the growth of non-equidistance with twist and curvature using three ansatzes: stereographic projections of the equidistant Seifert fibrations of S^3 into E^3 [9, 75]; splay-free tori, for which $\mathrm{tr}(\mathbf{H}) = 0$ [76]; and a third class, characterized by $\det(\mathbf{H}) = 0$. By constructing a numerical measure of non-equidistance, we compare asymptotic increases in non-equidistance with the lateral thickness (minor radius) of the twisted toroidal bundles,

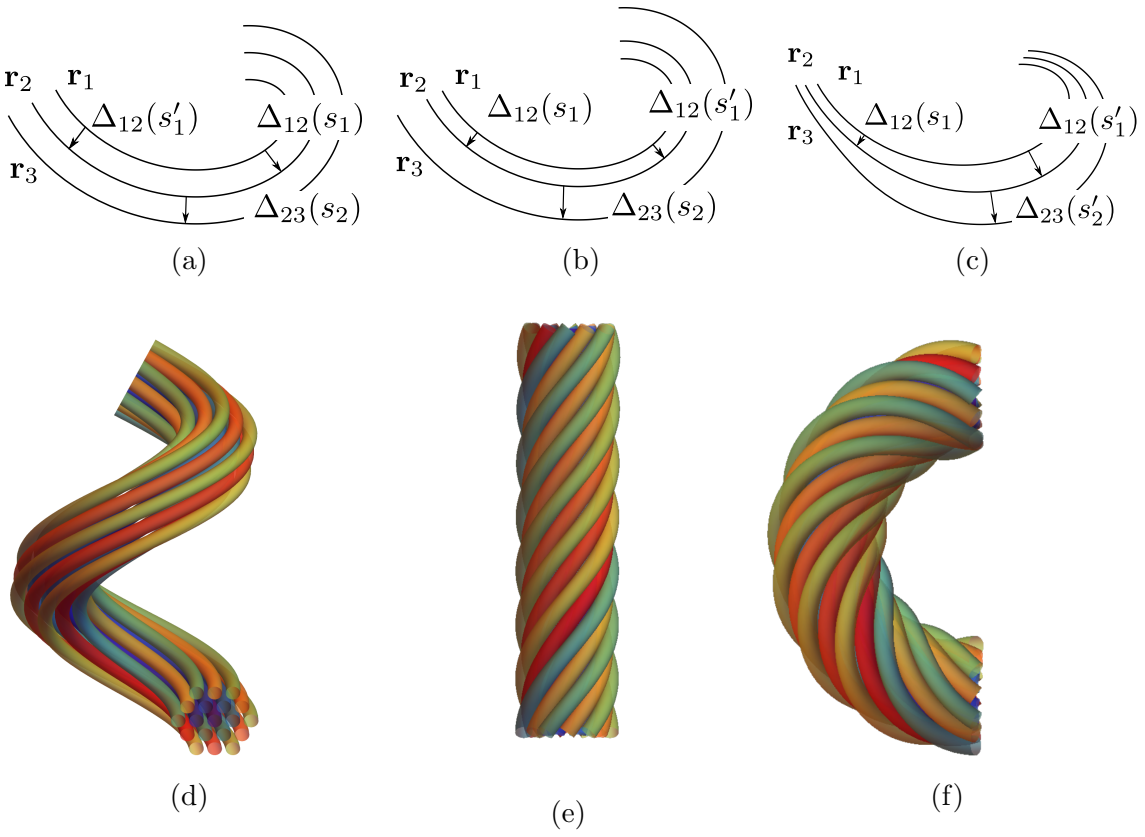

Figure 2.1: Examples of curve arrays that illustrate the distinction between *equidistant* and *isometric* configurations. The schematics in 2.1a–2.1c show three local inter-curve distances: $\Delta_{12}(s_1)$ and $\Delta_{12}(s_1')$, which denote the distance of closest approach between neighbor curves at arc positions s_1 and s_1', respectively; and $\Delta_{23}(s_2)$, the distance of closest approach between an alternate pair. In 2.1a, an *equidistant* and *isometric* array (where $\Delta_{12}(s_1) = \Delta_{12}(s_1') = \Delta_{23}(s_2)$); in 2.1b, an *equidistant* but *non-isometric* array, $(\Delta_{12}(s_1) = \Delta_{12}(s_1') \neq \Delta_{23}(s_2))$; and in 2.1c, a *non-equidistant* array (where, in general, $\Delta_{12}(s_1) \neq \Delta_{12}(s_1') \neq \Delta_{23}(s_2)$). While in two dimensions, every equidistant array is compatible with an isometric packing, there are equidistant, volume-filling curve textures of E^3 which are incompatible with isometric packing [43]. As shown in Section 2.3, there are only two families of equidistant curve fields in E^3. Developable domains, as in 2.1d, are equidistant, and allow isometric filament packings [38, 39], while helical domains, as in 2.1e, are equidistant, but do not allow isometric packings due to their effective positive Gaussian curvature [43]. Filament textures which are both bent and twisted, such as the toroidal bundle in 2.1f, cannot be equidistant.

showing by construction that longitudinal variations between curves in the optimal structures will vanish at least as fast as thickness cubed in the limit of narrow bundles.

These results extend the understanding of geometric frustration in multi-filament packings well beyond previous studies, which have focused either on the frustration of filament and column shape in isometric packings [38, 39] or the frustration of the lateral spacing between filaments in non-isometric (twisted) packings [5, 43, 46, 77]. Specifically, this analysis highlights the nature of *longitudinal* frustration of constant spacing as distinct from, and complementary to, the *transverse* frustration of lateral spacing between neighbors in a large N packing. As experiments on isometric filament packings subject to twist have shown [52, 53], the response of bundles to constraints of non-equidistance imposed by its global geometry will depend on the specifics of the filament packings. Nevertheless, because the constraints for equidistance in these large N packings are rather rigid, we anticipate several scenarios where the failure of equidistance triggers new structural and mechanical responses in physical models of bundles, including hierarchical packing of wires and cables.

We conclude with a discussion of the bifurcation of equidistant bundles as additional curves are added, conjecturing that there exists some finite $N_c > 3$ such that any equidistant bundle with $N \geq N_c$ non-collinear curves falls into one of the $N \gg 1$ families: either the helical or developable domains.

2.2 Equidistance in multi-filament arrays

In models of multi-filament packings, interactions between neighboring elements are often approximated by isotropic interactions between one-dimensional *central curves* [78–80]. In this context, local close-packing of two constant-diameter neighboring filaments requires that the distance of closest approach, Δ, between their central curves is constant *along the entire length of the curves*. In multi-filament bundles, uniform close-packing also requires that Δ is the same for any two nearest neighbors. For simplicity, we call packings with longitudinally constant Δ, as in Figs. 2.1a and

2.1b, *equidistant*, and those with uniform nearest neighbor distances, as in Fig. 2.1a, *isometric*.

Although equidistance is a necessary condition for isometric packing, since there cannot be a single well-defined distance between neighboring filaments unless this distance is constant, it is useful to consider the implications of equidistance independent of isometry. Equidistant packings are particularly valuable as they reduce the problem of inter-element distances in a three-dimensional bundle to the lower dimensional problem of packing elements on a two-dimensional surface. This perspective has enabled in-depth explorations of the (non-isometric) ground-state structure of close-packed, twisted bundles [11, 43]. Beyond this, cohesive interactions naturally impose a cost for variations in the local spacing between attractive filaments, and it is therefore natural to anticipate that equidistant geometries (if they are compatible with topological constraints or mechanical loading) are ground-state configurations of many models, particularly when inter-filament cohesion dominates over the mechanical costs of intra-filament bend and twist.

At a pairwise level, the conditions for equidistance are found by demanding that the shortest distance between two curves, $\mathbf{r}_1$ and $\mathbf{r}_2$, is constant along their arc lengths, s_1 and s_2, respectively. This is shown by considering the closest separation from $\mathbf{r}_1$ at s_1 to $\mathbf{r}_2$, which can be defined as $\Delta_{12}(s_1) \equiv \min_{s_2}\big[|\mathbf{r}_1(s_1) - \mathbf{r}_2(s_2)|\big]$. For a given s_1, this requires that the closest arc position, $s_2 = s_2(s_1)$ on $\mathbf{r}_2$, satisfies

$$\Big(\partial_{s_2}\big|\mathbf{r}_1(s_1) - \mathbf{r}_2(s_2)\big|^2\Big)_{s_2=s_2(s_1)} = -2\ \mathbf{T}_2\big[s_2(s_1)\big] \cdot \mathbf{\Delta}_{12}(s_1) = 0, \tag{2.1}$$

where $\mathbf{T}_2 = \mathbf{r}_2'\big[s_2(s_1)\big]$ is the tangent to $\mathbf{r}_2$ at the distance of closest approach, and $\mathbf{\Delta}_{12}(s_1) = \mathbf{r}_1(s_1) - \mathbf{r}_2\big[s_2(s_1)\big]$ is the closest separation vector to $\mathbf{r}_2$ from $\mathbf{r}_1(s_1)$ [2].

[2]In general, there may be multiple extrema of $\big|\mathbf{r}_1(s_1) - \mathbf{r}_2(s_2)\big|^2$, corresponding to multiple solutions for $s_2(s_1)$ to Eq. (2.1), for a given pair; in extreme cases, such as the tight Hopf link [81],

The solution to this condition induces a reparameterization $s_2(s_1)$ of $\mathbf{r}_2$ in terms of s_1, such that we can rewrite this second curve as $\mathbf{r}_2(s_1) \equiv \mathbf{r}_2\big[s_2(s_1)\big]$. Equidistance between $\mathbf{r}_1$ and $\mathbf{r}_2$ then requires that $\Delta_{12}(s_1)$ is constant in s_1, so

$$\partial_{s_1}\big|\mathbf{\Delta}_{12}(s_1)\big|^2 = 2\,\Big[\mathbf{T}_1(s_1) - \frac{\partial s_2(s_1)}{\partial s_1}\mathbf{T}_2(s_1)\Big]\cdot\mathbf{\Delta}_{12}(s_1) = 0. \tag{2.2}$$

While Eq. (2.2) is generically quite difficult to solve explicitly, when $s_2(s_1)$ is invertible ($\partial s_2/\partial s_1 \neq 0$), it has a straightforward geometric interpretation. In particular, $\mathbf{\Delta}_{12}(s_1)$ has constant magnitude, and remains perpendicular to the tangents of both $\mathbf{r}_1$ and $\mathbf{r}_2$ at the points of closest approach, s_1 and $s_2(s_1)$, respectively. In the language of, e.g., Ref. [81], equidistant curves pairs are *doubly-critical* at all points.

2.2.1 Equidistance in the Plane

For plane curves, as shown in Figs. 2.1a–c, a pair of curves $\mathbf{r}_1$ and $\mathbf{r}_2$ can be written in terms of the local distance between the two curves, Δ_{12}, the arc length s_1 of $\mathbf{r}_1$, $\mathbf{r}_1$, and its normal, $\mathbf{N}_1$, as

$$\mathbf{r}_2(s_1) = \mathbf{r}_1(s_1) + \Delta_{12}(s_1)\mathbf{N}_1(s_1). \tag{2.3}$$

If the two filaments are equidistant (i.e. $\partial_{s_1}\Delta_{12} = 0$), then the curves must be parallel (i.e. $\mathbf{T}_1 = \mathbf{T}_2$) at the points of closest approach. It is then straightforward to embed a field of curves $\mathbf{r}_n$ that are all parallel to $\mathbf{r}_1$, using a similar parameterization $\mathbf{r}_n(s_1) = \mathbf{r}_1(s_1) + \Delta_n\mathbf{N}_1(s_1)$, where Δ_n is the distance between the nth curve and $\mathbf{r}_1$. Note that Δ_n can be extended only up to the global radius of curvature of $\mathbf{r}_1$, at which point $\mathbf{r}_n$ becomes singular and its distance map from $\mathbf{r}_1$ becomes noninvertible [82]. If $\Delta_{n+1} - \Delta_n$ is constant for all n, then the equidistant curves are also *isometric*.

---

every point on the curve $\mathbf{r}_1$ is a minima. Our analysis assumes the minimal distance for solutions $s_2(s_1)$ for a given s_1.

Hence, any planar curve $\mathbf{r}_1(s_1)$ can be extended to an equidistant family on the plane (at least in a neighborhood of $\mathbf{r}_1(s_1)$ smaller than its global radius of curvature), and every equidistant family is compatible with isometric packing. As there are no constraints imposed by constant spacing on the shape of $\mathbf{r}_1(s_1)$ (beyond smoothness), we say that packings of planar curves are *unfrustrated*.

2.2.2 Equidistant pairs and ruled surfaces in E^3

In contrast, the geometry of equidistant pairs of curves in E^3 is much more flexible than that of planar curves. For a curve $\mathbf{r}_1$ in three dimensions, there are two linearly independent directions locally perpendicular to $\mathbf{T}_1$. Notably, this means that there are curves $\mathbf{r}_1$ and $\mathbf{r}_2$ that are equidistant but *not* parallel, so that $\mathbf{T}_1 \neq \mathbf{T}_2$ at the points of closest approach (i.e. points separated by $\mathbf{\Delta}_{12}(s_1) = -\mathbf{\Delta}_{21}(s_2)$). Furthermore, as we show in Appendix 2.A, for any sufficiently differentiable curve $\mathbf{r}_1$ and distance Δ_{12} less than the global radius of curvature, there exist multiple curves $\mathbf{r}_2$ such that $\mathbf{r}_1$ and $\mathbf{r}_2$ are equidistant but not parallel. Heuristically, one can understand this flexibility in terms of the "tubular" construction illustrated in Fig. 2.2a, where a circular tube of fixed radius Δ_{12} encloses $\mathbf{r}_1$. Any curve, $\mathbf{r}_2$, on this tubular surface for which $\mathbf{T}_1 \cdot \mathbf{T}_2 = \cos\theta_{12}$ has a constant sign is equidistant to $\mathbf{r}_1$.

Given any two equidistant curves $\mathbf{r}_1$ and $\mathbf{r}_2$, there is an infinite family of equidistant curves that lie along a ruled surface spanned by the vectors, $\mathbf{\Delta}_{12}(s) = \mathbf{r}_2(s) - \mathbf{r}_1(s)$, which we call the *separating surface* [3]. To see this, let $\hat{\rho}_{12}(s) \equiv (\mathbf{r}_2(s) - \mathbf{r}_1(s))/\Delta_{12}$. Then, we define a family of curves, parameterized by the distance ρ from $\mathbf{r}_1$ towards $\mathbf{r}_2$,

$$\mathbf{r}_\rho(s) = \mathbf{r}_1(s) + \rho\ \hat{\rho}_{12}(s). \tag{2.4}$$

[3] We again adopt the reparameterization of $\mathbf{r}_2$ in terms of the arc length of $\mathbf{r}_1$, which we call s for simplicity of notation.

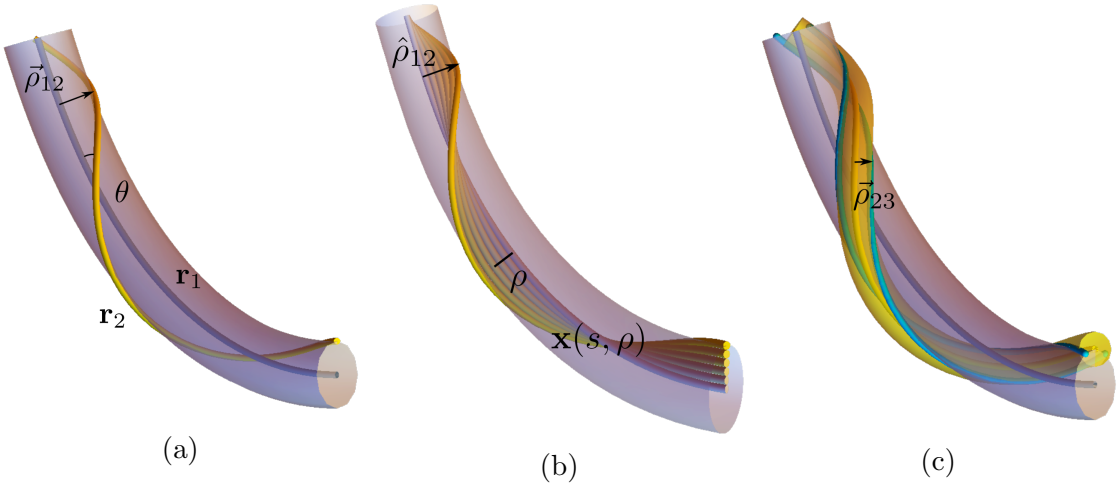

Figure 2.2: A simple heuristic argument suggests that for any sufficiently smooth space curve $\mathbf{r}_1$ in E^3 there are at least two additional curves, $\mathbf{r}_2$ and $\mathbf{r}_3$ such that $\mathbf{r}_1$, $\mathbf{r}_2$, and $\mathbf{r}_3$ are all equidistant. To see this, imagine extending a tube of constant radius ρ_{12} around $\mathbf{r}_1$, as in 2.2a. A curve $\mathbf{r}_2$ that lives on this tube is equidistant to $\mathbf{r}_1$. This construction can be extended to a one-dimensional family of equidistant and isometric curves, as in 2.2b, where the curves mark lines of constant ρ on the ruled *separating surface* generated by $\mathbf{r}_1$ and $\mathbf{r}_2$. These filaments are equidistant, as shown in Eq. (2.6), and isometric, as the distance of closest approach between neighboring curves is equivalent for any pair of neighbors. Extending a tube of radius ρ_{23} (not necessarily equal to ρ_{12}) around $\mathbf{r}_2$, as in 2.2c, we see that the curve $\mathbf{r}_3$, which traces out the intersection of the tubes, is equidistant to both $\mathbf{r}_1$ and $\mathbf{r}_2$, but in contrast to the separating surface in 2.2b, the three curves are *not* collinear.

It is straightforward to verify the equidistance of two curves at ρ_1 and ρ_2 by verifying that their tangents are perpendicular to their separation vector. Specifically,

$$\partial_s \mathbf{r}_{\rho_1}(s) \cdot \big[\mathbf{r}_{\rho_1}(s) - \mathbf{r}_{\rho_2}(s')\big] = \Big(\mathbf{T}_1(s) + \frac{\rho_1}{\Delta_{12}}\Big[\frac{\partial s_2}{\partial s}\mathbf{T}_2(s) - \mathbf{T}_1(s)\Big]\Big) \cdot \big[\mathbf{r}_{\rho_1}(s) - \mathbf{r}_{\rho_2}(s')\big], \tag{2.5}$$

which is zero when $s' = s$ because curves $\mathbf{r}_1$ and $\mathbf{r}_2$ are equidistant with distance of closest approach at s. The equivalent necessary condition for $\mathbf{r}_{\rho_2}$ also holds. This family of equidistant curves forms a ruled surface, the separating surface of $\mathbf{r}_1$ and $\mathbf{r}_2$,

$$\mathbf{x}_{12}(s, \rho) = \mathbf{r}_1(s) + \rho\ \hat{\rho}_{12}(s), \tag{2.6}$$

ruled by the vectors $\hat{\rho}_{12}(s)$ (as shown by Fig. 2.2b).

The regular spacing of curves on one such surface, the helicoid, has been suggested by Archad, et. al. [83] as an explanation for the structure of the $B7^*$ phase of bent core liquid crystals [84]. These ruled separating surfaces are also a natural generalization of the equidistant plane curves discussed in Subsection 2.2.1 to three dimensions, showing that the torsion of one or both curves allows for equidistant curves to be non-parallel. Any sufficiently smooth curve in E^3 permits such ruled surface families, and, as in the planar case, a subset of the equidistant curves on a separating surface can always be chosen such that the curves are isometric.

2.2.3 Non-collinear equidistant triplets

The families of equidistant and isometric curve packings described above are strictly two-dimensional, as they lie on the ruled, separating surface that is uniquely defined for any equidistant pair in E^3. Before continuing on to the problem of three-dimensional fields of equidistant curves, we first give a simple construction to show that it is generically possible, for a given equidistant pair, $\mathbf{r}_1$ and $\mathbf{r}_2$, to find at least one additional curve, $\mathbf{r}_3$, which is mutually equidistant to the first two, but that does not lie on their separating surface.

As shown in Fig. 2.2c, we can illustrate the constraints of equidistance by surrounding the curves with tubes of fixed radii perpendicular to their local tangents. This guarantees that the separation vector between the curves has constant length (say, Δ_{12}), is along the radial direction, and is, by construction, perpendicular to the central curve (say, $\mathbf{r}_1$) and the curve defined on its surface (say, $\mathbf{r}_2$). Likewise, it is straightforward to construct tubes around the two equidistant curves $\mathbf{r}_1$ and $\mathbf{r}_2$. The radii for these tubes can be chosen rather arbitrarily (up to the limits placed by the global radius of curvature) to be Δ_{13} and Δ_{23}. These tubes intersect along two curves that do not lie on the ruled surface spanning $\mathbf{r}_1$ and $\mathbf{r}_2$, but are, by construction, equidistant to both of those curves. Either one these curves can be taken as $\mathbf{r}_3$, forming an equidistant triplet.

We note that while the geometry of three equidistant, non-collinear curves constructed sequentially, as described above, is relatively flexible, it is far from clear how the addition of more curves alters the constraints on their shapes and relative arrangement. For example, adding a fourth equidistant curve to the triplet in Fig. 2.2c, requires the intersection of *three* tubular surfaces surrounding those curves along a single 1D curve, a condition that can only be satisfied for a subset of equidistant triplets. One might reasonably expect that, for N sufficiently large, this becomes a very restrictive constraint, a point we return to in the discussion.

2.3 Fields of Equidistant Curves

Thus motivated to find families of multi-curve packings corresponding to bundles of $N \gg 1$ non-collinear filaments in E^3, we adopt a continuum description based on the integral curves of unit vector fields. In many physical examples of bundles, like DNA condensates or carbon nanotube ropes, a combination of dense-packing and intra-filament stiffness keeps filaments in quasi-parallel orientation. In such a dense, multi-filament bundle (in the absence of filament ends in the array), the geometry of a

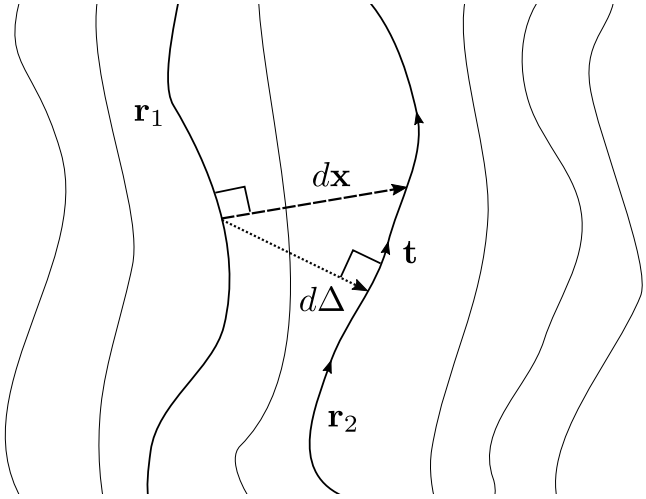

Figure 2.3: The distance of closest approach Δ from a curve $\mathbf{r}_1$ to a curve $\mathbf{r}_2$ is perpendicular to the tangent $\hat{t}$ of $\mathbf{r}_2$. Given a tangent field $\mathbf{t}$, the distance of closest approach between $\mathbf{r}_1$ at $\mathbf{x}$ and $\mathbf{r}_2$ at $\mathbf{x}+d\mathbf{x}$ can be found by projecting out the tangent field $\mathbf{t}$, giving an infinitesimal distance of closest approach $d\Delta = d\mathbf{x} - \mathbf{t}(\mathbf{t} \cdot d\mathbf{x})$.

finite set of backbone curves indexed by m, $\{\mathbf{r}_m(s)\}$, can be analyzed by a unit vector field $\mathbf{t}(\mathbf{x})$ that smoothly interpolates between their tangents, so that $\mathbf{t}\big[\mathbf{r}_m(s)\big] = \hat{t}_m(s)$.

In this section, we derive the conditions under which the integral curves of a given unit tangent field $\mathbf{t}(\mathbf{x})$ are all mutually equidistant in a region of E^3. These families of fields of equidistant curves are particularly valuable for physical models of multi-filament bundles, in that they permit the embedding of an arbitrary number of equidistant curves in a finite volume of three-dimensional space, in contrast to the 2D submanifolds of E^3 spanned by ruled separating surfaces. In the following section, we show that conditions imposed by equidistance lead to strong constraints on the relative shapes and orientations of the integral curves in the set.

2.3.1 Local metric and convective flow tensor

Given a unit tangent field $\mathbf{t} : E^3 \mapsto S^2$, we can find the distance of closest approach between two integral curves that pass through infinitesimally close points $\mathbf{x}$ and $\mathbf{x}+d\mathbf{x}$ by projecting out the component of $d\mathbf{x}$ along $\mathbf{t}$, as shown in Figure 2.3. The resulting

local distance of closest approach is given by

$$d\Delta^2 = (\delta_{ij} - t_i t_j) dx^i dx^j. \tag{2.7}$$

We note that this projection can be written as a 2D metric

$$g_{ij}(\mathbf{x}) = \delta_{ij} - t_i(\mathbf{x}) t_j(\mathbf{x}) \tag{2.8}$$

by considering $d\mathbf{x}$ in a planar section of E^3 whose normal $\mathbf{N}$ satisfies $\mathbf{N} \cdot \mathbf{t}(\mathbf{x}) > 0$ in some region (e.g. a plane which is perpendicular to $\mathbf{t}(\mathbf{x})$ at some $\mathbf{x}$) [43, 51].

In this local formulation, the distance between two curves is constant along their length when $\partial_s d\Delta^2 = 0$, where $\partial_s = \mathbf{t} \cdot \nabla$ is the directional derivative along $\mathbf{t}$. Differentiating, and using the convective flow of the separation between integral curves $\partial_s d\mathbf{x} = d\mathbf{x} \cdot \nabla \mathbf{t}(\mathbf{x})$, we find that

$$\partial_s d\Delta^2 = [\partial_i t_j + \partial_j t_i - t_k \partial^k (t_i t_j + t_j t_i)] dx^i dx^j = h_{ij} dx^i dx^j. \tag{2.9}$$

Because $\mathbf{t}$ is a unit vector, and hence $t_i \partial_k t_i = 0$, h_{ij} is zero for all components along $\mathbf{t}$. The remaining terms belong to a 2D block whose components can be associated with locally orthonormal directions $\hat{\mathbf{e}}_1(\mathbf{x})$ and $\hat{\mathbf{e}}_2(\mathbf{x})$ that span the plane perpendicular to $\mathbf{t}(\mathbf{x})$ (i.e., $\hat{\mathbf{e}}_1(\mathbf{x}) \times \hat{\mathbf{e}}_2(\mathbf{x}) = \mathbf{t}(\mathbf{x})$). Projecting h_{ij} onto this two-dimensional basis defines

$$H_{\alpha\beta} \equiv (\hat{\mathbf{e}}_\alpha)_i h_{ij} (\hat{\mathbf{e}}_\beta)_j \tag{2.10}$$

where $\alpha, \beta = 1, 2$. $\mathbf{H} = (H_{\alpha\beta})$ is a symmetric 2-tensor, which we call the *convective flow tensor*, that measures the longitudinal deviations from equidistance. Hence,

equidistance requires $H_{\alpha\beta} = 0$. We can gain some geometrical intuition for this condition by noting that

$$H_{\alpha\beta} = 2\Gamma_{\alpha\beta} + (\nabla \cdot \mathbf{t})\delta_{\alpha\beta}, \tag{2.11}$$

where $\mathbf{\Gamma} = (\Gamma_{\alpha\beta})$ is the "biaxial splay" tensor, $\Gamma_{ij} = \frac{1}{2}(\partial_i t_j + \partial_j t_i - (t^k \partial_k t_i)t_j - t_i(t^k \partial_k t_j) - \partial_k t^k(\delta_{ij} - t_i t_j)$, in its nonzero 2D block, following Refs. [35, 36]. The modes of zero $\mathbf{H}$, then, have both locally isotropic gradients of $\mathbf{t}$ (vanishing biaxial splay), and constant cross-sectional area per filament (vanishing splay).

These conditions can be recast in terms of the directional derivatives of the tangent field perpendicular to $\mathbf{t}(\mathbf{x})$,

$$(\nabla \mathbf{t})^{(2D)}_{\alpha\beta} \equiv (\hat{\mathbf{e}}_\alpha)_i \partial_i t_j (\hat{\mathbf{e}}_\alpha)_j \tag{2.12}$$

from which we have $H_{\alpha\beta} = (\nabla \mathbf{t})^{(2D)}_{\alpha\beta} + (\nabla \mathbf{t})^{(2D)}_{\beta\alpha}$. Therefore, a field $\mathbf{t}$ is equidistant only when these transverse directional derivatives are skew symmetric, with

$$(\nabla \mathbf{t})^{(2D)}_{\alpha\beta} = f(\mathbf{x})\epsilon_{\alpha\beta} \qquad \text{for } H_{\alpha\beta} = 0, \tag{2.13}$$

where f is any function and $\epsilon_{\alpha\beta}$ is the totally antisymmetric Levi-Civita symbol. This skew-symmetric structure is closely related to the *double-twist texture* of the blue phases of chiral liquid crystals [8]. In the context of the blue phases, it is well appreciated that the geometry of E^3 is incompatible with uniformly double-twisted textures [7], leading to the formation of defect-ordered phases of finite-diameter double-twist tubes. In the context of the present problem, however, the condition of Eq. (2.13) is slightly weaker, and the rate of double-twist, as parameterized by the function $f(\mathbf{x})$, may vary spatially without disrupting the equidistance of the field lines.

Before moving on to solve for the equidistant curve fields, we note that the equidistance of integral curve fields promotes the metric description of Eq. (2.8) from one

that measures local distances between infinitesimally spaced curves, to one in which the metric $g_{ij}(\mathbf{x})$ relates the true Euclidean distances of closest approach of *finitely-separated curves* to their coordinate separations in some reference plane (e.g. in a given 2D plane cutting through $\mathbf{t}(\mathbf{x})$). When $H_{\alpha\beta}(\mathbf{x}) = 0$ everywhere within some volume, distances of closest approach between finitely separated curves can be found as geodesic arc lengths computed according to the induced metric. In the language of differential geometry, equidistance is the necessary and sufficient condition for a Riemannian foliation, where the metric properties of the leaves (curves) inherited from the embedding space (the distance of closest approach in E^3) are encoded by the Riemannian metric of a lower dimensional base manifold (in this case, a 2D surface) [85]. In the following section, we classify the isometry of equidistant curve fields in terms of the Gaussian curvature of these foliations.

2.3.2 Equidistant solutions

The skew symmetry of $(\nabla\mathbf{t})^{(2D)}$ in Eq. (2.13) gives three independent differential equations for $\mathbf{t}$, which can be solved to find every equidistant tangent field. We begin by choosing coordinates $\{s, \rho, \phi\}$ adapted to some integral curve $\mathbf{r}_0$ of the tangent field, where s is an arc length parameterization of $\mathbf{r}_0$, ρ is a polar distance in the plane perpendicular to $\hat{t}_0$ at some s, and ϕ the polar angle in the same plane (see Appendix 2.B for details), such that

$$\mathbf{x}(s, \rho, \phi) = \mathbf{r}_0(s) + \rho\ \hat{\rho}(s, \phi), \tag{2.14}$$

as shown schematically in Fig 2.4. In these coordinates, any field $\mathbf{t}$ whose integral curves are equidistant to $\mathbf{r}_0$ will be perpendicular to the separation vector $\rho\ \hat{\rho}(s, \phi)$ and hence can be written

$$\mathbf{t}(s, \rho, \phi) = \cos\big[\theta(s, \rho, \phi)\big]\hat{t}_0(s) + \sin\big[\theta(s, \rho, \phi)\big]\hat{\phi}(s, \phi), \tag{2.15}$$

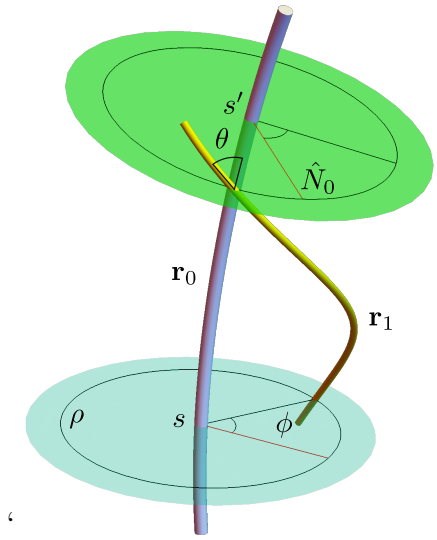

Figure 2.4: A schematic diagram of the coordinates described in Eq. (2.14), showing the radial distance ρ from a central curve, $\mathbf{r}_0$; ϕ, the polar angle in the plane normal to $\mathbf{r}_0$ measured with respect to the principle normal, $\hat{N}$; and s, the position along $\mathbf{r}_0$ in terms of its arc length.

where $\hat{t}_0 \equiv \partial_s \mathbf{r}_0$, $\hat{\phi} \equiv \partial_\phi \hat{\rho}$ and θ is a scalar field which characterizes the tilt of integral curves with respect to $\hat{t}_0$.

We can analyze the components of $(\nabla \mathbf{t})^{(2D)}_{\alpha\beta}$ in the two orthonormal directions, $\hat{\rho}$ and $\hat{b} = \mathbf{t} \times \hat{\rho}$, in the plane normal to $\mathbf{t}$ at $\mathbf{x}$. All $\mathbf{t}(\mathbf{x})$ of this form satisfy $(\nabla \mathbf{t})^{(2D)}_{\rho\rho} = 0$ explicitly. Using the coordinate transformations given in Appendix 2.B, the other components of $\nabla \mathbf{t}$ can be found exactly:

$$(\nabla \mathbf{t})^{(2D)} = \begin{bmatrix} 0 & \partial_\rho \theta \\ -\frac{\sin\theta\cos\theta}{\rho(1-\rho\kappa_0\cos\phi)} & \frac{1}{\rho}\partial_\phi\theta\left(\frac{\sin\theta\tau_0\rho}{1-\rho\kappa_0\cos\phi} + \cos\theta\right) + \frac{\sin\theta(\kappa_0\sin\phi - \partial_s\theta)}{1-\rho\kappa_0\cos\phi} \end{bmatrix}. \tag{2.16}$$

The skew symmetry of $(\nabla \mathbf{t})^{(2D)}$ required for equidistance gives us the differential equations:

$$(H_{\rho b} = 0) \quad \partial_\rho \theta = \frac{\sin\theta\cos\theta}{\rho(1-\rho\kappa_0\cos\phi)} \tag{2.17}$$

$$(H_{bb} = 0) \quad \sin\theta\partial_s\theta = [(\tfrac{1}{\rho} - \kappa_0\cos\phi)\cos\theta + \tau_0\sin\theta]\partial_\phi\theta + \kappa_0\sin\phi\sin\theta. \tag{2.18}$$

The first of these differential equations, Eq. (2.17), can be integrated directly, giving us

$$\tan\theta = \Omega(s,\phi)\frac{\rho}{1-\rho\kappa_0\cos\phi}, \tag{2.19}$$

where $\Omega(s,\phi)$ is a constant of ρ. Substituting into Eq. (2.18) and rearranging, we find that:

$$\begin{aligned} H_{bb} = 0 = -\big[(1-\rho\kappa_0\cos\phi)^2+(\rho\Omega)^2\big]^{-3/2}\Big\{ &\big[\rho^2\tau_0\Omega(1-\rho\kappa_0\cos\phi)+(1-\rho\kappa_0\cos\phi)^3\big]\partial_\phi\Omega \\ &- \rho^3\Omega^2\partial_s\kappa_0\cos\phi + \big[\rho\kappa_0\Omega\cos\phi-\Omega\big]\rho^2\partial_s\Omega + \rho^3\kappa_0\Omega^2(\tau_0-\Omega)\sin\phi\Big\}, \end{aligned} \tag{2.20}$$

where $\partial_s\mathbf{t}_0 = \kappa_0\mathbf{n}_0$ and $\partial_s(\mathbf{t}_0\times\mathbf{n}_0) = -\tau_0\mathbf{n}_0$ give, respectively, the curvature (κ_0) and torsion (τ_0) of the reference curve $\mathbf{r}_0$. The numerator of Eq. (2.20) is a cubic polynomial of ρ, so, grouping by powers of ρ and recognizing that solutions to $H_{bb}=0$ require the coefficients of these linearly independent terms to vanish, we find only two possible solutions for equidistant fields. In the first case we have

$$\Omega = 0, \tag{2.21}$$

which gives us solutions that are locally parallel in the plane normal to t_0 (i.e., $\theta = 0$). The second family of solutions require

$$\begin{aligned} \partial_\phi\Omega &= 0 \\ \partial_s\Omega &= 0 \\ \kappa_0'\cos\phi &= \kappa_0(\Omega-\tau_0)\sin\phi, \end{aligned} \tag{2.22}$$

so that every twisted equidistant field has constant pitch Ω, and includes an integral curve with constant curvature and torsion. Because any curve with constant curvature and torsion is a helix, the torsion is fixed by the pitch Ω, and the curvature is fixed

by the torsion and its distance from some straight line, this second family of solutions is the one parameter family of bundles of constant pitch circular helices.

2.4 The Equidistant Packings

In the previous section, we find that the conditions for equidistance are only satisfied by two restrictive families of curve fields, corresponding to the respective conditions in Eqs. (2.21) and (2.22). In this section, we describe in turn the geometric properties of these two families and the physical scenarios in which they have been invoked. We focus on the distinguishing features of inter-filament texture, intra-filament shape, inter-filament spacing (or metric geometry), and constraints on the lateral thickness of bundles of smoothly embeddable curves.

Motivated by applications of multi-filament packing in liquid crystals and soft matter [76, 86–88], it is natural to analyze the inter-filament texture in terms of the Frank elastic gradients of the tangent field, in particular, first derivatives of $\mathbf{t}$ that constitute generalized "orientational strains" in the Frank-Oseen free energy [89]. Because $(\nabla \cdot \mathbf{t}) = \frac{1}{2}\mathrm{tr}(\mathbf{H})$, all equidistant curve fields are splay-free. The twist, $\mathbf{t} \cdot (\nabla \times \mathbf{t})$, provides a measure the neighbor-average inter-filament skew angle in the packing, that is, the local rate of mutual rotation of neighbors [45]. The final first-order Frank term is associated with bending of the tangent field, that is, it is a measure of *intra-filament curvature* κ, which is computed from the convective derivative of $\mathbf{t}$ itself, namely $(\mathbf{t} \cdot \nabla)\mathbf{t} = \kappa\mathbf{n}$ where again, $\mathbf{n}(\mathbf{x})$ is the local normal to the integral curve at $\mathbf{x}$. In addition to the curvature, intra-filament shape is characterized by the *torsion* τ which is given by the rotation of the binormal $\mathbf{b} = \mathbf{t} \times \mathbf{n}$ around the tangent, $(\mathbf{t} \cdot \nabla)\mathbf{b} = -\tau\mathbf{n}$.

In addition to these measures of intra- and inter-filament gradients we analyze the metric properties of the equidistant packings in terms of the Gaussian curvature K of the 2D metric $g_{ij}(\mathbf{x})$ induced on a planar section through the bundle, as in Eq. (2.8),

Equidistant family	**Twist**	**Curvature**	**Torsion**	$\mathbf{K_G}$	**Thickness**
Developable domains	0	$\frac{\kappa_0}{1-\kappa_0\rho\cos\phi}$	$\frac{\tau_0}{1-\kappa_0\rho\cos\phi}$	0	$\min_s[1/\kappa_0]$
Helical domains	$\frac{2\Omega}{1+(\Omega\rho)^2}$	$\frac{\Omega^2\rho}{1+(\Omega\rho)^2}$	$\frac{\Omega}{1+(\Omega\rho)^2}$	$\frac{3\Omega^2}{[1+(\Omega\rho)^2]^2}$	∞

Table 2.1: Summary of geometric properties of the distinct families of equidistant curves. Inter-filament *twist* is defined by $\mathbf{t}\cdot(\nabla\times\mathbf{t})$. *Curvature*, κ, of filaments at $\mathbf{x}$ is derived from $(\mathbf{t}\cdot\nabla)\mathbf{t}=\kappa\mathbf{n}$, while *torsion*, τ, is derived from $(\mathbf{t}\cdot\nabla)\mathbf{b}=-\tau\mathbf{n}$, where $\mathbf{n}$ and $\mathbf{b}=\mathbf{t}\times\mathbf{n}$ are the normal and binormal, respectively. The *metric curvature*, K_G, is the Riemannian curvature of the inter-filament metric $g_{ij}(\mathbf{x})$, and the *max thickness* describes the largest lateral diameter of the domain that is embeddable without self intersection. For developable domains, generalized cylindrical coordinates are given with respect to a reference curved of respective curvature and torsion, κ_0 and τ_0, and for helical domains, coordinates are defined with respect to a straight central curve.

which may be directly derived via standard formulas [17]. Finally, we define the *maximum thickness* as the diameter of a bundle of filaments that can be smoothly extended normal to a given central curve in the packing. That is, beyond this maximum thickness, continuing the equidistant field introduces shape singularities in the integral curves, features which we exclude from our analysis due to the prohibitive costs of kinks in physical realization of multi-filament packings. Table 2.1 summarizes the geometric comparisons between the two families of equidistant curve fields. we describe each family in turn.

2.4.1 ($\Omega = 0$): Developable Domains

The first equidistant family, described by Eq. (2.21), corresponds to what have been called *developable domains* (see example in Fig. 2.1d). These textures were originally described by Bouligand [38] and Kléman [39] in the context of columnar liquid crystals. Developable domains have neither twist (i.e. $\mathbf{t}\cdot(\nabla\times\mathbf{t})=0$) nor splay ($\nabla\cdot\mathbf{t}=0$), and thus the filament tangents are all parallel at the point of closest approach, their tangents are normal to a common set of planes (i.e. $\theta=0$), and the closest separations between curves lie in these 2D planes. Hence, it is straightforward

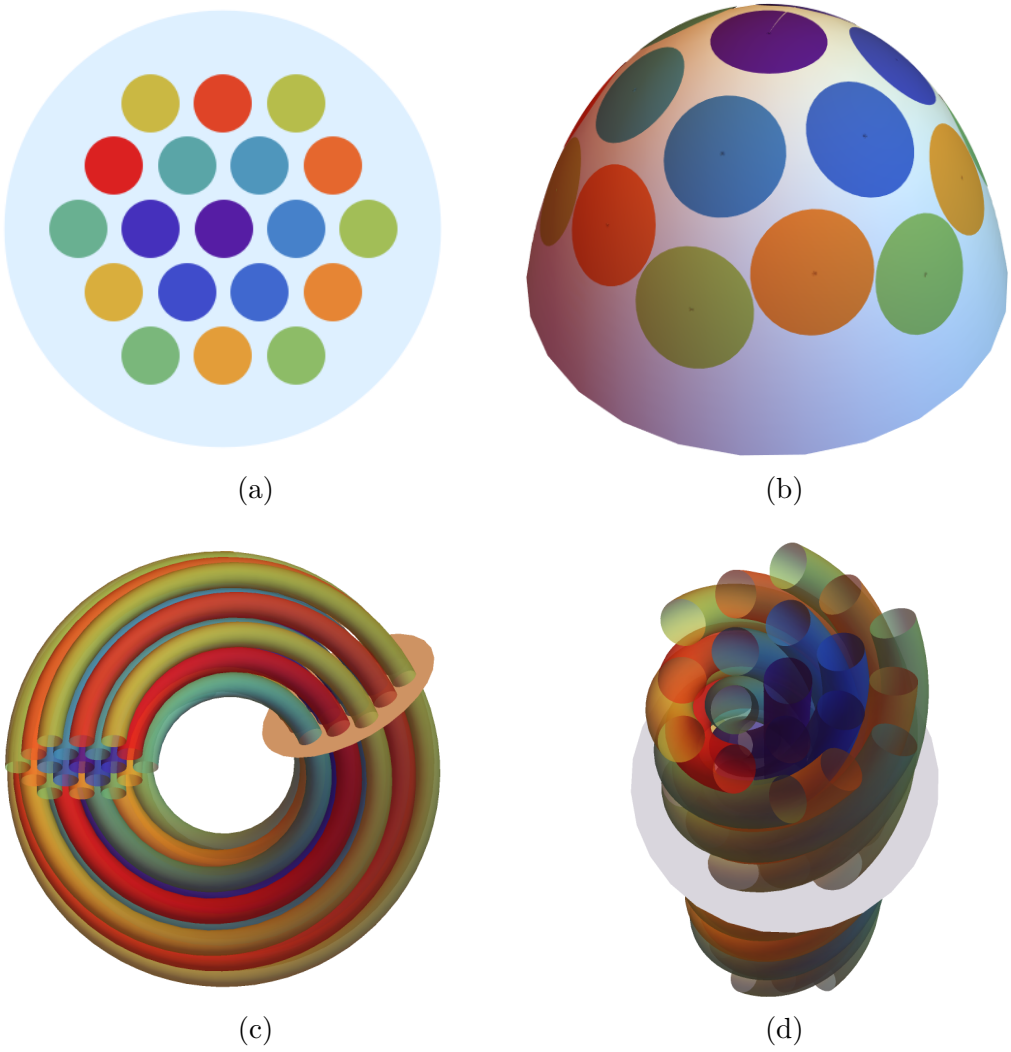

(a) (b)

(c) (d)

Figure 2.5: The quotient surfaces to the equidistant filament packings, showing the flat metric of the developable domains in 2.5a and the curved metric of the helical domains in 2.5b. These surfaces represent the true distance of closest approach between filaments, which are represented by colored disks of constant geodesic radius. The colors in the disk packings correspond to filaments in planar sections of the developable domains, in 2.5c, and helical domains, in 2.5d.

to see that their metric geometry is Euclidean, as in Fig 2.5a. Indeed, the developable domains are the *only isometric family* of $N \gg 1$ curves dense in E^3.

Because the curves are normal to a common set of planes and they do not twist around one another, they also share the same Frenet frames at points of closest contact, giving closely related shapes. Constructing a developable domain around a given curve with curvature κ_0 and torsion τ_0, the shape of all other curves in the domain are fully determined [65], such that

$$\kappa(\mathbf{x}) = \frac{\kappa_0}{1 - \kappa_0 \rho \cos\phi};\ \tau(\mathbf{x}) = \frac{\tau_0}{1 - \kappa_0 \rho \cos\phi}, \tag{2.23}$$

where ρ is the closest distance to the central curve and ϕ is the angle between the separation to the reference curve and its normal (see Fig. 2.4). Hence, for non-zero bending, these normal planes intersect along the cuspidal edge of the developable surface generated by the locus of all the centers of curvature of the filaments in the bundle [38]. Bouligand and Kléman argued that such curvature singularities manifest as characteristic topological defects in columnar phases. Here, we argue further that this same geometry places constraints on the maximum size of isometric filament packings with finite bending. While the developable domains permit isometric filament packings and can be embedded around reference curves of any (smooth) shape, embeddings of finite curvature filaments are spatially limited to a thickness around the central curve less than its global curvature radius [82] as they become singular along this developable surface.

2.4.2 ($\Omega \neq 0$): Constant-Pitch, Helical Domains

We first discuss the second equidistant family, described by Eq. (2.22), in terms of a straight central curve (i.e. $\kappa_0 = 0$) that threads through its center along an axis $\rho = 0$ (see example in Fig. 2.1e). Relative to this axis, these curves are easily seen to be helices with a tilt angle, $\theta = \arctan(\Omega\rho)$, with respect to the center which increases

with radius ρ, but has constant pitch $2\pi/\Omega$ (the corresponding curvature and torsion are given in Table 2.1). Indeed, the geometry of these equidistant *helical domains* closely corresponds to the "double-twist tube" that is the fundamental building block of the liquid crystal blue phases [8]. Unlike the developable domains, which do not permit twist, this second family is twisted, with $\mathbf{t}\cdot(\nabla\times\mathbf{t}) = 2\Omega/[1+(\Omega\rho)^2]$. As inter-filament twist is generically favored in chiral filamentous materials such as biopolymer assemblies [45, 90, 91], helical domains are important structural models of the compromise between the preference for chiral inter-filament packing and the cohesive preference for equidistance. Recent experiments show further that the constant-pitch helical texture emerges in mechanically twisted filament packings [52, 53].

While helical domains are the only twisted family of equidistant curves in E^3, twist is incompatible with isometric packing in the cross section [43, 51]. This can be seen from the metric in polar coordinates (as defined in Fig. 2.4) centered on the straight curve:

$$g = \begin{bmatrix} 1 & 0 \\ 0 & \rho^2\cos^2\theta. \end{bmatrix} \tag{2.24}$$

Because $\cos\theta = 1/\sqrt{1+(\Omega\rho)^2}$ decreases with ρ, hoops of constant distance from the center are effectively shortened relative to the Euclidean plane, as in Fig. 2.5b, consistent with positive Gaussian curvature [85],

$$K = \frac{3\Omega^2}{(1+\Omega^2\rho^2)^2}. \tag{2.25}$$

This is a special case of O'Neill's formula [50], which gives the curvature of any Riemannian fibration in terms of the curvature of the fibered space and the twist of the fibration; specifically, the curvature above can be written $K = \frac{3}{4}(\mathbf{t}\cdot(\nabla\times\mathbf{t})^2$. The effect of this positive Gaussian curvature is to frustrate constant lateral spacing of filaments (e.g. equi-triangular packing). Physical models of twisted cohesive bundles have shown that this metric frustration promotes accumulation of inter-filament

stresses [92] or else stabilize topological defects [43] in the cross sectional order of twisted cohesive bundles. Notably, the Gaussian curvature of helical domains is concentrated in the core, as the metric flattens in the limit $\Omega\rho \to \infty$. Hence, the disruption of uniform lateral spacing at the core of helical domains notwithstanding, this equidistant family can be extended smoothly to fill all of E^3, in contrast to the spatially limited, developable domains.

While the above description assumes a straight central curve, the choice of the central curve is arbitrary, provided that it satisfies Eqs. (2.22), such that it is a helix whose torsion is equal to Ω. It is straightforward to show that choosing one such helix simply gives a reparameterization of the same family of helical domains. For example, in terms of generalized cylindrical coordinates (ρ', ϕ') around a reference curve with curvature κ_0 we have the Gaussian curvature distribution,

$$K = \frac{3\Omega^2}{\left[(1 - \rho'\kappa_0 \cos\phi')^2 + (\Omega\rho')^2\right]^2}. \tag{2.26}$$

It can be shown that this metric derives from considering a planar slice through the helical bundle that is normal to a curve at finite radius, $\kappa/(\kappa^2 + \Omega^2)$.

Thus, up to the orientation and position of a central axis of rotation, every equidistant helical domain is parameterized by a single real number, Ω, which can be viewed as a simple rescaling of the same structure.

2.5 Almost Equidistant Bundles

In the previous section, we showed that equidistant curve packings fall into two strict families. These two families are either strictly untwisted but arbitrarily bent, or uniformly twisted around a straight axis. In this section, we illustrate the consequences of falling outside these strict geometrical constraints for inter-filament spacing in multi-filament bundles (e.g. a bundle that is simultaneously bent *and* twisted).

Such generic geometric conditions are encountered in widely varying rope-like structures, from hierarchical strands of wire-ropes [25], to twisted, curved bundles of condensed biopolymers [66–68].

Here, we study arguably the simplest possible non-equidistant geometry, the *twisted toroidal bundles*, a family of architectures that conveniently spans both equidistant families (see example, Fig. 2.1f). Notably, several previous models of close-packed toroidal bundles have been developed to describe the structure and thermodynamics of biopolymer toroids. A primary focus of many of these model has been the relationship between their geometry and their orientational order [76, 93] without regard to their metric geometry. Work of Sadoc, Charvolin and others have considered idealized metric geometries possible in S^3, but to date, the limits to the uniformity of filament spacing in toroids embedded in E^3 have not been explored.

Below we consider three ansatzes for non-equidistant, twisted-toroidal bundles. Two are related to previous models of either "splay-free" bundles or projections of ideal fibrations of S^3 to Euclidean space. In the context of the present study, we can contrast all three ansatzes in terms of the structure of the convective flow tensor $\mathbf{H}$. As described in Sec. 2.3.1, $\mathbf{H}$ describes the first-derivative of the local separation between integral curves and equidistance requires all three independent components of $H_{\alpha\beta}$ to vanish. Forcing a bundle to be simultaneously bent and twisted hence requires at least one of the components to be non-zero. Below, we compare the variable filament spacing in three toroidal ansatzes: stereographic projection of the Seifert fibrations of S^3 to E^3, for which $H_{\alpha\beta} = H(\mathbf{x})\delta_{\alpha\beta}$ and the biaxial splay, $\mathbf{\Gamma}$, vanishes; splay-free toroidal bundles, for which $\mathrm{tr}(\mathbf{H}) = 2\nabla \cdot \mathbf{t} = 0$; and twisted toroidal bundles, for which $\det(\mathbf{H}) = 2(\nabla \cdot \mathbf{t})^2 - 2\mathrm{tr}(\mathbf{\Gamma}^2) = 0$.

To compare the inter-filament spacing within these toroidal ansatzes quantitatively, we construct bundles from integral curves of each construction. The cross section of each bundle has 1+6+12 filaments, whose initial centers are chosen from

three concentric layers of a hexagonal packing of unit spacing. Each filament is then discretized in to $N = 10000$ arc positions, from which the distance matrix between all positions on each neighboring filament pair is calculated. Minimizing over the set of distances between a point s_i on curve $\mathbf{r}_i$ and all the positions s_j in $\mathbf{r}_j$, gives the distance of closest approach from $\mathbf{r}_i(s_i)$ to $\mathbf{r}_j$, $\Delta_{ij}(s_i)$, from which we can compute a pointwise measure of non-equidistance, δr, and the total non-equidistance, $\langle \delta r^2 \rangle$, as defined in Appendix 2.C. The Supplemental Video shows an example of the variation of $\delta r_i(s_i)$ throughout a bent and twisted packing (generated via the $\det(\mathbf{H}) = 0$ ansatz described below).

We analyze filament bundles from tangent fields that are constructed to twist around a planar, circular central curve of radius κ_0^{-1}, the major radius of the torus, with a minor radius R, which is defined by the outer filament in the bundle. As detailed below, for a general non-equidistant family of tangent fields, the winding rate of filaments around the minor cycle of the torus is non-uniform. we therefore impose an additional constraint that all curves in the cross section have the same average circulation rate around the minor cycle of the torus. In terms of the dependence of the angular position ϕ of a given curve (parameterized by the arc position s along the central curve), this takes the form of constant pitch

$$P = 2\pi/\Omega \equiv \int_0^{2\pi} d\phi \Big(\frac{\partial \phi}{\partial s}\Big)^{-1}. \tag{2.27}$$

Using this definition of Ω, we compare the uniformity of spacing in each ansatz as a function of reduced curvature $\kappa_0 R$ and reduced twist ΩR. When computing length averages, we average over the pitch length, or a half-circumference of the central circle $L = \pi/\kappa_0$ when $L/P < 1$.

Comparing the scaling of the convective flow tensor, $\mathbf{H}$, with bundle radius to the numerically calculated non-equidistance, $\langle \delta r^2 \rangle^{1/2}$, for each of the toroidal ansatzes, we show that nonequidistance in the Seifert fibrations scale linearly with the radius,

while the splay-free and determinant-free structures scale as the radius cubed. The agreement between the analytic scaling arguments and numerical calculations suggests the convective flow tensor accurately captures the growth of nonequidistance for each of the three ansatzes.

2.5.1 S^3 fibrations projected to Euclidean space

While there are no equidistant filament textures in E^3 which are both twisted and bent, the same is not true of more general curved spaces. In particular, S^3, the unit sphere in E^4, permits a family of twisted, equidistant curves called Clifford parallels [10]. These uniformly double-twisted curves, which generate the Hopf fibration, are equidistant in S^3, but when stereographically projected into E^3 induce a twisted, toroidal structure of interlinking circles. Stereographic projections of the Hopf fibration to E^3 generate twisted toroidal bundles with a particular linking number, or ratio of bend to twist, $|\Omega|/\kappa_0 = 1$. Projection of a more general class of fibrations, the Seifert fibrations, which are also equidistant in S^3, permit a variable ratio of bend to twist [51, 75] . Because stereographic projection preserves metric properties at the pole of the projection, which is chosen to be the major cycle at the center of the bundle, these projections of Seifert fibrations of S^3 have been proposed as physical models of cyclized, chiral polymer condensates that compromise between uniform packing and twist, [9, 94, 95].

Here, we construct projections of Seifert fibrations following the toroidal coordinates of Sadoc and Charvolin [75]. With coordinates for the sphere in E^4 of radius κ_0^{-1} given by

$$
\begin{aligned}
x_1 &= \kappa_0^{-1} \cos\varphi \sin\Theta \\
x_2 &= \kappa_0^{-1} \sin\varphi \sin\Theta \\
x_3 &= \kappa_0^{-1} \cos\psi \cos\Theta \\
x_4 &= \kappa_0^{-1} \sin\psi \cos\Theta,
\end{aligned}
\tag{2.28}
$$

the fibers of a Seifert fibration are defined by $\varphi(\psi) = \varphi_0 + \alpha\psi$, where ψ is a parameter that travels along the fibers and α parameterizes the ratio of turns per minor cycle of the torus to the turns per major cycle [4]. The coordinate Θ parameterizes different tori, each of which is foliated by curves of distinct values of $\varphi_0 \in [0, 2\pi]$. Stereographically projecting a fiber to E^3 through a pole of S^3 (where $\Theta = 0$ corresponds to the major cycle of radius κ_0^{-1} in E^3) a fiber at Θ and ϕ_0 parameterized by ψ is given in Cartesian coordinates by

$$
\begin{aligned}
x(\psi) &= \kappa_0^{-1} \frac{\cos\psi \cos\Theta}{1 - \cos(\varphi_0 + \alpha\psi)\sin\Theta} \\
y(\psi) &= \kappa_0^{-1} \frac{\sin\psi \cos\Theta}{1 - \cos(\varphi_0 + \alpha\psi)\sin\Theta} \\
z(\psi) &= \kappa_0^{-1} \frac{\sin(\varphi_0 + \alpha\psi)\sin\Theta}{1 - \cos(\varphi_0 + \alpha\psi)\sin\Theta}.
\end{aligned}
\tag{2.29}
$$

This projection is composed of curves defined on nested tori of increasing minor radius, $\kappa_0^{-1}\tan\Theta$. However, the tori are not concentrically nested around a fixed major circle, and instead, are centered around major circles of increasing radius $\kappa_0^{-1}\sec\Theta$. Because the arc distance along the central curve is simply $(\Delta\psi)\kappa_0^{-1}$, it is straightforward to see that the twist, as defined in Eq. (2.27), is $\Omega = \alpha\kappa_0$.

Due to the non-concentric nature of toroidal stacking in this projection, it is convenient to analyze the tangent field in terms of orthonormal directions $\hat{t}_0 = \kappa_0 \partial_\psi \mathbf{x}\big|_{\Theta=0}$,

[4] Strictly, α is a rational number such that the (a, b) Seifert fibration of S^3 has $\alpha = \frac{a}{b}$.

$\hat{\varphi} = \partial_\varphi \mathbf{x}/|\partial_\varphi \mathbf{x}|$ and $\hat{\Theta} = \hat{t}_0 \times \hat{\varphi}$. The tangent vector field of the texture induced by the Seifert fibers can now be found by differentiating Eq. (2.29), with respect to ψ:

$$\mathbf{t} = \frac{\cos\Theta\ \hat{t}_0 + \alpha \sin\Theta\ \hat{\varphi}}{\sqrt{\cos^2\Theta + \alpha^2 \sin^2\Theta}}. \tag{2.30}$$

From this, the components of $H_{\alpha\beta}$ along $\hat{\Theta}$ and $\hat{b} = \mathbf{t} \times \hat{\Theta}$ can be found explicitly:

$$H_{\Theta\Theta} = H_{bb} = -2\sqrt{2}\Omega \frac{\sin\Theta \sin\varphi}{\sqrt{\cos^2\Theta + \alpha^2 \sin^2\Theta}}$$
$$H_{\Theta b} = H_{b\Theta} = 0.$$

This diagonal structure of the convective flow of separation follows from the stereographic projection: relative to the equidistant fibrations in S^3, the local distances between curves is locally stretched by the projection to E^3 by equal amounts in both directions normal to $\mathbf{t}$. Qualitatively, the spatial variation of non-equidistance follows that illustrated for the $\det(\mathbf{H}) = 0$ structure in the Supplemental Video, with respective bunching and of filaments on the inner and outer sides of the torus. While similar topology and spatial distribution of non-equidistance, we find that the magnitude of spacing variation differs considerably among the ansatzes.

We note that in the limit of narrow bundles ($\Theta \to 0$), we can estimate the growth of non-equidistance from $H \sim \Omega\kappa_0\rho$. When $\Omega \gg \kappa_0$ we average this over one P (a minor cycle of the torus) to estimate $\delta r \sim \kappa_0\rho$. Alternatively, for small twist when $\Omega \ll \kappa_0$ this should be averaged over the bundle length $2\pi/\kappa_0$, leading to $\delta r \sim \Omega\rho$. From these two regimes, we estimate the scaling of non-equidistance with bundle thickness

$$\lim_{R\to 0} \langle \delta r^2 \rangle_{\text{Seifert}} \propto \min[\Omega^2, \kappa_0^2] \times R^2. \tag{2.31}$$

We compare this estimate to numerical calculations of $\langle \delta r^2 \rangle$ in the $\kappa_0 R$ and ΩR plane for projections of Seifert fibrations in Fig. 2.6a.

2.5.2 Splay-free toroids

The non-equidistance of stereographic projections of fibrations of S^3 derives from the locally isotropic (conformal) dilation of inter-filament spacing. An alternative ansatz, and one which is typically invoked in models of polymeric liquid crystal textures, is the assumption of zero splay, which corresponds to constant area per filament transverse to its normal [96]. Hence, in the plane transverse to each filament, the polygonal region bounded by the neighboring filaments maintains constant area, and exhibits only area-preserving (shear) deformations as it flows along its contour.

A splay-free tangent field requires that $\nabla \cdot \mathbf{t} = \frac{1}{2}\mathrm{tr}(\mathbf{H})$ vanishes. Since $H_{\rho\rho} = 0$ by construction in the generalized cylindrical coordinates of Sec. 2.3.2, this imposes the additional condition that $H_{bb} = 0$, or Eq. (2.18). For a circular central curve, which has constant curvature and zero torsion, this equation can be solved by the method of characteristics, giving:

$$\sin\theta = \frac{f(\rho)}{1 - \rho\kappa_0 \cos\phi}, \tag{2.32}$$

where $f(\rho)$ is any function of ρ. Previous studies for splay-free liquid crystalline toroids have assumed the simple linear ansatz, e.g. $f(\rho) = \Omega\rho$. Notably, a splay-free toroidal texture is spatially limited to $f(\rho) + \rho\kappa_0 < 1$, beyond which it becomes singular. The additional constraint that all curves wind around the minor cycle of the toroid at the same pitch, Eq. (2.27), constrains the specific radial dependence of $f(\rho)$ and $\kappa_0\rho$. The rate of angular circulation of a filament's position relative to the inward pointing normal of the major circle is

$$\frac{\partial\phi}{\partial s} = \frac{f(\rho)}{\rho\sqrt{1 - \frac{f(\rho)^2}{(1-\rho\kappa_0\cos\phi)^2}}}. \tag{2.33}$$

Inserting this into Eq. (2.27), we have the additional condition that

$$\kappa_0 P = \int_{-\pi}^{+\pi} d\phi \; \kappa_0\rho\sqrt{\frac{1}{f(\rho)^2} - \frac{1}{(1 - \rho\kappa_0\cos\phi)^2}} \tag{2.34}$$

is independent of ρ. From this condition, we derive the relationship between $f(\rho)$ and $\kappa_0\rho$ for general values of $\kappa_0 P$ in splay-free bundles with mean winding which is notably more complex than the linear ansatz assumed in refs. [76, 93]. Notably, in the slender bundle limit (as $\Omega\rho$, $\kappa_0\rho \to 0$). Eq. (2.34) satisfies

$$f(\rho) \simeq \frac{\Omega\rho}{\sqrt{1+\Omega^2\rho^2}}\big[1 - 18\Omega^2\kappa_0^2\rho^4 + \mathcal{O}(\rho^6)\big], \tag{2.35}$$

which, as $\kappa_0\rho \to 0$, recovers the equidistant helical domains, for which $f(\rho) = \Omega\rho/\sqrt{1+\Omega^2\rho^2}$.

We can estimate the magnitude of this variable spacing by considering the off-diagonal, non-vanishing component of $\mathbf{H}$ for Eq. (2.32),

$$\begin{aligned} H_{b\rho} = H_{\rho b} &= \partial_\rho\theta - \frac{\sin\theta\cos\theta}{\rho(1-\rho\kappa_0\cos\phi)} \\ &= \tan\theta\Big(\frac{\partial_\rho f}{f} + \frac{\kappa_0\cos\phi}{f}\sin\theta\Big) - \frac{\sin\theta\cos\theta}{\rho(1-\rho\kappa_0\cos\phi)}. \end{aligned} \tag{2.36}$$

In the limit of narrow splay-free bundles, we have $H_{b\rho} \approx \Omega^3\kappa_0\rho^3 + \mathcal{O}(\rho^4)$. Integrating this over the shorter of lengths P and $L = \pi\kappa_0^{-1}$, we find that this separation averages to $\delta r \sim \min[\Omega, \kappa_0]\Omega^2\rho^3$, from which we estimate,

$$\lim_{R\to 0}\langle\delta r^2\rangle_{splay-free} \propto \min[\Omega^2, \kappa_0^2] \times \Omega^4 R^6. \tag{2.37}$$

The suppression of splay notwithstanding, we find that the growth of spacing variation (shears) in narrow splay-free bundles grows as ρ^3, as opposed to the linear scaling with thickness of the stereographically projected fibrations of S^3 [5]. Fig. 2.6b shows the numerical calculation of $\langle\delta r^2\rangle$ in the $\kappa_0 R$ and ΩR plane for splay-free bundles.

[5]It can be shown that neglect of the constant circulation constraint of Eq. (2.34) in the linear ansatz $f(\rho) = \Omega\rho$ studied in refs. [76, 93] leads to less equidistanct splay-free textures, with $\delta r \sim \min[\Omega, \kappa_0]\Omega\rho^2$

Notably, due to the condition $f(R) \leq \kappa_0 R$, the continuous class of solutions extend only up to a critical thickness $R_{max} < \kappa_0$, whose value decreases with ΩR.

2.5.3 $\det(\mathbf{H}) = 0$ toroids

Finally, we consider a nearly-equidistant ansatz that satisfies $\det(\mathbf{H}) = 0$, as opposed to vanishing trace. In particular, we adopt the solution to $H_{\rho\rho} = H_{\rho b} = H_{b\rho} = 0$ of Eq. (2.19), and further take Ω to be a constant, such that the tangent field (in the coordinates of Eq. (2.14)) is

$$\tan\theta = \frac{\Omega\rho}{1 - \kappa_0 \cos\phi}, \tag{2.38}$$

which can be extended continuously up to thicknesses equal to the major radius of the torus. Using the fact that τ_0 and κ_0 are also constant, we find from Eq. (2.20) that the non-vanishing component of $\mathbf{H}$ is

$$H_{bb} = -\frac{2\rho^3\kappa_0\Omega^3 \sin\phi}{[(1 - \rho\kappa_0\cos\phi)^2 + (\rho\Omega)^2]^{3/2}}, \tag{2.39}$$

which notably grows as $\sim \rho^3$ for small thicknesses. Integrating over the shorter of P or κ_0, we estimate the growth of non-equidistance for this class of toroids to be

$$\lim_{R\to 0} \langle \delta r^2 \rangle_{\det(\mathbf{H})=0} \propto \min[\Omega^2, \kappa_0^2] \times \Omega^4 R^6. \tag{2.40}$$

Thus, like the splay-free toroids, the $\det(\mathbf{H}) = 0$ ansatz remains more equidistant than S^3 fibrations (i.e. $\langle \delta r^2 \rangle^{1/2} \sim R^3$ as opposed to $\sim R$). In Fig. 2.6d we compare the numerical calculations for $\langle \delta r^2 \rangle^{1/2}$ for the three *ansatz* with $\Omega = \kappa_0$ for increasing twist. For increasing thickness $\Omega R \lesssim 1$, we see that $\langle \delta r^2 \rangle$ ultimately grows larger for splay-free structures than for the $\det(\mathbf{H}) = 0$ ansatz, indicating that the incorporation of a small amount of splay leads to more equidistant structures. How close the $\det(\mathbf{H}) = 0$ structure comes to the true minimizer of $\langle \delta r^2 \rangle$ remains an open question.

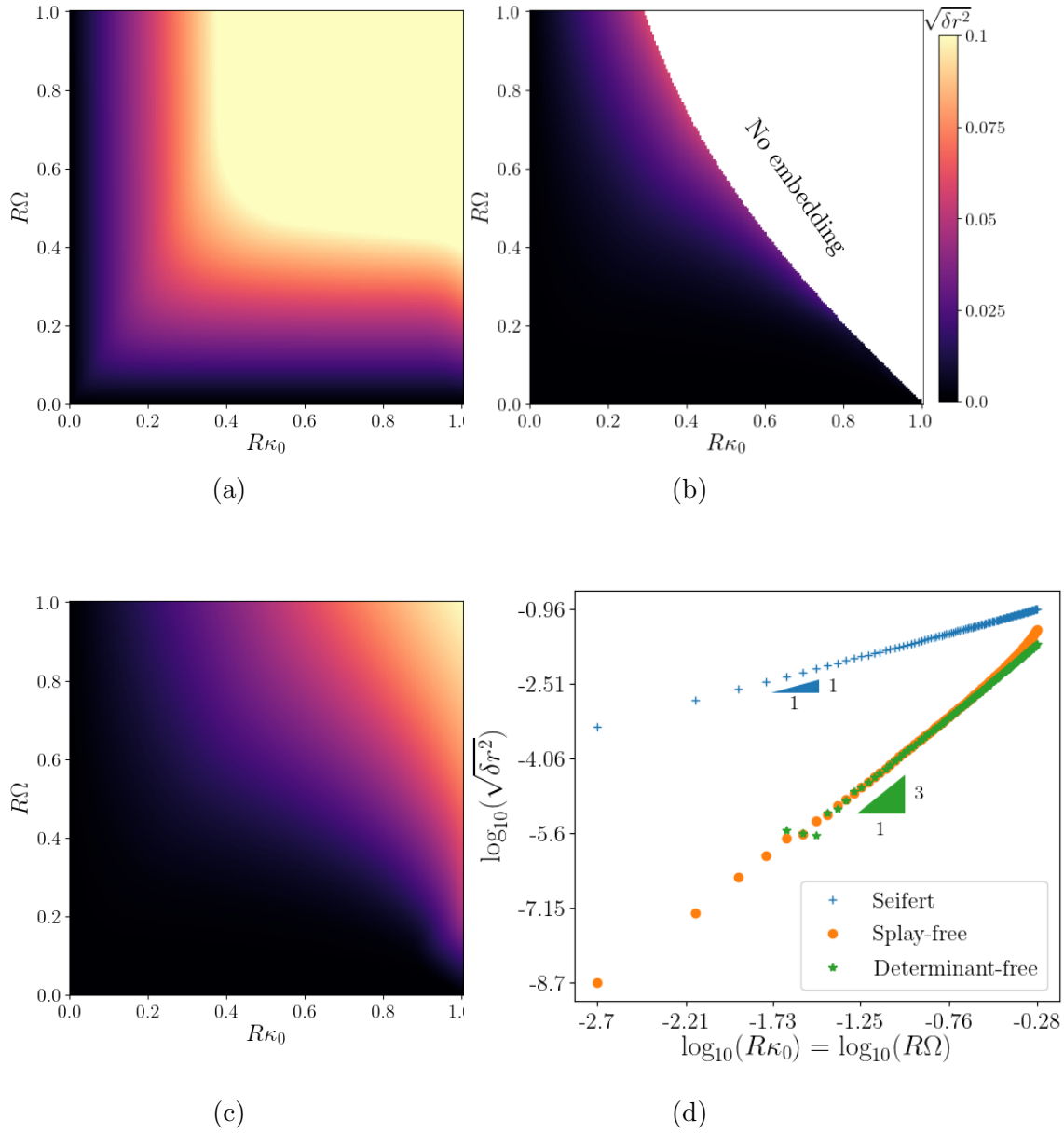

Figure 2.6: Numerically calculated deviations from equidistance for the Seifert fibrations 2.6a, splay-free ($\mathrm{tr}(\mathbf{H}) = 0$) 2.6b, and $\det(\mathbf{H}) = 0$ 2.6c textures, varying $R\kappa_0$ and $R\Omega$, where R is the bundle radius. $R\Omega = R\kappa_0$ slices for Seifert, splay-free, and determinant-free structures, in 2.6d show, respectively, the R scaling of the Seifert fibrations (Eq. (2.31)) and the R^3 scaling of the splay-free (Eq. (2.37)), and determinant-free (Eq. (2.40)) textures.

2.6 Discussion

In this chapter, we have presented several results on packings of multiple curves in E^3 constrained by mutual equidistance. First, we showed that any two mutually equidistant curves $\mathbf{r}_1$ and $\mathbf{r}_2$ in E^3 are spanned by the ruled surface generated by the vector distance of closest approach between the curves, and the one parameter family of curves perpendicular to these rulings is itself equidistant. We call this the *separating surface* defined by the equidistant pair, and between two equidistant curves, it is possible to fill in an arbitrary number of mutually equidistant curves embedded in the separating surface. Although such families of curves are clearly unlimited in number, they are strictly two-dimensional in the sense that the family is collinear: the 1D line separating any two curves perpendicularly intersects all the curves in the set.

In contrast, we find that non-collinear, volume filling, curve fields of E^3 fall into two strictly distinct families, and in comparison to the collinear families, the geometries of curves that these permit are highly constrained. Crudely speaking, bundles of curves can be twisted (uniformly) but not bent, or bent but not twisted. However, like the collinear family, these equidistant curve fields have the property that they allow for embedding an arbitrary number of equidistant curves ($N \to \infty$) within a finite tubular neighborhood of some central curve in E^3.

The relatively restrictive geometry of equidistant fields raises interesting questions about the relationship between the problem of packing finite vs. infinite equidistant curves. The existence of only two distinct equidistant fields, along with the tube argument in Fig. 2.2 suggests that the structure of finite N equidistant bundles may be much less constrained than equidistant fields. Discrete equidistant bundles of this sort have ready applications to physical systems, from collagen triple helices [97] and other dense packed biological systems, to the (conventional) seven strands that make up most wire rope [25]. A particularly relevant restriction of this problem is that of

locally isometric packings, where each filament is only constrained to lie equidistant to its nearest neighbors at some characteristic distance a, as in typical physical systems, where filaments packings are governed by an interfilament spacing set by an effective size.

We also expect the constraint satisfaction problem for N equidistant filaments to yield novel and complex geometries, since, as shown in Subsection 2.2.3, twisted equidistant triplets can be constructed around any smooth curve in E^3, but only constant twist helical bundles have a continuous field realization. We conjecture that there exists $N_c > 3$ such that the only bundles of $N \geq N_c$ regular, equidistant, non-collinear curves in E^3 are either parallel (developable domain) or helical (constant twist), i.e. they are integral curves of equidistant fields.

For relatively small numbers of filaments, ($N \leq 3$), these and related close packing problems have been studied in the context of ideal (or tight) knots and tangles [98]. Ideal knots, which are embeddings in E^3 that minimize the ratio of knot length to filament-width [99], demand a fully global treatment that considers self-contact phenomena. To this end, the principle object of study for single stranded knots becomes not the distance of closest approach, but the global radius of curvature [82]. Interestingly, ideal knot embeddings are not equidistant in general, even when equidistant embeddings exist. For example, the ideal trefoil is known to make close (self-)contact over only a subset of its length [100]. The existence of geometrically rigid families of equidistant curve packings suggest that knot optimization problems that account for the energetic penalty of broken cohesive contacts are likely to yield new classes of minimizers [101]. For example, one may consider a generalization of the "Möbius energy" [102], that incorporates a pair-wise potential between different arc-elements of a knotted curve, parameterized by some $V(x)$ that diverges as $x \to 0$,

$$E[\boldsymbol{\gamma}] = \int ds \int d\sigma V(|\boldsymbol{\gamma}(\sigma) - \boldsymbol{\gamma}(s)|), \tag{2.41}$$

where s and σ are arc length parameterizations of curve $\boldsymbol{\gamma}$. When $V(x)$ is a strictly hard-core repulsive potential, we recover the ideal knot problem, while if $V(x)$ has an attractive minimum at finite $x = \delta$, we might expect solutions which favor equidistance. In particular, in the limit that the cohesive attraction becomes infinitely strong in depth but infinitely narrow in range (relative to the repulsive core thickness), we anticipate a new class of minimizers that maximize the length and number of cohesive contacts. In light of the conjectured rigidification of the constraints on equidistance with increasing numbers of curves (or, here, curve segments) in equidistant contact, we further anticipate that such minimizers will be strongly dependent on the knot topology. For example, because torus knots are necessarily simultaneously bent and twisted, we expect uniformly equidistant cohesive contact to be possible only when the number of strands arrayed around the minor cycle of the knot is less than N_c.

Beyond possible applications to problems in knot theory, the geometric constraints of equidistance would seem to have important and heretofore unexplored mechanical and structural consequences for a range of multi-filament structures. Recent experimental studies, for example, have shown that 2D packings of initially straight filaments tend to adopt constant-pitch, helical shapes when subjected to mechanical twist at their ends [52]. The emergence of this texture, even in the absence of cohesion between filaments, suggests that equidistance may be favored due to generic mechanical arguments (e.g. due to inward pressures generated by flexed or stretched outer strands). This observation, in combination with the restrictive constraints imposed by equidistance in large N packings, as described herein, raises further questions about the additional mechanical responses of filament packings associated with driving the structure to a non-equidistant geometry, such as when one simultaneously bends and twists a packing. Bent and twisted assemblies of filaments, twisted toroids, are observed in condensates of collagen [68] and DNA [67], and physical models constructed

to date have yet to account for necessary energetic costs of non-equidistance required by this geometry.

Beyond even structures of physical filament, twisted toroidal structures appear as topological solitons in range of classical field theories, for example, the extended non-linear σ model [103, 104], which supports knotted solutions whose topology is closely connected to the Hopf fibration of S^3. In these "hopfion" structures, 1D preimages of constant order parameter orientation (corresponding to a point on S^2) correspond to "virtual filaments" that are twisted into closed toroidal bundles. Above, we showed that the simultaneously twisted and bent structure of hopfions is incompatible with equidistance between preimages. Recent studies show that hopfions emerge in models with preferred chiral pitch, such as models of chiral liquid crystals [69–71], and chiral [73, 74], or frustrated ferromagnets [72]. In such models, a preferred rotation rate corresponds to a favored constant local spacing between preimage "filaments" of the field configuration. Hence, we expect that equidistant (but not necessarily isometric) textures of constant-preimage filaments are energetically favored. Thus, at least in models with a preferred twist wavelength, the incompatibility between twist, bend and equidistance in curve fields in E^3 represents an intrinsic, and previously unrecognized, source of frustration in the formation of hopfionic structures.

Addressing questions about the structural and mechanical consequences for complex, non-equidistant bundle geometries requires new theoretical descriptions, since canonical approaches, such as the generalized elasticity theory of columnar liquid crystals [89], account for only small deviations around an unstrained reference. The relevant physics for twisted and bent filament bundles (e.g. twisted toroids) requires a fully geometrically non-linear theory that couples the metric properties of the cross-sectional filament packing to the flow generated by the filament texture, a framework which will be addressed in future work.

Of particular interest is the coupling of metric (2D solid) to textural (1D fluid) degrees of freedom in geometrically frustrated materials. In the simplest case of helical filament bundles, the increase in twist leads to an effective positively curved metric and the stability of excess 5-fold disclinations in an otherwise hexagonally-coordinated bundle [43]. The total integrated Gaussian curvature of a straight twisted bundle is 2π, implying a maximum number of six excess 5-fold defects [43]. For combined twisted and bent geometries, such as a twisted toroid, a naive analysis of the "local metric" induced in a planar cut of the bundle suggests that the effective integrated curvature of the section exceeds the value for the straight bundle, presumably implying that simultaneously twisting and bending a bundle increases the total number of defects in the ground state order. It remains to be understood whether, and to what extent, this "local" perspective on the metric structure in a give planar cut of a non-equidistant bundle truly underlies even a heuristic understanding of the coupling between defects and the 3D geometry of bundles beyond the equidistant cases studied so far.

For straight filament bundles, similar work has shown that the introduction of packing defects can generate highly non-trivial textures in cohesive filament bundles, through their ability to reshape the "target metric" of a filament packing from planar to non-Euclidean [47]. This effect neatly demonstrates one important repercussion of our result in Section 2.3: that the response of positive and negative topological defects (5- and 7-fold disclinations in hexagonal packings) is highly asymmetric *because* there is an equidistant field with positive effective curvature, while there are no equidistant fields with negative effective curvature. The consequences of the restrictive nature of equidistance in bundles with negative curvature are therefore even more severe, as evidenced by the non-trivial elastic instabilities observed in simulated bundles with trapped negative disclinations. A theoretical approach to predict equilibrium configurations of bundles whose target metrics (controlled by either distributions of

defects or by patterns of inhomogeneous filament diameter) are incompatibile with equidistance remains an open challenge.

2.A Existence of Equidistant Pairs

Let $\mathbf{r}_1$ be a curve embedded in E^3 with Darboux frame $\{\hat{T}, \hat{e}_1, \hat{e}_2\}$, arc length s, and frame curvatures and torsion κ_1, κ_2, and τ_g. Then any curve $\mathbf{r}_2$ parameterized by

$$\mathbf{r}_2(s) = \mathbf{r}_1(s) + \rho\Big\{ \cos\big[\phi(s)\big]\hat{e}_1(s) + \sin\big[\phi(s)\big]\hat{e}_2(s)\Big\}, \tag{2.42}$$

is equidistant to $\mathbf{r}_1$. To see why, note that for any such $\mathbf{r}_2$, the point of closest approach to $\mathbf{r}_2(s)$ on $\mathbf{r}_1$ is the corresponding point $\mathbf{r}_1(s)$. Then $\mathbf{r}_1$ and $\mathbf{r}_2$ are equidistant when $\partial_s\mathbf{r}_2 \cdot (\mathbf{r}_2 - \mathbf{r}_1) = 0$, as in Eq. (2.2). Since

$$\mathbf{r}_2 - \mathbf{r}_1 = \rho\Big\{ \cos\big[\phi(s)\big]\hat{e}_1(s) + \sin\big[\phi(s)\big]\hat{e}_2(s)\Big\}, \tag{2.43}$$

all that remains is to show that $\partial_s\mathbf{r}_2$ is perpendicular to $\cos\big[\phi(s)\big]\hat{e}_1(s)+\sin\big[\phi(s)\big]\hat{e}_2(s)$. Since

$$\partial_s\mathbf{r}_2 = (1 - \rho\kappa_1\cos\phi - \rho\kappa_2\sin\phi)\hat{T} + \rho(\partial_s\phi + \tau_g)(-\sin\phi\hat{e}_1 + \cos\phi\hat{e}_2), \tag{2.44}$$

the two vectors are always orthogonal, so we have that $\mathbf{r}_2$ and $\mathbf{r}_1$ are equidistant whenever $(1 - \rho\kappa_1\cos\phi - \rho\kappa_2\sin\phi)$ and $\rho(\partial_s\phi + \tau_g)$ are finite and nonzero.

2.B Quasi-cylindrical coordinates for filament bundles

We can write down any generic position $\vec{x}$ in coordinates centered around some curve $\mathbf{r}_0$ as follows:

$$\mathbf{x} = \mathbf{r}_0 + \rho\hat{\rho}. \tag{2.45}$$

An infinitesimal displacement $d\vec{x}$ can then be found by

$$d\mathbf{x} = \frac{\partial \mathbf{x}}{\partial s} ds + \frac{\partial \mathbf{x}}{\partial \rho} d\rho + \frac{\partial \mathbf{x}}{\partial \phi} d\phi, \tag{2.46}$$

where the partial derivatives are:

$$\frac{\partial \mathbf{x}}{\partial s} = \hat{t}_0 + \rho \frac{\partial \hat{\rho}}{\partial s} \tag{2.47}$$

$$\frac{\partial \mathbf{x}}{\partial \rho} = \hat{\rho} \tag{2.48}$$

$$\frac{\partial \mathbf{x}}{\partial \phi} = \rho \hat{\phi}, \tag{2.49}$$

and

$$\frac{\partial \hat{\rho}}{\partial s} = -\kappa_0 \cos\phi \hat{t}_0 + \tau_0 \hat{\phi}. \tag{2.50}$$

So, we find the Jacobian for this coordinate transformation:

$$J = \begin{bmatrix} 1 - \rho\kappa_0 \cos\phi & 0 & 0 \\ 0 & 1 & 0 \\ \rho\tau_0 & 0 & \rho \end{bmatrix} \tag{2.51}$$

with its inverse

$$J^{-1} = \begin{bmatrix} \frac{1}{1-\rho\kappa_0 \cos\phi} & 0 & 0 \\ 0 & 1 & 0 \\ -\frac{\tau_0}{1-\rho\kappa_0 \cos\phi} & 0 & \frac{1}{\rho}. \end{bmatrix} \tag{2.52}$$

Note that this inverse does not exist for $\rho\kappa_0 \cos\phi = 1$ or $\rho = 0$, for which we can't take these derivatives.

We can now write down the tensor $\nabla \mathbf{t}$ in these coordinates, represented in the basis $\{\mathbf{t}, \hat{\rho}, \hat{b}\}$, where $\hat{b} = \mathbf{t} \times \hat{\rho}$. The $\rho\rho$ component of this matrix, $\hat{\rho} \cdot \nabla = \frac{\partial}{\partial \rho}$ doesn't do much, but $\hat{e} \cdot \nabla$ is slightly more exciting:

$$\hat{e} \cdot \nabla = (J^{-1}\hat{e}) \cdot \nabla \tag{2.53}$$

$$= \left(\begin{bmatrix} \frac{1}{1-\rho\kappa_0 \cos\phi} & 0 & 0 \\ 0 & 1 & 0 \\ -\frac{\tau_0}{1-\rho\kappa_0\cos\phi} & 0 & \frac{1}{\rho} \end{bmatrix} \cdot \begin{bmatrix} -\sin\theta \\ 0 \\ \cos\theta \end{bmatrix} \right) \cdot \nabla \tag{2.54}$$

$$= [-\sin\theta \frac{1}{1-\rho\kappa_0\cos\phi}\hat{t}_0 + (\sin\theta \frac{\tau_0}{1-\rho\kappa_0\cos\phi} + \cos\theta\frac{1}{\rho})\hat{\phi}] \cdot \nabla \tag{2.55}$$

$$= -\sin\theta \frac{1}{1-\rho\kappa_0\cos\phi}\frac{\partial}{\partial s} + (\sin\theta \frac{\tau_0}{1-\rho\kappa_0\cos\phi} + \cos\theta\frac{1}{\rho})\frac{\partial}{\partial\phi}. \tag{2.56}$$

We can now find these derivatives acting on the tangent field, noting that to find derivatives on $\hat{\phi}$, we can write it explicitly in the Frenet-Serret frame $\hat{\phi} = -\sin\phi\hat{N}_0 + \cos\phi\hat{B}_0$, with

$$\partial_s \hat{N}_0 = -\kappa_0 \hat{t}_0 + \tau_0 \hat{B}_0 \tag{2.57}$$

$$\partial_s B_0 = -\tau_0 \hat{N}_0 \tag{2.58}$$

$$\implies \partial_s \hat{\phi} = \kappa_0 \sin\phi \hat{t}_0 - \tau_0 \hat{\rho}. \tag{2.59}$$

This gives us derivatives as follows:

$$\partial_\phi \hat{t} = \partial_\phi(\cos\theta\hat{t}_0) + \partial_\phi(\sin\theta\hat{\phi} \tag{2.60}$$

$$= -\sin\theta\partial_\phi\theta\hat{t}_0 + \cos\theta\partial_\phi\theta - \sin\theta\hat{\rho} \tag{2.61}$$

$$\partial_s \hat{t} = \cos\theta\kappa_0(\cos\phi\hat{\rho} - \sin\phi\hat{\phi}) + \sin\theta(\kappa_0\hat{t}_0 - \tau_0\hat{\rho}) - \sin\theta\partial_s\theta\hat{t}_0 + \cos\theta\partial_s\theta\hat{\phi} \tag{2.62}$$

$$\partial_\rho \hat{t} = -\sin\theta\partial_\rho\theta\hat{t}_0 + \cos\theta\partial_\rho\theta\hat{\phi} \tag{2.63}$$

These now let us write down explicitly the components of $\nabla \mathbf{t}$, and give us Eq. (2.16).

2.C Measuring non-equidistance numerically

Averaging the distance of closest approach between filaments i and j at all positions s_i gives the average separation from i to j, $\langle \Delta_{ij} \rangle$. To compare longitudinal uniformity of inter-filament spacing in these distinct textures, we define the following measure of local deviation from equidistance:

$$\delta r_i(s_i) = \frac{1}{n_i} \sum_{\langle ij \rangle} \frac{\Delta_{ij}(s_i) - \langle \Delta_{ij} \rangle}{\langle \Delta_{ij} \rangle}, \tag{2.64}$$

where $\sum_{\langle ij \rangle}$ denotes the sum over the n_i neighbors of the ith filament in the initial hexagonal packing.

This quantity measures the extent to which a point s_i on $\mathbf{r}_i$ is relatively closer or further than its average separation from other filaments in the bundle. we define a measure of the total variability of spacing in the bundle $\langle \delta r^2 \rangle$ as the average of the square of this local measure over the lengths of all filaments,

$$\langle \delta r^2 \rangle = \frac{1}{N_f} \sum_{i=1}^{N_f} \int ds_i \ \frac{\delta r_i^2(s_i)}{\ell_i}. \tag{2.65}$$

where $N_f = 17$ is the number of filaments in the bundle and ℓ_i is the arc length used in the averaging of the ith filament. we note that both quantities are insensitive to variations in spacing from pair to pair throughout the cross section (i.e. whether a packing is isometric or not), and only measure longitudinal variations.

CHAPTER 3

WHEN YOUR FIBERS ARE FILAMENTS: A GAUGE THEORY OF ELASTICITY FOR COLUMNAR LIQUID CRYSTALS

She flung herself on her bed and drew a line with a pencil on a piece of paper. And another line, carefully, and another. A world was born around her, like a bright forest with a million shimmering leaves

The Price of Salt
Patricia Highsmith

3.1 Introduction

It is a truth universally acknowledged, that a physicist in possession of an interesting problem, must be in want of an energy. However well or poorly understood the phenomena may be on first coming to her attention, this truth is so well fixed in the minds of her colleagues that it is considered the rightful content of some or other chapter of her dissertation [105].

Soft elasticity—where certain deformations are necessarily zero modes of the elastic energy—is a ubiquitous feature of soft materials, from mechanical metamaterials [106**?** , 107], in which the presence of continuous zero modes of rigid networks can tune bulk elastic properties; to smectic and columnar liquid crystals, and liquid crystal elastomers [108]; and in biological systems as diverse as DNA condensates [67] and cell monolayers. Because soft-elastic materials can undergo large deformations with minimal strain, effective continuum descriptions depend heavily on strain tensors which capture the materials' *geometric nonlinearities*.

Since soft-elastic materials are often described by their zero modes [1], we can try to build a modified elasticity theory based on these continuous symmetries. This *gauge theoretic* view of soft elasticity has the advantages of accounting explicitly for the large deformations associated with elastic zero modes. Moreover, the elastic response of a more general class of materials with *soft modes*, which, while not true elastic zero modes, cost much lest energy than other deformations, can often be well modeled by an "ideal" soft-elastic theory.

Soft-elastic liquid crystals, like the smectic-A and columnar phases [89, 109], are both prototypical soft-elastic materials, and important geometric templates for diverse materials across a wide range of lengthscales, from nucleic acid condensates [23, 66] like those in viral capsids [67, 110, 111], biopolymer bundles [11, 60, 68, 112], and lamellar phases of surfactants [109] and solid sheets [113] to wire ropes [25], yarns [21, 22, 114], bundles of elastomer filaments [52, 53], and stacks of paper [115]. While there are well established models which capture the geometrical nonlinearities in smectic-A liquid crystals [116], longitudinal frustration in columnar liquid crystals and filamentous materials associated with strict geometric constraints on *equidistance* [1] means that prior two dimensional descriptions [40–42] cannot adequately describe the elastic response of many columnar textures.

In the absence of a validated energetic description for the geometric non-linearities which dominate the response of twisted-toroidal filament bundles, theoretical models to date have focused on a variety of geometric ansatzes[1, 9, 75, 76, 93, 95], which draw on the coupling between the nematic and crystalline degrees of freedom for these materials [96]. Because non-vanishing splay necessarily corresponds to areal dilation or expansion of the columns, and because typical shear moduli for columnar mesophases are lower than the bulk modulus [109], splay-free textures, in which each

[1] After all, the difference between a columnar liquid crystal and a smectic liquid crystal is that columnar phases have one uncorrelated, fluid like direction, while smectics have two

column experiences purely local shear, without bulk dilation, are preferred to textures with splay [1, 76, 93]. However, recent developments [1], which we reproduce in Ch. 2, have shown that some of these geometric templates fair quite poorly on measures of their longitudinal geometric frustration, and, while these ansatzes have the advantage of a clear geometrical motivation, it remains unclear whether any are actually elastic equilibria.

In this chapter, we develop a geometrically non-linear, gauge-theoretic description for the elasticity of soft-elastic liquid crystals. We first present a brief introductory example, which shows that the minimally non-linear two-dimensional theory introduced by J. Selinger and R. Bruinsma [42] is inadequate for descriptions of non-equidistant filament bundles [1]. Then, to capture the geometric non-linearities inherent in non-equidistant, longitudinally frustrated filament bundles, we introduce a modified deformation gradient, as in classical gauge theories [117], so that any continuous symmetry of the material is a zero of this *covariant derivative*. Unlike classical gauge theories, however, for soft-elastic materials, all physical degrees of freedom are determined by a particular deformation of the material. What follows provides a generic procedure for deriving elasticity theories of *fibered materials*, like smectic and columnar liquid crystals, in which the embedding space is 'nicely' divided into submanifolds called *fibers* [2] [1, 85].

Unlike gauge-theory inspired treatments of the nematic to smectic-A transition [120, 121] and it's columnar analog [40, 41, 48, 122], in which the gauge symmetry of a density-wave model is explicitly broken by, e.g., the splay elasticity of the underlying

[2]For smectics, the layers corresponding to density level sets; for columnar liquid crystals, the constituent columns. For an introduction to the mathematical literature on the topology and geometry of smooth fiber bundles, see, for example [118, 119]. The connection between a metric on the embedding space and on the fiber bundle is fundamental to the study of Riemannian fibrations, see [50, 85], with the additional constraint of equidistance between the fibers.

nematic order, here the elastic energy in the ideal case will be invariant under the *embedded* gauge transformations [3].

The resultant Lagrangian elasticity theory has a simple geometric interpretation in terms of the local *distance of closest approach* between the fibers, providing a correspondence between the global symmetries under reptations and the local geometric structure of these materials. In contrast to density wave models of nonlinear elasticity (such as [2, 122, 123]), the theory we describe here neither depends on the presence of a well defined planar reference crystal, nor presupposes the possibility of regular 2d lattice packings, allowing us both to accommodate the effective curvature of bundles of constant pitch helices [43], and providing for a natural generalization to arbitrary target metrics.

We next derive the conditions of force balance for filamentous materials by finding the Euler-Lagrange equations of the Hookean elastic energy. As in thin sheets, force balance perpendicular to the filament tangents is given by gradients of the stress tensor (with corrections to account for non-integrability due to inter-filament twist). Unlike the case of thin sheets, however, force balance along the filaments is controlled not by the curvature tensor, but by the *convective flow tensor*, as introduced in Ch. 2, which measure the local deviations from equidistance [1].

3.2 Non-equidistance and non-linearities

Having shown in Ch. 2 that non-equidistance is an all but generic feature of twisted filament bundles, it becomes quite important to consider whether current continuum descriptions of filament bundles and columnar liquid crystals account for these longitudinal variations in length. The minimally rotationally-invariant strain tensor, introduced by Selinger and Bruinsma [42], is given by

[3] So the symmetries of the material are a subgroup of the diffeomorphism group [119], rather than a symmetry of the density wave-vector.

$$\epsilon_{\alpha\beta} = \partial_\alpha u_\beta + \partial_\beta u_\alpha - \partial_\alpha \mathbf{u} \cdot \partial_\beta \mathbf{u} - t_\alpha t_\beta, \tag{3.1}$$

where $t_\alpha \approx \partial_\alpha u_z$. We can hexplicitly calculate the strains by assuming that the initial configuration is given by a developable domain around a central curve $\vec{r}_0$ with tangent vector $\hat{t}_0$. We then take the tangent vector field of the deformed filament bundle to be

$$\mathbf{t} = \cos\theta \hat{t}_0 + \sin\theta \hat{\phi}, \tag{3.2}$$

with $\theta = \Omega\rho$ for two different central curves: one a straight line, as in Fig. 3.1a, and one a circle with curvature κ_0, as in Fig. 3.1b. If we then calculate the Selinger-Bruinsma strain tensor, we find that

$$\epsilon_{ij} = \begin{pmatrix} 0 & 0 \\ 0 & -\frac{\Omega^2\rho^2}{1+\Omega^2\rho^2} \end{pmatrix} \tag{3.3}$$

for both bundles; clearly in contradiction of our proof in Ch. 2 that the twisted toroid must be non-equidistant. While this may seem like a small failing, it makes it difficult to distinguish between different candidate textures for twisted-toroidal bundles. For example, Kulić, et al. [76] have suggested that splay-free textures (which has $\mathrm{tr}(h) = 0$, and is defined in Eq. 2.32) are likely candidate solutions based on the observation that zero splay implies constant area per filament; however, in Ch. 2 we have shown that this splay-free solution is strictly less equidistant than a $\det(h) = 0$ ansatz, which incorporates a little splay [1]. Without the ability to determine the importance of longitudinal length variations in the elastic energy, the equilibrium states of non-equidistant filament bundles, which are both common and important in real materials, are beyond our reach.

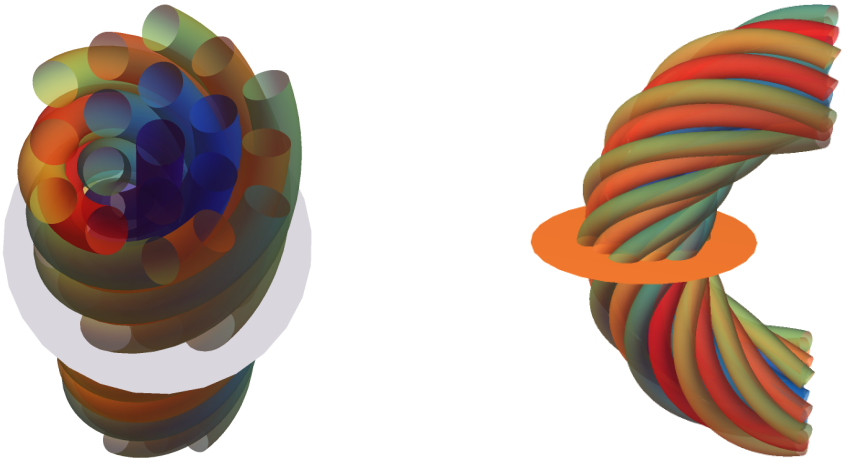

(a) (b)

Figure 3.1: We can make the shortfalls of two dimensional models explicitly by constructing two filament bundles with the same projection of the filament tangents into the plane perpendicular to the central curve. For 3.1a, reproduced from [1], the central curve is a straight line, whereas in 3.1b, it's a circle with curvature κ_0, but both have the same cross-sectional profile, given by Eq. (3.2) with $\theta = \Omega\rho$. The two-dimensional strain tensor in [42] doesn't distinguish between the two, whereas we have shown in Ch. 2 that there must be longitudinal fluctuations in the distance of closest approach for the torodial bundle in 3.1b.

3.3 Gauge theory elasticity for soft-elastic liquid crystals

In order to address this problem in the continuum elasticity for filament bundles, we turn to an approach inspired both by classical gauge theories and the geometry of fiber bundles. We first note that soft-elastic liquid crystals, like the columnar phase, are naturally described by their fluid-like directions, with crystalline order between columns, but not between molecules within the same column.

As with gauge theories for fields with a continuous field, like electrodynamics [117], we work at the level of the derivative, demanding that a modified deformation gradient, or **covariant derivative** of a deformation, remains invariant under symmetries. To avoid the introduction of unphysical auxiliary fields, and in contrast to typical gauge field theories, we here insist that all modifications to the deformation gradient depend solely on the deformation, $\mathbf{r}$ of the material. More formally, we are looking for a modified gradient D_I, so that if $\mathbf{r}$ and $\tilde{\mathbf{r}}$ are related by a continuous symmetry, then $D_I\mathbf{r} = \tilde{D}_I\tilde{\mathbf{r}}$, and so that $D_I\mathbf{r}$ is entirely determined by $\mathbf{r}$.

3.3.1 Elasticity of filament fields

We can apply the basic concepts of gauge theories to filament bundles and columnar liquid crystals by noting that they have a family of continuous zero modes corresponding to *reptations*, in which filaments slither along their length. Unlike classical gauge theories, however, the symmetries of soft-elastic materials are embedded, and correspond to a subset of its possible deformations, and so we demand that the covariant derivative also be solely determined by the current material configuration. Given any energy functional for columnar materials $\mathcal{W}$ [4], and a coordinate system on a manifold so that $\partial_s\mathbf{r}(s,\mathbf{v}) \parallel \mathbf{t}$, then for a deformation

$$\mathbf{r}'(s,\mathbf{v}) = \mathbf{r}(s+\sigma(s,\mathbf{v}),\mathbf{v}), \tag{3.4}$$

[4] so this is a statement about a quasi-static, elastic deformation

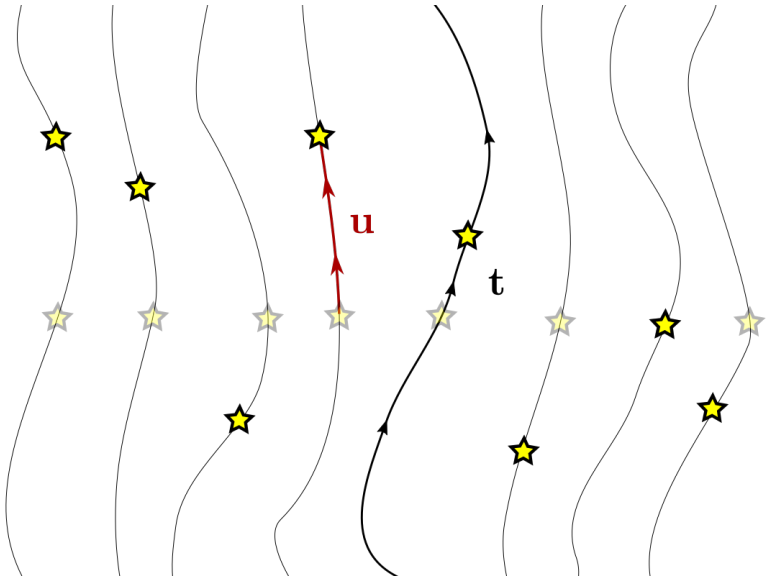

Figure 3.2: A displacement field $\mathbf{u}$, as shown above, which slides an initial material configuration (faded stars) to points all along the same filaments (stars) without changing the conformation, $\mathbf{t}$, is a *gauge transformation* or *reptation*.

as shown in Fig. 3.2, we should have that $\mathcal{W}[\mathbf{r}] = \mathcal{W}[\mathbf{r}']$. We also want to note here that any good elasticity theory should be local and determined solely by the deformation, so this will depend only on the deformation gradient $\partial_I \mathbf{r}$. Unfortunately, the deformation gradient here is not invariant under σ, the reptation or *gauge transformation*:

$$\partial_I \mathbf{r}' = \partial_I \mathbf{r} + \partial_I \sigma \partial_s \mathbf{r}. \tag{3.5}$$

Inspired by gauge theories such as classical electrodynamics, we want to work at the level of the deformation gradient, and see if we can find a covariant derivative D_I so that $D_I \mathbf{r} = D'_I \mathbf{r}'$. So, first, we'll break up this covariant derivative so that $D_I \mathbf{r} = \partial_I \mathbf{r} - \mathbf{A}_I$. Then, in order for $D_I \mathbf{r}$ to be gauge invariant, we have that $D'_I \mathbf{r}' - D_I \mathbf{r} = -\mathbf{A}'_I + \mathbf{A}_I = \partial_I \sigma \partial_s \mathbf{r}$, and so $-\mathbf{A}'_I + \mathbf{A}_I = -(\mathbf{t} \cdot \partial_I \mathbf{r}')\mathbf{t} + (\mathbf{t} \cdot \partial_I \mathbf{r})\mathbf{t}$, where $\mathbf{t} = \frac{\partial_s \mathbf{r}}{|\partial_s \mathbf{r}|}$.

$\mathbf{A}_I$ has a gauge degree of freedom associated with reptations, but if we impose the additional constraint that $D_s \mathbf{x} = 0$, which is to say that the s component of the

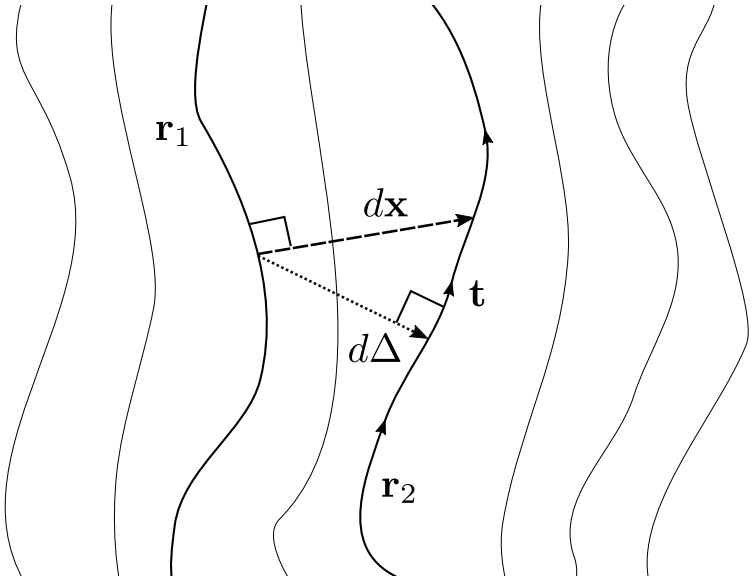

Figure 3.3: The covariant derivate $D_I\mathbf{r}$ has a natural geometric interpretation as the linearized distance of closest approach $d\mathbf{\Delta} = d\mathbf{x} - (\mathbf{t}\cdot d\mathbf{x})\mathbf{t}$ between two integral curves of the tangent field $\mathbf{t}$ separated by an infintessimal coordinate distance $d\mathbf{x}$ [1].

identity deformation vanishes [5], we have that

$$D_I\mathbf{r} = \partial_I\mathbf{r} - (\mathbf{t}\cdot\partial_I\mathbf{r})\mathbf{t}. \tag{3.6}$$

Notably, we can derive this covariant derivative from just the local geometry of our filament bundle, as the local *distance of closest approach* between nearby filaments, as shown in Fig. 3.3, where $d\mathbf{\Delta} = D_I\mathbf{r}dx^I$. This profound connection between the *local geometry* and continuous symmetries of fiber-elastic materials underlies much of the power of this description of their elastic behavior.

3.3.2 Elasticity of smectic stacks

We can implement a similar program for smectic liquid crystals by projecting onto the nematic director, $\mathbf{n}$, rather than the space perpendicular to it, to account for arbi-

[5]This is the equivalent of absorbing the s component of the target metric into the deformation gradient

trary material deformations within the smectic layers. For smectics, our symmetries are given by

$$\mathbf{r}(s, \mathbf{v}) \mapsto \mathbf{r}(s, \mathbf{v} + \mathbf{w}(s, \mathbf{v})), \tag{3.7}$$

and so our covariant derivative becomes

$$D_I \mathbf{r} = N_I \mathbf{n}, \tag{3.8}$$

where $N_I \equiv \mathbf{n} \cdot \partial_I \mathbf{r}$. So, the strain tensor for a smectic liquid crystal (with $\mathbf{r} = \mathbf{x} + \mathbf{u}$ becomes

$$\epsilon_{IJ} = [\mathbf{n} \cdot \partial_I (\mathbf{x} + \mathbf{u})][\mathbf{n} \cdot \partial_J (\mathbf{x} + \mathbf{u})] - g^{\text{tar}}_{IJ}, \tag{3.9}$$

where a Euclidean g^{tar}_{IJ} here is just $g^{\text{tar}}_{IJ} = (\mathbf{n} \cdot \partial_I \mathbf{x})(\mathbf{n} \cdot \partial_J \mathbf{x})$, the thing that's one along the director directions and zero everywhere else. So, we can work out the strain tensor in terms of the displacement field, and we find:

$$\epsilon_{IJ} = (\mathbf{n} \cdot \partial_I \mathbf{x})(\mathbf{n} \cdot \partial_J \mathbf{u}) + (\mathbf{n} \cdot \partial_I \mathbf{u})(\mathbf{n} \cdot \partial_J \mathbf{x}) + (\mathbf{n} \cdot \partial_I \mathbf{u})(\mathbf{n} \cdot \partial_J \mathbf{u}). \tag{3.10}$$

Taking the trace, and noting that $(\mathbf{n} \cdot \partial_I \mathbf{x})(\mathbf{n} \cdot \partial_I \mathbf{u}) = \mathbf{n} \cdot (\mathbf{n} \cdot \nabla)\mathbf{u}$, we find that

$$\epsilon^I_I = 2\mathbf{n} \cdot (\mathbf{n}^I \partial_I)\mathbf{u} + (\mathbf{n} \cdot \partial^I \mathbf{u})(\mathbf{n} \cdot \partial_I \mathbf{u}). \tag{3.11}$$

When $\mathbf{n} \approx \hat{z}$, we see that this reduces to

$$\text{tr}(\epsilon) = 2\partial_z u + (\nabla u)^2, \tag{3.12}$$

which is just twice the usual non-linear smectic strain contribution (up to a sign, which is just the difference between the Eulerian and Lagrangian forms) [116, 124]. Additionally, noting that (ϵ) as defined above is zero except on the 1×1 block along $\mathbf{N}$, we see that this is the only contribution we get to the strain energy (no other scalar invariants).

3.4 Geometry and elasticity for filament bundles

Now that we have a gauge covariant deformation gradient for filament bundles, we construct a rotationally invariant effective metric, $g^{\text{eff}}_{IJ} = D_I\mathbf{r} \cdot D_J\mathbf{r}$ and strain tensor,

$$\epsilon_{IJ} = D_I\mathbf{r} \cdot D_J\mathbf{r} - g^{\text{tar}}_{IJ}, \tag{3.13}$$

in the usual way [30, 31]. We can also write this in a form that will be a little more familiar, by breaking our deformation into an identity component $\mathbf{x}$ and a displacement field $\mathbf{u}$, so $\mathbf{r} = \mathbf{x}+\mathbf{u}$. Then, in euclidean space, and with a 2-dimensional euclidean target metric, we have that

$$\epsilon_{\alpha\beta} = \partial_\alpha u_\beta + \partial_\beta u_\alpha + \partial_\alpha\mathbf{u} \cdot \partial_\beta\mathbf{u} - (\mathbf{t} \cdot \partial_\alpha\mathbf{r})(\mathbf{t} \cdot \partial_\beta\mathbf{r}), \tag{3.14}$$

for $\alpha,\ \beta \in \{1, 2\}$, and with $\epsilon_{sI} = 0$ otherwise. If we restrict ourself to a plane perpendicular to $\mathbf{t}$ and drop higher-than-quadratic terms in $\mathbf{u}$, this reduces to the less non-linear, rotationally invariant description for filament assemblies, with again a sign difference due to the Lagrangian, rather than Eulerian form of the elasticity [42, 123],

$$U_{\alpha\beta} = \partial_\alpha u_\beta + \partial_\beta u_\alpha + \partial_\alpha\mathbf{u} \cdot \partial_\beta\mathbf{u} - \partial_s u_\alpha \partial_s u_\beta, \tag{3.15}$$

which has been used with great success to describe the elastic properties of equidistant filament configurations.

Since our covariant derivative, and thus our strain tensor, are all gauge invariant, as long as the elastic energy is a scalar in target space, this will be a gauge-invariant description of the elasticity of filamentous materials. In order to get a tractable model, we can make the usual assumptions that the strain tensor is relatively small, even

if the deformations of the material are large, we can write down a Hookean elastic energy, so that

$$E_{\text{strain}} = \tfrac{1}{2}\int dV S^{IJ}\epsilon_{IJ}, \tag{3.16}$$

where $S^{IJ} = \frac{\partial E}{\partial \epsilon_{IJ}} = C^{IJKL}\epsilon_{KL}$ is the nominal stress tensor, and C^{IJKL}, is a tensor of elastic constants which behaves in the usual way, and will in general depend on both the crystalline symmetries of the underlying columnar order and the target metric, g^{tar}_{IJ}.

3.5 Force balance for frustrated filaments

While there are other terms which are higher order in some microscopic lengthscale which are also gauge invariant (like the terms of the Frank-Oseen free energy), for simplicity and clarity, we first derive the Euler-Lagrange equations for just the strain elastic energy, and return to the bending Euler-Lagrange equations, which stabilize against arbitrary filament writhing, for a later subsection. Taking as our variational principle that, in the absence of body forces (we can always add them back in later),

$$\delta E = \int dV S^{IJ}\delta\epsilon_{IJ} = 0. \tag{3.17}$$

What remains then is to work out $\delta\epsilon_{IJ}$, and apply the divergence theorem to derive the conditions of force balance. First, recall that $\epsilon_{IJ} = D_I\mathbf{r}\cdot D_J\mathbf{r} - g^{tar}_{IJ}$. Then, taking $\delta\epsilon_{IJ}$, and defining $\delta\mathbf{r}$ as the variation of our deformation, we find:

$$\delta\epsilon_{IJ} = 2D_J\mathbf{r}\big[\partial_I\delta\mathbf{r} - \mathbf{t}\cdot\partial_I\mathbf{r}\frac{\partial_s\delta\mathbf{r}}{\|\partial_s\mathbf{r}\|}\big], \tag{3.18}$$

where in all the above we have used that $D_J\mathbf{r}\cdot\mathbf{t} = 0$. Plugging this back into our integral, we find:

$$\delta E = 2\int dV S^{IJ}D_J\mathbf{r}\cdot\big[\partial_I\delta\mathbf{r} - \mathbf{t}\cdot\partial_I\mathbf{r}\frac{\partial_{\mathbf{s}}\delta\mathbf{r}}{|\partial_{\mathbf{s}}\mathbf{r}|}\big]. \tag{3.19}$$

Now we just apply the divergence theorem, finding that:

$$\begin{aligned} 0 &= -2\int \partial_I\big[dVS^{IJ}D_J\mathbf{r}\big]\cdot\delta\mathbf{r} \\ &\quad + 2\int \partial_{\mathbf{s}}\big[dVS^{IJ}D_J\mathbf{r}\frac{\mathbf{t}\cdot\partial_I\mathbf{r}}{\|\partial_s\mathbf{r}\|}\big]\cdot\delta\mathbf{r} = 0 \qquad (3.20) \\ 0 &= 2\int dA\hat{N}_I\big[dVS^{IJ}D_J\mathbf{r}\big]\cdot\delta\mathbf{r} \\ &\quad - 2\int dA\hat{N}_K\hat{T}^K\big[dVS^{IJ}D_J\mathbf{r}\frac{\mathbf{t}\cdot\partial_I\mathbf{r}}{\|\partial_s\mathbf{r}\|}\big]\cdot\delta\mathbf{r}, \qquad (3.21) \end{aligned}$$

where $\hat{N}$ here is the vector normal to the boundary ∂V of the material and $\hat{T}$ is the tangent field in the material frame.

Projecting out and onto $\mathbf{t}$, and noting that $\mathbf{t}\cdot\partial_I D_J\mathbf{r} = -\partial_I\mathbf{t}\cdot D_J\mathbf{r}$ and $\mathbf{t}\cdot\partial_s D_J\mathbf{r} = -\partial_s\mathbf{t}\cdot D_J\mathbf{r}$, we recognize that the parallel component of bulk force balance can be written in terms of the *convective flow tensor* of the bundle,

$$\begin{aligned} h_{IJ} &= \partial_I\mathbf{t}\cdot\partial_J\mathbf{r} + \partial_J\mathbf{t}\cdot\partial_I\mathbf{r} \\ &\quad - \frac{\mathbf{t}\cdot\partial_I\mathbf{r}}{|\partial_s\mathbf{r}|}\partial_s\mathbf{t}\cdot\partial_J\mathbf{r} - \frac{\mathbf{t}\cdot\partial_J\mathbf{r}}{|\partial_s\mathbf{r}|}\partial_s\mathbf{t}\cdot\partial_I\mathbf{r}, \qquad (3.22) \end{aligned}$$

which measures the local deviations from equidistance of a deformation [1], as

$$S^{IJ}h_{IJ} = 0 \qquad (3.23)$$

The convective flow tensor measures the symmetric changes in the tangent vector as you move orthogonal (as shown in Fig. 3.4), similar to how the second fundamental form for a surface measures the local change in the normal vector.

The remaining bulk components of the Euler-Lagrange equations can then be formulated as

$$0 = D_I\big[S^{IJ}D_J\mathbf{r}\big] - D_s\big[S^{IJ}\frac{\mathbf{t}\cdot\partial_I\mathbf{r}}{\|\partial_s\mathbf{r}\|}D_J\mathbf{r}\big], \qquad (3.24)$$

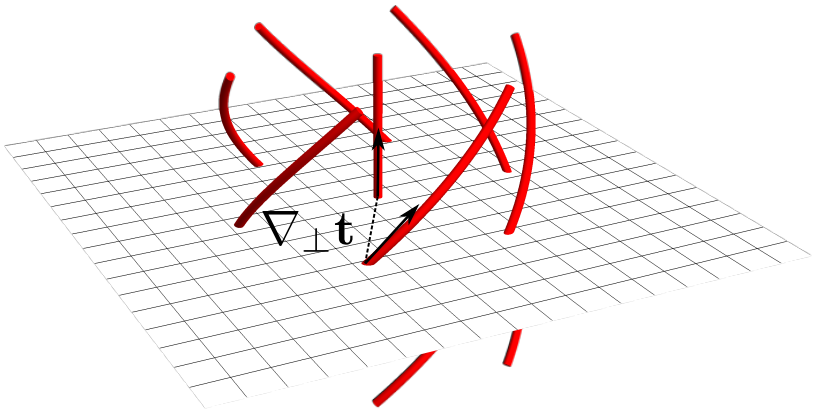

Figure 3.4: The convective flow tensor, h_{IJ}, which governs tangent force balance in filament bundles, is a symmetric combination of perpendicular gradients of $\mathbf{t}$, as shown above [1]. The related second fundamental form for a surface in E^3 measures the tilt of the normal vector to the surface, $\hat{n}$, as you move tangent to the surface.

where D_I is again the gauge-covariant derivative on vectors in the target space, modified so that it acts covariantly on tensors in the material space.

The physical meaning of the Euler-Lagrange equations for filament bundles is now more straightforward: tangent force balance couples *non-equidistance*, as measured by the convective flow tensor, to the stress tensor in a way reminiscent of the Young-Laplace law [125]. It's also useful, for interpreting the force balance equations perpendicular to $\mathbf{t}$, to note that these reduce to the usual force-balance equations for thin sheets in the absence of inter-filament twist. To see why, remember that $\mathbf{t} \cdot (\nabla \times \mathbf{t}) = 0$ is the necessary condition for a family of surfaces to be orthogonal to $\mathbf{t}$. Put another way, this means that, for zero twist, there are coordinates x_i such that $\partial_s \mathbf{r} \cdot \partial_{x_i} \mathbf{r} = 0$. Choosing these, we see that

$$S^{IJ} \frac{\mathbf{t} \cdot \partial_I \mathbf{r}}{|\partial_s \mathbf{r}|} = 0, \tag{3.25}$$

and so the force balance equations perpendicular to $\mathbf{t}$ reduce to those for thin sheets. Similarly, when the twist is zero, the convective flow tensor reduces to the second fundamental form on the surface normal to $\mathbf{t}$, and so the force balance conditions

are exactly those for these orthogonal surfaces. These observations help clarify the meaning of this $\frac{\mathbf{t}\cdot\partial_I\mathbf{r}}{\|\partial_s\mathbf{r}\|}$ contribution in the force balance equations, which also arises in the Selinger-Bruinsma model [46]. We can now see that this term corrects for the global *non-integrability* of twisted filament bundles, and serves to cancel out the components of $\partial_I\mathbf{r}$ which lie along the filament tangent.

3.5.1 Bending contributions to force balance

While splay, twist, and biaxial splay of filaments are penalized by their cross-sectional elasticity, the bending contributions which are important to the phenomenology of columnar liquid crystals, are not. Energetic contributions from Bending elasticity which penalize, for example, the writhing of developable domains, must then be included explicitly. The bending energy of a liquid crystal mesophase is:

$$\tfrac{1}{2}K_{33}\big[(\mathbf{n}\cdot\nabla)\mathbf{n}\big]^2 \tag{3.26}$$

In Lagrangian coordinates, we can rewrite the bend vector, $\mathbf{b}$:

$$\mathbf{b} = -\frac{\partial_s\mathbf{t}}{|\partial_s\mathbf{r}|}. \tag{3.27}$$

So we can make the bending term in the Frank free energy as:

$$f_{\text{bend}} = \tfrac{1}{2}K_{33}\frac{\partial_s\mathbf{t}\cdot\partial_s\mathbf{t}}{|\partial_s\mathbf{r}|^2}. \tag{3.28}$$

So the bending contributions to the Euler-Lagrange equations are:

$$\delta f_{\text{bend}} = K_{33}\frac{\partial_s\mathbf{t}}{|\partial_s\mathbf{r}|}\cdot\big[\frac{1}{|\partial_s\mathbf{r}|}\partial_s(\frac{\partial_s\delta\mathbf{r}-\mathbf{t}\cdot\partial_s\delta\mathbf{r}\mathbf{t}}{|\partial_s\mathbf{r}|}) - \frac{\partial_s\mathbf{t}}{|\partial_s\mathbf{r}|^2}\mathbf{t}\cdot\partial_s\delta\mathbf{r}\big]. \tag{3.29}$$

Simplifying and distributing the derivative, we have:

$$\delta f_{\text{bend}} = K_{33}\frac{\partial_s\mathbf{t}}{|\partial_s\mathbf{r}|}\cdot\big[\frac{\partial_s^2\delta\mathbf{r}}{|\partial_s\mathbf{r}|^2} - \frac{\partial_s\delta\mathbf{r}}{|\partial_s\mathbf{r}|^3}\partial_s^2\mathbf{r}\cdot\mathbf{t} - 2\frac{\partial_s\mathbf{t}}{|\partial_s\mathbf{r}|^2}\mathbf{t}\cdot\partial_s\delta\mathbf{r}\big] \tag{3.30}$$

Integrating by parts, we find that

$$EL_{\text{bend}} = K_{33}\big[\partial_s^2 \frac{\partial_s \mathbf{t}}{|\partial_s \mathbf{r}|^3} + \partial_s \frac{\partial_s \mathbf{t} \partial_s^2 \mathbf{r} \cdot \mathbf{t}}{|\partial_s \mathbf{r}|^4} + 2\partial_s \frac{\partial_s \mathbf{t} \cdot \partial_s \mathbf{t}}{|\partial_s \mathbf{r}|^3} \mathbf{t}), \tag{3.31}$$

with appropriate boundary contributions. Breaking this up into components along and perpendicular to $\mathbf{t}$, we have,

$$EL_{\text{bend}}^{\parallel} = K_{33}\big[\frac{\partial_s^2 \mathbf{t} \cdot \mathbf{t}(\partial_s^2 \mathbf{r} \cdot \mathbf{t})}{|\partial_s \mathbf{r}|^4} - \frac{\partial_s^2 \mathbf{t} \cdot \partial_s \mathbf{t}}{|\partial_s \mathbf{r}|^3}\big] \tag{3.32}$$

$$= -K_{33} \frac{1}{2|\partial_s \mathbf{r}|} \partial_s \frac{\partial_s \mathbf{t} \cdot \partial_s \mathbf{t}}{|\partial_s \mathbf{r}|^2}. \tag{3.33}$$

This is pretty straightforward, and is just the derivative of the squared curvature, and so tells us that there are forces along the tangent direction whenever the curvature is both varying and nonzero. Then, the perpendicular components are:

$$EL_{I\text{bend}}^{\perp} = K_{33}\big[\partial_s \mathbf{t} \cdot D_I \mathbf{r}(2\frac{\partial_s \mathbf{t} \cdot \partial_s \mathbf{t}}{|\partial_s \mathbf{r}|^3} - 2\partial_s \frac{\partial_s^2 \mathbf{r} \cdot \mathbf{t}}{|\partial_s \mathbf{r}|^4}) - 5\partial_s^2 \mathbf{t} \cdot D_I \mathbf{r} \frac{\partial_s^2 \mathbf{r} \cdot \mathbf{t}}{|\partial_s \mathbf{r}|^4} + \frac{\partial_s^3 \mathbf{t} \cdot D_I \mathbf{r}}{|\partial_s \mathbf{r}|^3}\big]. \tag{3.34}$$

3.6 To finite twist... and beyond! the Föppl-von Kármán limit for helical filament bundles

While helical bundles have been examined in depth in the limit of small twist, our new geometrically non-linear elastic energy provides us with the opportunity to both validate calculations done in the Föppl-von Kármán (FvK) limit, and investigate behavior at large twists, and incorporating elastic costs for filament bending and stretching. To start, recall that all together, the force balance equations for filament bundles are given by:

$$0 = S^{IJ}h_{IJ} - K_{33}\frac{1}{2|\partial_s \mathbf{r}|}\partial_s \frac{\partial_s \mathbf{t}\cdot\partial_s \mathbf{t}}{|\partial_s \mathbf{r}|^2} \tag{3.35}$$

$$\begin{aligned} 0 = {} & D_I\big[S^{IJ}D_J\mathbf{r}\big] - D_s\big[S^{IJ}\frac{\mathbf{t}\cdot\partial_I\mathbf{r}}{|\partial_s\mathbf{r}|}D_J\mathbf{r}\big] \\ & - K_{33}\big[\partial_s\mathbf{t}\cdot D_I\mathbf{r}(2\frac{\partial_s\mathbf{t}\cdot\partial_s\mathbf{t}}{|\partial_s\mathbf{r}|^3} - 2\partial_s\frac{\partial_s^2\mathbf{r}\cdot\mathbf{t}}{|\partial_s\mathbf{r}|^4}) - 5\partial_s^2\mathbf{t}\cdot D_I\mathbf{r}\frac{\partial_s^2\mathbf{r}\cdot\mathbf{t}}{|\partial_s\mathbf{r}|^4} + \frac{\partial_s^3\mathbf{t}\cdot D_I\mathbf{r}}{|\partial_s\mathbf{r}|^3}\big]. \end{aligned} \tag{3.36}$$

Stable configurations of helical bundles with constant pitch, $\frac{2\pi}{\Omega}$, can be described by the deformation

$$\mathbf{r}(s,\rho,\phi) = s\hat{z} + f(\rho)\hat{\rho}(\phi+\Omega s), \tag{3.37}$$

where s is the arclength along the central straight curve, $\hat{\rho}$ the typical radial unit vector in cylindrical coordinates, and the radial deformation field $f(\rho)$ is determined by the boundary value problem above. If we assume that our helical bundles are isotropic or hexagonal in the cross-section, then the linear relationship between the stress and strain tensor is given by:

$$S^{IJ} = \lambda g^{IJ\mathrm{tar}}\mathrm{tr}(\epsilon) + 2\mu\epsilon^{IJ}, \tag{3.38}$$

where $g^{IJ\mathrm{tar}}$ is the inverse target metric (which we have also used in taking the trace and raising the indices of the strain tensor), and λ and μ are the Lamé parameters [2], which can be written in terms of the Young's modulus, E, and the 2d Poisson ratio ν as:

$$\begin{aligned} \lambda &= \frac{E}{2(1+\nu)} \\ \mu &= \frac{\nu E}{(1+\nu)(1-2\nu)}. \end{aligned} \tag{3.39}$$

If we put all of this together with force-free boundary conditions on the sides, we find that $f(\rho)$ must satisfy

$$
\begin{aligned}
0 &= -\partial_\rho\big[\rho f'(\rho)\{\frac{(\lambda+2\mu)}{2}(f'(\rho)^2-1)+\tfrac{\lambda}{2}(\frac{f(\rho)^2}{\rho^2(1+\Omega^2 f(\rho)^2)}-1)\}\big] \\
&\quad -\frac{\rho f(\rho)}{\rho^2(1+\Omega^2 f(\rho)^2)^2}\big[\tfrac{\lambda}{2}(f'(\rho)^2-1)+\frac{(\lambda+2\mu)}{2}(\frac{f(\rho)^2}{\rho^2(1+\Omega^2 f(\rho)^2)}-1)\big] \\
&\quad + K_{33}\rho\Omega^4 f(\rho)\frac{1-\Omega^2 f(\rho)^2}{f'(\rho)(1+\Omega^2 f(\rho)^2)^3} \qquad (3.40)\\
0 &= f(0) \qquad (3.41)\\
0 &= \frac{(\lambda+2\mu)}{2}(f'(R)^2-1)+\tfrac{\lambda}{2}(\frac{f(R)^2}{R^2(1+\Omega^2 f(R)^2)}-1),
\end{aligned}
$$

where R is the bundle radius. Generically, our solutions to these are just going to be numerical, but we can find series solutions for the first several terms. Because the cylindrical symmetry of the problem, even terms in the power series expansion for $f(\rho)$ vanish, so, taking

$$
f(\rho) = a_1\rho + a_3\Omega^2\rho^3 + a_5\Omega^4\rho^5 + \cdots , \qquad (3.42)
$$

we find (with a_1 the slope at $\rho = 0$, which is fixed by the outer boundary condition), that

$$
\begin{aligned}
a_3 &= \frac{2a_1K_{33}\Omega^2 + 2a_1^3\lambda - a_1^5\lambda + 2a_1^3\mu - 3a_1^5\mu}{8(-\lambda+2a_1^2\lambda-\mu+3a_1^2\mu)} \qquad (3.43)\\
a_5 &= \frac{a_1}{384(-\lambda+2a_1^2\lambda-\mu+3a_1^2\mu)^3}\Big\{K_{33}^2\big[-8\Omega^4\lambda-60a_1^2\Omega^4\lambda-8\Omega^4\mu-108a_1^2\Omega^4\mu\big] \\
&\quad + K_{33}\big[-160a_1^2\Omega^2\lambda^2-160a_1^2\Omega^2\mu^2+424a_1^2\Omega^2\lambda^2+672a_1^4\Omega^2\mu^2 \qquad (3.44)\\
&\quad -436a_1^6\Omega^2\lambda^2-972a_1^6\Omega^2\mu^2-320a_1^2\Omega^2\lambda\mu+1096a_1^4\Omega^2\lambda\mu-1320a_1^6\Omega^2\lambda\mu\big] \\
&\quad + \big[-72a_1^4\lambda^3-72a_1^4\mu^3+204a_1^6\lambda^3+420a_1^6\mu^3-258a_1^8\lambda^3-990a_1^8\mu^3+105a_1^{10}\lambda^3+837a_1^{10}\mu^3 \\
&\quad -216a_1^4\lambda^2\mu^2-216a_1^4\lambda\mu^2+828a_1^6\lambda^2\mu+1044a_1^6\lambda\mu^2-129-a_1^8\lambda^2\mu-2022a_1^8\lambda\mu^2 \\
&\quad +663a_1^{10}\lambda^2\mu+1323a_1^{10}\lambda\mu^2\big]\Big\}.
\end{aligned}
$$

While most of the results we present in this chapter will rely instead on on numerical solutions to the BVP in Eq. (3.40) and (3.41), series analysis of force-balance

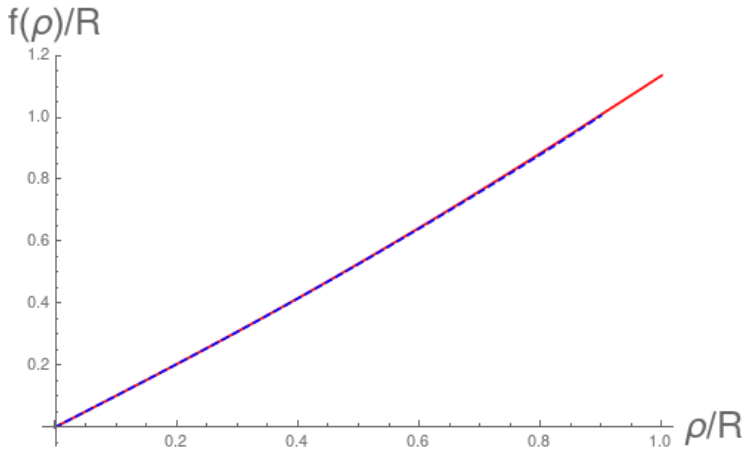

Figure 3.5: The power series solution (dashed blue) to $f(\rho)$ to $\mathcal{O}(\rho^7)$ plotted against the numerical solution (solid red) to Eq. (3.40) for $\Omega R = 1.45$, $\nu = .49$, and $K_{33} = 0$, demonstrating excellent agreement. Even at higher ΩR, this stays in qualitative agreement for small ρ (less than $\approx .5R$) until about $\Omega R = 4$.

equations for twisted-toroidal filament bundles in Ch. 4 will rely in part on the series solutions in Eq. (3.44). We can also solve the BVP numerically by shooting from $\rho = 0$, and compare to the series solution, as in Fig. 3.5. When using the series solution to evaluate filament behavior, we'll calculate a_1 [6] from the slope of numerical value of $f'(\rho)$ at $\rho/R = 10(-6)$.

Numerical evaluation of the deformation field for helical bundles allows us to examine their behavior beyond the small twist limit, including evaluating contributions from filament bending and stretching elasticity. Figures 3.6a and 3.6b shows cross-sectional pressure, $P = -\mathrm{tr}(S)$ in a helical bundle with $\Omega R = 1.45$. A convenient measure for the difference in the non-linear behavior from the low twist behavior is the dimensionless critical radius, r_c/R, at which the pressure inside the bundle vanishes, so that $P|_{r_c} = 0$. In the low twist limit and in the absence of longitudinal elasticity, this critical radius is constant, at $r_c = \frac{R}{\sqrt{2}}$ [46]. In comparison, we can

[6] generically, a function of ΩR due to contributions from the outer boundary conditions

see in Fig 3.6c, that for larger twists, the critical radius decreases, concentrating the compressive regime at the center of the bundle.

Similarly, by incorporating a non-zero modulus for filament bending, K_{33}, as in Fig. 3.7, we can push bundles away from the small twist behavior. Nonlinearities in the force-balance equations produce qualitatively different responses to varying bending moduli at low (Fig. 3.7a) and high (Fig. 3.7b) twist. And, while the deeper understanding of this behavior necessary for comparison with relevant experimental systems (such as [52, 53]), this once again serves to emphasize the importance of geometric non-linearities in the phenomenology of even equidistant filament packings.

3.7 Discussion

In this chapter, we have introduced at general procedure for deriving geometrically nonlinear strain tensors for soft-elastic liquid crystals, drawing on their geometric structure as fiber bundles embedded in Euclidean space. In columnar liquid crystals and filament bundles, the geometric nonlinearities introduced by this gauge theoretic description are of fundamental importance, because two-dimensional models fail to capture the longitudinal variations in length characteristic of non-equidistant geometries.

The force balance equations for filament bundles derived from this geometrically non-linear theory reinforce the conceptual importance of constant spacing for understanding the behavior of soft-elastic liquid crystals [1]. For filament bundles, while the conditions for equilibrium are qualitatively similar to those for thin sheets, normal force balance couples transverse strains to the longitudinal fluctuations in spacing described by the convective flow tensor, while in-plane force balance incorporates corrections for the tortured coordinates of twisted configurations. In a sense, the force balance equations derived above are the natural generalization of the classical Euler-Lagrange equations for thin sheets to the more general setting of filament

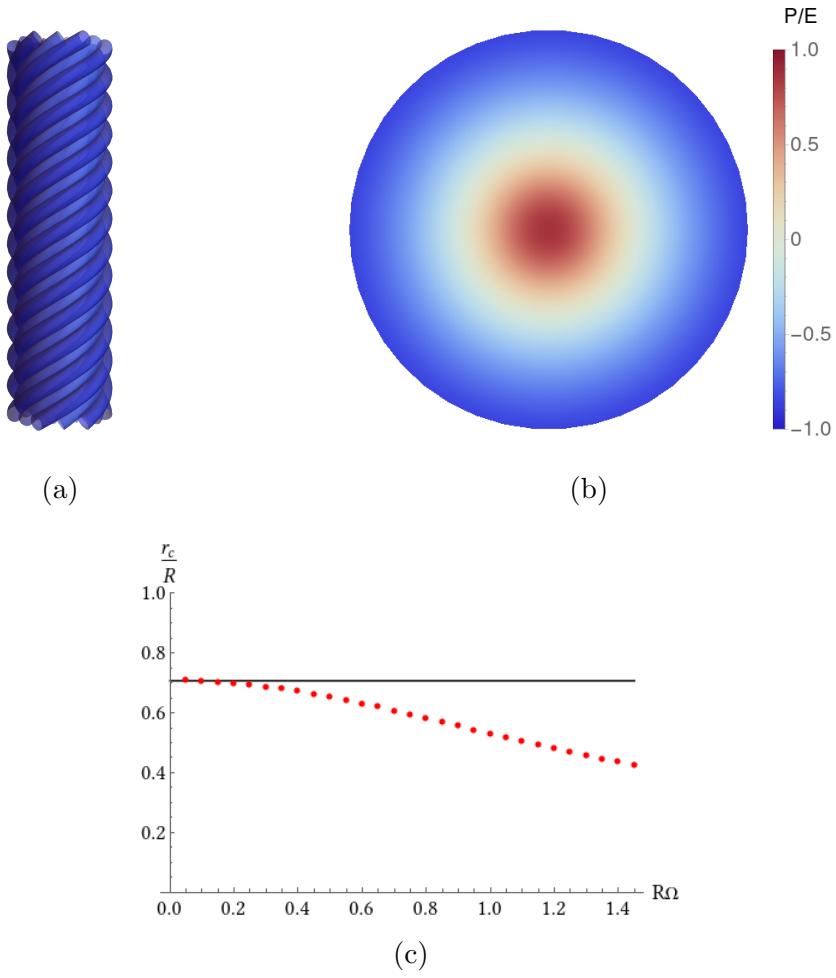

Figure 3.6: By solving for the radial deformation field, $f(\rho)$, for the fully non-linear force balance equations for helical filament bundles, we can extract information like the position of filaments at varying radii, as in 3.6a, and the pressure distribution in the cross-section, as in 3.6b with $\Omega R > 1$ (shown here with $\nu = .49$, $\Omega R = 1.45$, and $K_{33} = 0$.) The ability to move to large ΩR allows us to examine deviations from behavior in the Föppl-von Kármán (FvK) limit, as in 3.6c, which shows the critical radius, at which $\mathrm{tr}(S) = 0$, plotted against ΩR for the non-linear force-balance equations (red dots), compared to the constant value in the FvK, $r_c/R = \frac{1}{\sqrt{2}}$ (black line) [46].

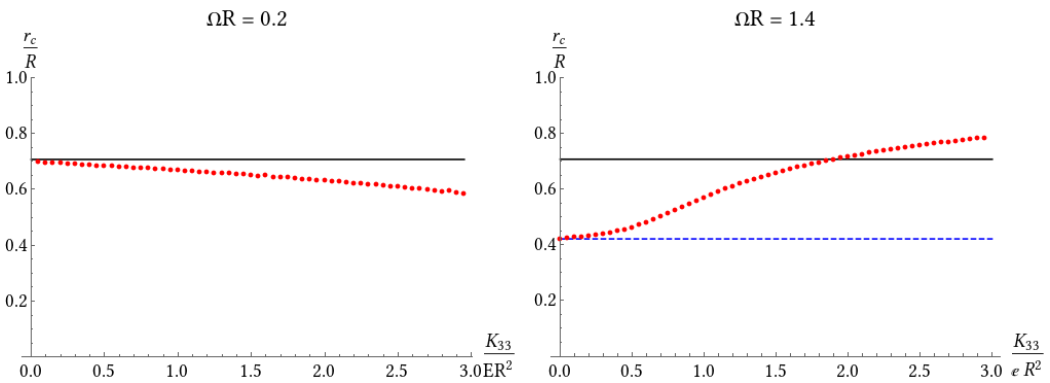

(a) (b)

Figure 3.7: The introduction of filament bending to the columnar elasticity of helical bundles qualitatively changes their behavior for large twists. For low twists, as in 3.7a, with $\Omega R = .2$, an increase in the bend elastic modulus, K_{33}, leads to a gradual decrease in the critical radius (red dots) from that of the FvK limit (black line). At large twists, however, as in 3.7b, with $\Omega R = 1.4$, the introduction of bending leads to qualitatively different behavior, driven by the elastic non-linearities. Here r_c/R increases from the $K_{33} = 0$ value (dashed blue line) to higher than the FvK value (black line). In all of the above, $\nu = .49$.

elasticity, where we are asked to measure changes in lengths of vectors in the plane perpendicular to *any* unit vector field, as opposed to one normal to a surface.

In Ch. 1, we briefly introduced the concept of *transverse frustration* in twisted filament bundles, where twist and splay in the field of local tangent vectors to the filaments in a bundle couple to strains in the bundle cross section. Our geometrically non-linear strain tensor allows us to further explore *longitudinal frustration*, where filaments are forced, either by boundary conditions or topological constraints, into necessarily non-equidistant configurations, as described in Ch. 2 [1]. As shown in Eq. 3.23, these longitudinal variations in lengths couple to stresses orthogonal to the filament tangents, much as curvatures in thin sheets must be met by in plane forces. It is worth noting that, in contrast to the surfaces, filament bundles can develop *metric curvature* in the cross-section without concomitant non-zero terms in the convective flow tensor, by twisting without splay or biaxial splay [1].

Because this geometric approach to the elasticity of soft-elastic liquid crystals is both incredibly general and nearly algorithmic, we speculate that it may have applications beyond liquid-crystalline systems. The general mathematical principles are the same for all soft-elastic materials: by considering the metric inherited from the embedding space (E^3 for us) by the space orthogonal to the continuous zero modes, we can "project out" the zero energy deformations of the material, leaving us with a strain that cares only about the "shortest distance" to the nearest zero-energy state. And while the applications of these techniques to, for example, conformal metamaterials [107], are for now put off for another day, we anticipate that the powerful theoretical framework developed in this chapter for the study of columnar liquid crystals will have broad applications across soft matter physics and materials science.

CHAPTER 4

GET IT TWISTED: THE LINEAR STABILITY OF TWISTED TOROIDAL FILAMENT BUNDLES

People—well, men, really—talk about art and science as though they are so noble. And they are! They're important and worthy and vital to the process of mankind! But... aside from all the talk, they look like quite a lot of work. Tedious, never-ending, unforgiving, excruciatingly demanding work.

The Lady's Guide to Celestial Mechanics
Olivia Waite

4.1 Introduction

Many mechanical [25, 126] and biological [67, 68, 110, 111, 127] filaments include stable twisted and bent configurations. Whether because of confinement, linking between neighboring filaments, mechanical loading, or entropic effects, buckling in chiral filament bundles is so ubiquitous as to be universal. Soft matter physicists, applied mathematicians, and materials scientists of all stripes have generally considered this inconvenient, at best, because of the difficulties presented by longitudinally varying geometries. When the number of strands is small, as for some varieties of wire rope, plies, tangled telephone cables, and supercoiled DNA, progress has been made by considering the interactions and elasticity of each strand [25, 59, 126, 128, 129]. As the number of filaments grows, however, and approaches a bulk, continuum columnar liquid crystalline state, frustration arising from geometric constraints on constant spacing muddles the matter. Past work on the continuum elastic response of filament

assemblies has considered the elastic response of twisted helical bundles [46, 47], this has, with the exception of our work in Ch. 3, been done in a less non-linear, Föppl-von Kármán (FvK) limit, and does not account for the longitudinal frustration which is characteristic of non-helical twisted filament bundles. Even working beyond the FvK limit, the geometrical nonlinearities associated with longitudinal variations in inter-filament spacing become important, as a consequence of the mutual incompatibility of twist, central filament curvature, and equidistance we explored in Ch. 2, and so prior treatments, which have depended on two-dimensional, minimally rotationally invariant models of columnar liquid crystals [42], are not up to the task.

While previous work has attempted to capture the consequences of frustration in these models with either geometric templates, based on fibrations of S^3 [9, 94, 95] or liquid crystalline models [76, 93] which look for zero splay solutions by enforcing the dual constraints of volume filling and no filament ends [96], there has as of yet been no succesful description of the elastic equilibria for continuum twisted-toroidal filament bundles.

Fortunately, we have just now developed a general method of accounting for the geometric non-linearities inherent in longitudinally frustrated filament bundles. Starting from the force-balance equations presented in Ch. 3, we can find the conditions for stability of twisted-tori by treating both the curvature of the center-line, κ_0, and the corrections to the deformation of the helical conformation as perturbations to the curvature-free solution, proportional to a formal parameter, ε in which we will expand. Starting with our numerical and power series solutions to the helical bundle solutions from Ch. 3, in Section 4.2 we then find the $\mathcal{O}(\varepsilon)$ correction to the force-balance equation, giving us the linear response of a stable bundle of constant pitch helices to a small curvature. By Fouriér transforming in polar and arclength coordinates, ϕ and s, in Section 4.3, the resulting linear partial differential equations can be reduced to three coupled, linear ordinary differential equations, which on a good

(a)

(b)

Figure 4.1: A schematic (4.1a) and common household example (4.1b) of twisted toroidal filament bundles, a common geometric motif. Twisted toroidal textures are easy to create with common household materials, occur naturally in viral capsids' confined coils of nucleic acids, and are a simple test case for the more general class of non-equidistant filament bundles, which have important applications in mechanical systems like cables, ropes, and yarns.

day, could be integrated numerically and analyzed with power series techniques to find solutions to the boundary value problem (BVP). In the process of deriving the force balance equations for twisted tori, we also delve a little deeper into the underlying geometry of these filament assemblies, as introduced in Ch. 3, and speculate about the nature of life and parallel transport on a nowhere integrable distribution of 2-planes equipped with a metric.

Unfortunately, as we will show in Section 4.4, force-free boundary conditions combine with the soft modes associated with reptations of the helical state and the coupling of non-equidistance to in-plane strains to render this BVP singular at both boundaries. For $\Omega\rho$ small, we can find a series expansion at the inner boundary, giving us intuition for the way that curvature couples to the resulting deformations. However, while the $\rho = 0$ solution can be well analyzed by a generalized, matrix Frobenius method [130], and thus made amenable to series and numerical solutions, the boundary at $\rho = R$ proves much more troublesome. Because, with force free

boundary conditions to the zero curvature case, the radial components of the stress tensor vanish at $\mathcal{O}(\varepsilon^0)$, if any of the terms they multiply at $\mathcal{O}(\varepsilon)$ (like the convective flow tensor in Eq. (3.23)) contain the highest order derivative in the perturbative functionals, the resulting BVP will be singular. In fact our lot is much worse than this, and we conclude Section 4.4 by showing that, in contrast to the inner boundary, there are no regular series solutions around $\rho = R$.

The great difficulty posed by the singularities in these differential equations leaves us in need of a slight change in course. We first briefly discuss possible palliatives, including including surface stresses [131] at $\mathcal{O}(\varepsilon^0)$, which would appropriately modify the singular behavior at the outer boundary. Since solutions to even this modified problem are fairly difficult to obtain, however, and because we do not yet understand the cause of the singular behavior discussed above, we turn instead to a problem mentioned several times previously in the dissertation.

While we may not yet be able to solve generically for stable states of toroidal bundles, we can still answer some questions. The technology developed in the vain pursuit of a general solution, for example, allows us to shed some light on the questions raised in Ch. 2, about whether the splay-free or determinant-free textures are energetically favorable [1]. By substituing into the force balance equations, we can show that neither are in elastic equilibrium in the bulk, but that the boundary tends towards a splay-free solution as the bending modulus goes to zero.

4.2 Linearized Euler-Lagrange equations for twisted toroidal filament bundles

The force balance equations for filament bundles are given by:

$$0 = S^{IJ}h_{IJ} - K_{33}\frac{1}{2|\partial_s \mathbf{r}|}\partial_s \frac{\partial_s \mathbf{t}\cdot\partial_s \mathbf{t}}{|\partial_s \mathbf{r}|^2} \tag{4.1}$$

$$\begin{aligned} 0 = {} & D_I\big[S^{IJ}D_J\mathbf{r}\big] - D_s\big[S^{IJ}\frac{\mathbf{t}\cdot\partial_I\mathbf{r}}{|\partial_s\mathbf{r}|}D_J\mathbf{r}\big] \\ & - K_{33}\big[\partial_s\mathbf{t}\cdot D_I\mathbf{r}(2\frac{\partial_s\mathbf{t}\cdot\partial_s\mathbf{t}}{|\partial_s\mathbf{r}|^3} - 2\partial_s\frac{\partial_s^2\mathbf{r}\cdot\mathbf{t}}{|\partial_s\mathbf{r}|^4}) - 5\partial_s^2\mathbf{t}\cdot D_I\mathbf{r}\frac{\partial_s^2\mathbf{r}\cdot\mathbf{t}}{|\partial_s\mathbf{r}|^4} + \frac{\partial_s^3\mathbf{t}\cdot D_I\mathbf{r}}{|\partial_s\mathbf{r}|^3}\big], \end{aligned} \tag{4.2}$$

In Ch. 3 we showed that a bundle of helices with constant pitch, $\frac{2\pi}{\Omega}$, can be described by the deformation

$$\mathbf{r}(s,\rho,\phi) = s\hat{z} + f(\rho)\hat{\rho}(\phi+\Omega s), \tag{4.3}$$

where s is the arclength along the central straight curve, $\hat{\rho}$ the typical radial unit vector in cylindrical coordinates, and the radial deformation field $f(\rho)$ satisfies the boundary value problem

$$\begin{aligned} 0 = {} & -\partial_\rho\big[\rho f'(\rho)\{\frac{(\lambda+2\mu)}{2}(f'(\rho)^2-1) + \tfrac{\lambda}{2}(\frac{f(\rho)^2}{\rho^2(1+\Omega^2 f(\rho)^2)} - 1)\}\big] \\ & - \frac{\rho f(\rho)}{\rho^2(1+\Omega^2 f(\rho)^2)^2}\big[\tfrac{\lambda}{2}(f'(\rho)^2-1) + \frac{(\lambda+2\mu)}{2}(\frac{f(\rho)^2}{\rho^2(1+\Omega^2 f(\rho)^2)} - 1)\big] \\ & + K_{33}\rho\Omega^4 f(\rho)\frac{1-\Omega^2 f(\rho)^2}{f'(\rho)(1+\Omega^2 f(\rho)^2)^3} \end{aligned} \tag{4.4}$$

$$0 = f(0) \tag{4.5}$$

$$0 = \frac{(\lambda+2\mu)}{2}(f'(R)^2-1) + \frac{\lambda}{2}(\frac{f(R)^2}{R^2(1+\Omega^2 f(R)^2)} - 1),$$

where R is the bundle radius. To describe twisted toroidal bundles, we instead take as the deformation field:

$$\mathbf{r}(s,\rho,\phi) = \mathbf{r}_0(s+\varepsilon\delta\tilde{s}) + (f(\rho)+\varepsilon\delta\tilde{\rho})\hat{\rho}(\phi+\varepsilon\delta\tilde{\phi}+\Omega s+\varepsilon\Omega\delta\tilde{s}), \tag{4.6}$$

where $\delta\tilde{s}$, $\delta\tilde{\rho}$, and $\delta\tilde{\phi}$ are generically independent functions of the coordinates s, ρ, and ϕ, and the central curve [1, 78–80] $\mathbf{r}_0$ is a circle with arclength parameter s, so

that $\partial_s^2 \mathbf{r}_0(s) = \varepsilon\kappa_0 \cos\tilde{\phi}\hat{\rho} - \varepsilon\kappa_0 \sin\tilde{\phi}\hat{\phi}$, where $\tilde{\phi} = \phi + \Omega s$. So, if we break up the deformation by orders, we have

$$\mathbf{r} = \mathbf{r}^{(0)} + \varepsilon\big[\delta\tilde{s}(\hat{t}_0 + \Omega f(\rho)\hat{\phi}) + \delta\tilde{\rho}\hat{\rho} + f(\rho)\delta\tilde{\phi}\hat{\phi}\big], \tag{4.7}$$

with additional contributions of $\mathcal{O}(\varepsilon)$ to the deformation gradient (and thus the force balance equations) arising from derivatives of the frame vectors: $\hat{t}_0$, $\hat{\rho}$, and $\hat{\phi}$, with

$$\partial_s \hat{t}_0 = \varepsilon\kappa_0 \cos(\tilde{\phi})\hat{\rho} - \varepsilon\kappa_0 \sin(\tilde{\phi})\hat{\phi}. \tag{4.8}$$

Considering contributions from both columnar elasticity and filament bending, our task is then to calculate the stress tensor, convective flow tensor, covariant derivative, and bending forces to linear order in ε.

4.2.1 Index form of the Euler-Lagrange equations

We begin by rearranging the Euler-Lagrange equations into a form slightly more convenient for calculation than was presented in Ch. 3. To avoid the proliferation of spaces that can result from dangling $D_I\mathbf{r}$s, we'll instead introduce a more intrinsic description, which will naturally result in Christoffel symbols modified to fit our 2-planes in E^3 context.

Recall that the orthogonal to $\mathbf{t}$ components of the elastic contributions to the Euler-Lagrange equations are given by:

$$0 = D_I\big[S^{IJ} D_J\mathbf{r}\big] - D_s\big[S^{IJ}\frac{\mathbf{t}\cdot\partial_I\mathbf{r}}{\|\partial_s\mathbf{r}\|}D_J\mathbf{r}\big]. \tag{4.9}$$

Since $D_I\mathbf{r}$ should be invertible when $I \neq s$, and we've already selected out the perpendicular components, we can project onto these coordinate basis vectors:

$$0 = \partial_I\big[S^{IJ} D_J\mathbf{r}\big]\cdot D_K\mathbf{r} - \partial_s\big[S^{IJ}\frac{\mathbf{t}\cdot\partial_I\mathbf{r}}{\|\partial_s\mathbf{r}\|}D_J\mathbf{r}\big]\cdot D_K\mathbf{r}. \tag{4.10}$$

Distributing the partial derivatives, we then have:

$$0 = \partial_I S^{IJ} g^{\text{eff}}_{JK} - \partial_s (S^{IJ} \frac{\mathbf{t} \cdot \partial_I \mathbf{r}}{\|\partial_s \mathbf{r}\|}) g^{\text{eff}}_{JK} + S^{IJ} \big[D_K \mathbf{r} \cdot \partial_I D_J \mathbf{r} - \frac{\mathbf{t} \cdot \partial_I \mathbf{r}}{\|\partial_s \mathbf{r}\|} D_K \mathbf{r} \cdot \partial_s D_J \mathbf{r} \big], \quad (4.11)$$

where $g^{\text{eff}}_{IJ} = D_{\mathbf{r}} \cdot D_J \mathbf{r}$. Then, multiplying by an inverse effective metric and renaming the floating index, we have:

$$0 = \partial_I S^{IJ} - \partial_s (S^{IJ} \frac{\mathbf{t} \cdot \partial_I \mathbf{r}}{\|\partial_s \mathbf{r}\|}) + S^{IL} g^{KJ\text{eff}} \big[D_K \mathbf{r} \cdot \partial_I D_L \mathbf{r} - \frac{\mathbf{t} \cdot \partial_I \mathbf{r}}{\|\partial_s \mathbf{r}\|} D_K \mathbf{r} \cdot \partial_s D_L \mathbf{r} \big]. \quad (4.12)$$

By analogy with the geometry of embeddings of sub-manifolds in Euclidean space, which inherit a connection given by the Christoffel symbol $\Gamma^l_{ij} = g^{kl} \mathbf{x}_k \cdot \mathbf{x}_{ij}$, we define

$$\Gamma^J_{IL} \equiv g^{KJ\text{eff}} D_K \mathbf{r} \cdot \partial_I D_L \mathbf{r}, \quad (4.13)$$

however, it turns out to be more convenient to instead combine both terms above into one modified Christoffel symbol

$$\Gamma^{J\text{mod}}_{IL} = g^{KJ\text{eff}} D_K \mathbf{r} \cdot \partial_I D_L \mathbf{r} - g^{KJ\text{eff}} \frac{\mathbf{t} \cdot \partial_I \mathbf{r}}{\|\partial_s \mathbf{r}\|} D_K \mathbf{r} \cdot \partial_s D_L \mathbf{r}. \quad (4.14)$$

Putting this all together, we have that

$$0 = (\partial_I - \partial_s \frac{\mathbf{t} \cdot \partial_I \mathbf{r}}{\|\partial_s \mathbf{r}\|}) S^{IJ} + S^{IL} \Gamma^{J\text{mod}}_{IL}. \quad (4.15)$$

It's useful to note here that, for a generic vector V^I,

$$V^I_{;K} \equiv (\partial_K - \partial_s \frac{\mathbf{t} \cdot \partial_K \mathbf{r}}{\|\partial_s \mathbf{r}\|}) V^I + \Gamma^{I\text{mod}}_{KL} V^L \quad (4.16)$$

is zero whenever $K = s$, and when s and u are orthogonal coordinates, so that $\partial_u \mathbf{r} \cdot \mathbf{t} = 0$ [1]:

$$V^I_{;u} \equiv (\partial_u - \partial_s \frac{\mathbf{t} \cdot \partial_u \mathbf{r}}{\|\partial_s \mathbf{r}\|}) V^I + \Gamma^{I\text{mod}}_{uL} V^L = \partial_u V^I + \Gamma^I_{uL} V^I. \tag{4.17}$$

In this sense, the "extra" terms with s derivatives are, again, corrections for the possible *non-integrability* of the tangent field, $\mathbf{t}$.

We can address the bending elasticity similarly. By rewriting $\partial_s \mathbf{t} = -b^K D_K \mathbf{r}$, we can rewrite Eq. (3.34) as:

$$\begin{aligned} EL^{\perp}_{I\text{bend}} = K_{33}\big[&- b^K g_{IK} (2\frac{\partial_s \mathbf{t} \cdot \partial_s \mathbf{t}}{|\partial_s \mathbf{r}|^3} - 2\partial_s \frac{\partial_s^2 \mathbf{r} \cdot \mathbf{t}}{|\partial_s \mathbf{r}|^4}) + 5(g_{IK} \partial_s b^K + b^K \Gamma_{IsK}) \frac{\partial_s^2 \mathbf{r} \cdot \mathbf{t}}{|\partial_s \mathbf{r}|^4} \\ &- (g_{IK} \partial_s^2 b^K + 2\partial_s b^K \Gamma_{IsK} + b^K \partial_s \Gamma_{IsK}) \frac{1}{|\partial_s \mathbf{r}|^3} \big]. \end{aligned} \tag{4.18}$$

Multiplying by an inverse metric (for comparison to columnar elastic bits) gives us:

$$\begin{aligned} EL^{J\perp}_{\text{bend}} = K_{33}\big[&- b^J (2\frac{\partial_s \mathbf{t} \cdot \partial_s \mathbf{t}}{\|\partial_s \mathbf{r}\|^3} - 2\partial_s \frac{\partial_s^2 \mathbf{r} \cdot \mathbf{t}}{\|\partial_s \mathbf{r}\|^4}) + 5(\partial_s b^J + b^K \Gamma^J_{sK}) \frac{\partial_s^2 \mathbf{r} \cdot \mathbf{t}}{\|\partial_s \mathbf{r}\|^4} \\ &- (\partial_s^2 b^J + 2\partial_s b^K \Gamma^J_{sK} + b^K g^{IJ} \partial_s \Gamma_{IsK} - b^K \Gamma_{LsK} \Gamma^{L\ J}_{s}) \frac{1}{\|\partial_s \mathbf{r}\|^3} \big]. \end{aligned} \tag{4.19}$$

4.2.2 Linear components of the Euler-Lagrange equations

Taking as our displacement field Eq. (4.6), we now proceed to find, up to linear order, the various components of the Euler-Lagrange equations. We'll suppress the formal parameter ε in what follows in the interest of clarity, and instead indicate the

[1] We can find coordinates s, u, and v, such that this is true when $\mathbf{t} \cdot (\nabla \times \mathbf{t}) = 0$, which is exactly the condition that there be a family of surfaces with $\mathbf{t}$ as the normal vector, so this makes a certain amount of sense.

order of the terms by a parenthetical superscript, so that $M = M^{(0)} + \varepsilon M^{(1)} + \cdots$, etc. Of principle interest is the strain tensor, given by:

$$\epsilon^{(0)} = \tfrac{1}{2}\begin{pmatrix} f'(\rho)^2 - 1 & 0 \\ 0 & \frac{f(\rho)^2}{1+\Omega^2 f(\rho)^2} - \rho^2 \end{pmatrix}, \tag{4.20}$$

and

$$\begin{aligned} \epsilon^{(1)}_{\rho\rho} &= f'(\rho)\partial_\rho \delta\tilde{\rho} \qquad (4.21)\\ \epsilon^{(1)}_{\rho\phi} &= \tfrac{1}{2} f'(\rho)\partial_\phi \delta\tilde{\rho} + \tfrac{1}{2}\frac{f(\rho)^2\partial_\rho \delta\tilde{\phi} - f'(\rho)\Omega f(\rho)^2 \partial_s \delta\tilde{\rho}}{1+\Omega^2 f(\rho)^2} \\ \epsilon^{(1)}_{\phi\phi} &= f(\rho)\Big[\frac{\delta\tilde{\rho} - \Omega^2\kappa_0 f(\rho)^4\cos(\tilde{\phi}) + (1+\Omega^2 f(\rho)^2) f(\rho)\partial_\phi\delta\tilde{\phi} - \Omega f(\rho)^3\partial_s\delta\tilde{\phi}}{1+\Omega^2 f(\rho)^2}\Big]. \end{aligned}$$

The stress tensor is then just linearly related to the strain tensor:

$$S = \begin{pmatrix} (\lambda+2\mu)\epsilon_{\rho\rho} + \frac{\lambda}{\rho^2}\epsilon_{\phi\phi} & 2\frac{\mu}{\rho^2}\epsilon_{\rho\phi} \\ 2\frac{\mu}{\rho^2}\epsilon_{\rho\phi} & \frac{\lambda}{\rho^2}\epsilon_{\rho\rho} + \frac{(\lambda+2\mu)}{\rho^2}\epsilon_{\phi\phi}. \end{pmatrix} \tag{4.22}$$

From here, the other contributions to the Euler-Lagrange equations we need are just the convective flow tensor, h, the modified Christoffel symbols, Γ^{mod}, and the corrections for integrability, $t_I = \mathbf{t}\cdot\frac{\partial_I \mathbf{r}}{\|\partial_s \mathbf{r}\|}$. The convective flow tensor vanishes as $\epsilon \to 0$, so at linear order here we have:

$$h^{(1)}_{\rho\rho} = 2\frac{f'(\rho)\partial_s\partial_\rho\delta\tilde{\rho}}{\sqrt{1+\Omega^2 f(\rho)^2}} \tag{4.23}$$

$$h^{(1)}_{\rho\phi} = \frac{f(\rho)^2\partial_s\partial_\rho\delta\tilde{\phi} + f'(\rho)(1+\Omega^2 f(\rho)^2)\partial_s\partial_\phi\delta\tilde{\rho} - \Omega f(\rho)^2 f'(\rho)\partial_s^2\delta\tilde{\rho}}{(1+\Omega^2 f(\rho)^2)^{3/2}} \tag{4.24}$$

$$h^{(1)}_{\phi\phi} = 2\frac{\Omega^3\kappa_0 f(\rho)^5 + f(\rho)\partial_s\delta\tilde{\rho} + f(\rho)^2(1+\Omega^2 f(\rho)^2)\partial_s\partial_\phi\delta\tilde{\phi} - \Omega f(\rho)^3\partial_s^2\delta\tilde{\phi}}{(1+\Omega^2 f(\rho)^2)^{5/2}} \tag{4.25}$$

For t_I, without further ado, we have:

$$t_I^{(0)} = \begin{pmatrix} 1 \\ 0 \\ \frac{\Omega f(\rho)^2}{1+\Omega^2 f(\rho)^2} \end{pmatrix}, \tag{4.26}$$

and

$$t_s^{(1)} = 0, \tag{4.27}$$

$$\begin{aligned} t_\rho^{(1)} &= \partial_\rho \delta\tilde{s} + \frac{\Omega f(\rho)^2 \partial_\rho \delta\tilde{\phi} + f'(\rho)\partial_s \delta\tilde{\rho}}{1+\Omega^2 f(\rho)^2} \\ t_\phi^{(1)} &= \partial_\phi \delta\tilde{s} + \frac{\Omega f(\rho)^2 \partial_\phi \delta\tilde{\phi} - \Omega f(\rho)^2 \partial_s \delta\tilde{s}}{1+\Omega^2 f(\rho)^2} \\ &\quad + \frac{2\Omega f(\rho)\delta\tilde{\rho} + f(\rho)^2(1-\Omega^2 f(\rho)^2)\partial_s \delta\tilde{\phi} + 2\Omega\kappa_0 f(\rho)^3 \cos(\tilde{\phi})}{(1+\Omega^2 f(\rho)^2)^2}. \end{aligned} \tag{4.28}$$

The last to be calculated are the modified Christoffel symbols, which are a bit of a pain, so it'll pay to think some more about which we need: We'll want all of these as $\varepsilon \to 0$, but at $\mathcal{O}(\varepsilon)$, we can use that $S^{\rho\phi(0)} = 0$, so we only need $\Gamma^{J\mathrm{mod}}_{\rho\rho}$ and $\Gamma^{I\mathrm{mod}}_{\phi\phi}$. With $\varepsilon = 0$, we find:

$$\begin{aligned} \Gamma^{\rho\mathrm{mod}(0)}_{\rho\rho} &= \frac{f''(\rho)}{f'(\rho)} \\ \Gamma^{\rho\mathrm{mod}(0)}_{\phi\phi} &= -\frac{f(\rho)}{(1+\Omega^2 f(\rho)^2)^2 f'(\rho)} \\ \Gamma^{\phi\mathrm{mod}(0)}_{\phi\rho} &= \frac{f'(\rho)}{f(\rho)(1+\Omega^2 f(\rho)^2)} \\ \Gamma^{\phi\mathrm{mod}(0)}_{\rho\phi} &= \frac{f'(\rho)}{f(\rho)(1+\Omega^2 f(\rho)^2)}, \end{aligned} \tag{4.29}$$

and all others vanishing. Then, at linear order in ε, (which we're going to suppress here) we find that

$$\Gamma_{\rho\rho}^{\rho\mathrm{mod}(1)} = \frac{-f''(\rho)\partial_\rho\delta\tilde{\rho} + f'(\rho)\partial_\rho^2\delta\tilde{\rho}}{f'(\rho)^2}$$
$$\Gamma_{\phi\phi}^{\rho\mathrm{mod}(1)} = \frac{\partial_\phi^2\delta\tilde{\rho}}{f'(\rho)} - \frac{2\Omega f(\rho)^2\partial_s\partial_\phi\delta\tilde{\rho}}{f'(\rho)(1+\Omega^2 f(\rho)^2)} + \frac{f(\rho)\partial_\rho\delta\tilde{\rho} - 2f(\rho)f'(\rho)\partial_\phi\delta\tilde{\phi}}{f'(\rho)^2(1+\Omega^2 f(\rho)^2)^2} \tag{4.30}$$
$$+ \frac{(-1+3\Omega^2 f(\rho)^2)\delta\tilde{\rho} + 4\Omega f(\rho)^3\partial_s\delta\tilde{\phi} + \Omega^2\kappa_0 f(\rho)^4\cos(\tilde{\phi})(5+\Omega^2 f(\rho)^2)}{(1+\Omega^2 f(\rho)^2)^3 f'(\rho)}$$

and

$$\Gamma_{\rho\rho}^{\phi\mathrm{mod}(1)} = \partial_\rho^2\delta\tilde{\phi} - \frac{f''(\rho)\partial_\rho\delta\tilde{\phi}}{f'(\rho)} + \frac{2f'(\rho)\partial_\rho\delta\tilde{\phi}}{f(\rho)(1+\Omega^2 f(\rho)^2)} - \frac{2\Omega f'(\rho)^2\partial_s\delta\tilde{\rho}}{f(\rho)(1+\Omega^2 f(\rho)^2)} \tag{4.31}$$
$$\Gamma_{\phi\phi}^{\phi\mathrm{mod}(1)} = \partial_\phi^2\delta\tilde{\phi} - 2\frac{\Omega f(\rho)^3\partial_s\partial_\phi\delta\tilde{\phi} - \partial_\phi\delta\tilde{\rho}}{f(\rho)(1+\Omega^2 f(\rho)^2)}$$
$$+ \frac{f(\rho)\partial_\rho\delta\tilde{\phi} - f'(\rho)\Omega f(\rho)\partial_s\delta\tilde{\rho} + \Omega^2\kappa_0 f(\rho)^3 f'(\rho)\sin(\tilde{\phi})}{f'(\rho)(1+\Omega^2 f(\rho)^2)^2}. \tag{4.32}$$

While it can be difficult to appreciate from down in the weeds, we can see some remarkable features of the preceding linear terms. Notably, we have here a linear force proportional to the curvature, κ_0, of the central curve, even in the absence of bending elasticity for the filaments themselves. This is in contrast to the developable domains, which can bend freely without penalty from the cross-sectional elasticity. We expect that this effective contribution to the bending stiffness becomes especially important for hierarchical, macroscopic assemblies of much smaller fibers, like yarns, ropes, and cables, where the thickness of the bundle is much larger than thickness of the constituent filaments.

We can now proceed to find the column bending contributions to the Euler-Lagrange equations. The only term which survives as $\varepsilon \to 0$ is the radial component:

$$EL_{\mathrm{bend}}^{\rho(0)} = K_{33}\Omega^4\rho f(\rho)\frac{1-\Omega^2 f(\rho)^2}{f'(\rho)(1+\Omega^2 f(\rho)^2)^3}. \tag{4.33}$$

At linear order, we get more exciting contributions. Parallel to $\mathbf{t}$, we have:

$$EL^{\parallel(1)}_{\text{bend}} = -\frac{K_{33}\Omega^2 f(\rho)}{(1+\Omega^2 f(\rho)^2)^{7/2}}\big[(1+\Omega^2 f(\rho)^2)\partial_s^3\delta\tilde{\rho} \tag{4.34}$$
$$-(1-\Omega^2 f(\rho)^2)(\Omega\kappa_0\sin(\tilde{\phi}) - \Omega^2\partial_s\delta\tilde{\rho}) - 2\Omega f(\rho)\partial_s^2\delta\tilde{\phi}\big],$$

While perpendicular to $\mathbf{t}$, we have

$$EL^{\rho(1)}_{\text{bend}} = \frac{K_{33}\rho f(\rho)}{(1+\Omega^2 f(\rho)^2)^4 f'(\rho)^2}\big[(1+\Omega^2 f(\rho)^2)^2 f'(\rho)\partial_s^4\delta\tilde{\rho} \tag{4.35}$$
$$-\Omega^2(6+\Omega^2 f(\rho)^2 - 5\Omega^4 f(\rho)^4)f'(\rho)\partial_s^2\delta\tilde{\rho} + \Omega^4(1-8\Omega^2 f(\rho)^2 + 3\Omega^4 f(\rho)^4)f'(\rho)\delta\tilde{\rho}$$
$$-\Omega^4 f(\rho)(1-\Omega^4 f(\rho)^4)\partial_\rho\delta\tilde{\rho} - \Omega f(\rho)(4+3\Omega^2 f(\rho)^2 - \Omega^4 f(\rho)^4)f'(\rho)\partial_s^3\delta\tilde{\phi}$$
$$+4\Omega^3 f(\rho)(1-2\Omega^2 f(\rho)^2)f'(\rho)\partial_s\delta\tilde{\phi} + \Omega^2 f(\rho)(1+\Omega^2 f(\rho)^2)^2 f'(\rho)\partial_s^3\delta\tilde{s}$$
$$+3\Omega^4\kappa_0 f(\rho)^2(5+\Omega^2 f(\rho)^2)f'(\rho)\cos(\tilde{\phi})\big]$$

and

$$EL^{\phi(1)}_{\text{bend}} = \frac{K_{33}\rho}{f(\rho)f'(\rho)(1+\Omega^2 f(\rho)^2)^3}\big[f(\rho)f'(\rho)(1+\Omega^2 f(\rho)^2)\partial_s^4\delta\tilde{\phi} \tag{4.36}$$
$$-2\Omega^2 f(\rho)f'(\rho)(3-2\Omega^2 f(\rho)^2)\partial_s^2\delta\tilde{\phi} - \Omega^4 f(\rho)^2(1-\Omega^2 f(\rho)^2)\partial_\rho\delta\tilde{\phi}$$
$$+4\Omega f'(\rho)(1+\Omega^2 f(\rho)^2)\partial_s^3\delta\tilde{\rho} - 4\Omega^3 f'(\rho)(1-2\Omega^2 f(\rho)^2)\partial_s\delta\tilde{\rho}$$
$$+2\Omega^3 f(\rho)f'(\rho)(1+\Omega^2 f(\rho)^2)\partial_s^2\delta\tilde{s} + 10\Omega^4\kappa_0 f(\rho)^2 f'(\rho)\sin(\tilde{\phi})\big].$$

4.2.3 Boundary conditions

The same linearization procedure also provides boundary conditions for the $\mathcal{O}(\varepsilon)$ force balance equations. Recall from Ch. 3 that force balance on the boundary is given by

$$\hat{N}_I\big[dVS^{IJ}\big]D_J\mathbf{r} - \hat{N}_K\hat{T}^K\big[dVS^{IJ}\frac{\mathbf{t}\cdot\partial_I\mathbf{r}}{|\partial_s\mathbf{r}|}\big]D_J\mathbf{r} = 0. \tag{4.37}$$

Thinking for a half second, choosing $\hat{N} = \rho$ and noting that ρ and s are orthogonal in the reference coordinates, we have:

$$S^{\rho J}D_J\mathbf{r} = 0. \tag{4.38}$$

Doing our usual trick, and adding in the possibility of a pressure P^I acting normal to the boundary here gives us:

$$P^I = S^{\rho J} D_J \mathbf{r} \cdot D_I \mathbf{r}$$
$$P^I = S^{\rho J} g^{\text{eff}}_{IJ} g^{IJ\text{eff}} = S^{\rho I}. \tag{4.39}$$

which is nice and straightforward. At linear order, this is then just the condition that $P^{J(1)} = S^{\rho J(1)}$, and so when $P^{J(1)} = 0$, $S^{\rho\rho(1)} = S^{\rho\phi(1)} = 0$. In terms of our δx_i, this is then

$$(\lambda + 2\mu) f'(\rho) \partial_\rho \delta\tilde{\rho} = -\frac{\lambda}{\rho^2} f(\rho) \big[\frac{\delta\tilde{\rho} - \Omega^2 \kappa_0 f(\rho)^4 \cos(\tilde{\phi}) + (1 + \Omega^2 f(\rho)^2) f(\rho) \partial_\phi \delta\tilde{\phi} - \Omega f(\rho)^3 \partial_s \delta\tilde{\phi}}{1 + \Omega^2 f(\rho)^2} \big] \tag{4.40}$$

$$\frac{\mu}{\rho^2} \frac{f(\rho)^2 \partial_\rho \delta\tilde{\phi}}{1 + \Omega^2 f(\rho)^2} = -\frac{\mu}{\rho^2} \big[f'(\rho) \partial_\phi \delta\tilde{\rho} + \frac{f'(\rho) \Omega f(\rho)^2 \partial_s \delta\tilde{\rho}}{1 + \Omega^2 f(\rho)^2} \big] \tag{4.41}$$

At the inner boundary, $\rho = 0$, we have also assumed that the central curve is parameterized by $\mathbf{r}_0$, and so we have that

$$\delta\tilde{\rho}|_{\rho=0} = 0 \tag{4.42}$$
$$\delta\tilde{\phi}|_{\rho=0} = 0 \tag{4.43}$$
$$\delta\tilde{s}|_{\rho=0} = 0. \tag{4.44}$$

4.3 Fourier expansion for perturbative fields

If we look a little more carefully about the structure of these differential equations, we notice that there's some nice groupings of terms here, if we collect the components of the Euler-Lagrange equations: since

$$EL^{\rho(1)} = \big[(\partial_I - \partial_s t_I) S^{I\rho} + S^{IJ} \Gamma^{\rho\text{mod}}_{IJ} \big]^{(1)} \tag{4.45}$$
$$EL^{\phi(1)} = \big[(\partial_I - \partial_s t_I) S^{I\phi} + S^{IJ} \Gamma^{\phi\text{mod}}_{IJ} \big]^{(1)}, \tag{4.46}$$

and so $EL^{\rho(1)}$ contains only even derivatives of s and ϕ of $\delta\tilde{\rho}$, and odd derivatives of s and ϕ of $\delta\tilde{\phi}$ and $\delta\tilde{s}$, and a source term, proportional to $\kappa_0 \cos(\tilde{\phi})$, where $EL^{\phi(1)}$ contains only odd derivatives of s and ϕ of $\delta\tilde{\rho}$, and even derivatives of s and ϕ of $\delta\tilde{\phi}$ and $\delta\tilde{s}$, and a source term, proportional to $\kappa_0 \sin(\tilde{\phi})$. This inspires us to make a simplifying assumption: that the lowest energy solutions in $\delta\tilde{\rho}$, $\delta\tilde{\phi}$, and $\delta\tilde{s}$ include only the first Fourier mode in $\tilde{\phi}$.

We can then find solutions of the form

$$\begin{aligned} \delta\tilde{\rho} &= \delta\tilde{\rho}(\rho)\cos(\tilde{\phi}) \\ \delta\tilde{\phi} &= \delta\tilde{\phi}(\rho)\sin(\tilde{\phi}) \\ \delta\tilde{s} &= \delta\tilde{s}(\rho)\sin(\tilde{\phi}), \end{aligned} \tag{4.47}$$

so that what were initially partial differential equations are now a system of ordinary differential equations. While we fail to make much progress in using these to find direct solutions in the rest of this chapter, it's worth noting that this already tells us a great deal about the linear response of twisted-toroidal bundles. Since it is implicit, as defined in Eq. (4.8), that $\phi = 0$ points along the normal vector, $\hat{N}_0$ to the central curve, we see that $\|\delta\tilde{\rho}\|$ is largest in the plane of the central curve, while $\|\delta\tilde{\phi}\|$ and $\|\delta\tilde{s}\|$, which move transversely to the radial coordinate, are largest along the top and bottom of the torus, suggesting a deformation field which points principally in the normal direction.

Substituting this ansatz into our Euler-Lagrange equations, we find the elastic contributions are:

$$EL^{\|(1)} = -\frac{2\Omega f'(\rho)\sin(\tilde{\phi})}{\sqrt{1+\Omega^2 f(\rho)^2}} S^{\rho\rho(0)}\delta\tilde{\rho}' \tag{4.48}$$
$$+ \frac{2\Omega f(\rho)\sin(\tilde{\phi})}{(1+\Omega^2 f(\rho)^2)^{5/2}} S^{\phi\phi(0)}\left[\Omega^2\kappa_0 f(\rho)^4 - \delta\tilde{\rho} - f(\rho)\delta\tilde{\phi}\right]$$

$$EL^{\rho(1)} = -\cos(\tilde{\phi})\Big\{A(\rho)\delta\tilde{\rho}'' + B(\rho)\delta\tilde{\rho}' + C(\rho)\delta\tilde{\rho} \tag{4.49}$$
$$+ D(\rho)\delta\tilde{\phi}' + E(\rho)\delta\tilde{\phi} + F(\rho)\delta\tilde{s}' + \text{  }(\rho)\kappa_0\Big\}$$

$$EL^{\phi(1)} = -\sin(\tilde{\phi})\Big\{\mathcal{A}(\rho)\delta\tilde{\rho}' + \mathcal{B}(\rho)\delta\tilde{\rho} \tag{4.50}$$
$$+ \mathcal{C}(\rho)\delta\tilde{\phi}'' + \mathcal{D}(\rho)\delta\tilde{\phi}' + \mathcal{E}(\rho)\delta\tilde{\phi} + \mathcal{F}(\rho)\delta\tilde{s} + \text{ 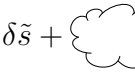 }(\rho)\kappa_0\Big\},$$

where we can calculate all of these coefficients explicitly in terms of the $\mathcal{O}(\varepsilon^0)$ solution. First, we find

$$A(\rho) = (\lambda+2\mu)\rho f'(\rho) + S^{\rho\rho(0)}\frac{\rho}{f'(\rho)} \tag{4.51}$$

$$B(\rho) = \lambda\frac{f(\rho)}{\rho(1+\Omega^2 f(\rho)^2)^2} + (\lambda+2\mu)(f'(\rho)+\rho f''(\rho)) + (\lambda+2\mu)\rho f''(\rho) \tag{4.52}$$
$$- \frac{\lambda f(\rho)}{\rho(1+\Omega^2 f(\rho)^2)^2} - S^{\rho\rho(0)}\frac{\rho f''(\rho)}{f'(\rho)^2} + S^{\phi\phi(0)}\frac{\rho f(\rho)}{f'(\rho)^2(1+\Omega^2 f(\rho)^2)^2}$$

$$C(\rho) = -\frac{\lambda f(\rho)(1+\Omega^2 f(\rho)^2) + \rho(\mu-\lambda)f'(\rho) + \Omega^2\rho f(\rho)f'(\rho)(3\lambda+\mu)}{\rho^2(1+\Omega^2 f(\rho)^2)^3}$$
$$+ \frac{\lambda f(\rho)f''(\rho)}{\rho f'(\rho)(1+\Omega^2 f(\rho)^2)^2} - \frac{(\lambda+2\mu)f(\rho)^2}{\rho^3 f'(\rho)(1+\Omega^2 f(\rho)^2)^4} \tag{4.53}$$
$$- S^{\rho\rho(0)}\frac{\rho\Omega^2 f'(\rho)}{1+\Omega^2 f(\rho)^2} - S^{\phi\phi(0)}\frac{2\rho(1-\Omega^2 f(\rho)^2)}{f'(\rho)(1+\Omega^2 f(\rho)^2)^3},$$

$$D(\rho) = \frac{(\lambda+\mu)f(\rho)^2}{\rho(1+\Omega^2 f(\rho)^2)^2} + S^{\rho\rho(0)}\frac{\Omega^2\rho f(\rho)^2}{1+\Omega^2 f(\rho)^2} \tag{4.54}$$

$$E(\rho) = -\frac{\lambda f(\rho)(f(\rho)(1+\Omega^2 f(\rho)^2) - 2\rho f'(\rho)(1-\Omega^2 f(\rho)^2))}{\rho^2(1+\Omega^2 f(\rho)^2)^3} + \frac{\lambda f(\rho)^2 f''(\rho)}{\rho f'(\rho)(1+\Omega^2 f(\rho)^2)^2}$$
$$- \frac{(\lambda+2\mu)f(\rho)^3}{\rho^3 f'(\rho)(1+\Omega^2 f(\rho)^2)^4} - S^{\phi\phi(0)}\frac{2\rho f(\rho)(1-\Omega^2 f(\rho)^2)}{f'(\rho)(1+\Omega^2 f(\rho)^2)^3} \tag{4.55}$$

$$F(\rho) = \Omega\rho S^{\rho\rho(0)} \tag{4.56}$$

 $(\rho) = \frac{\lambda\Omega^2 f(\rho)^4[f(\rho)(1+\Omega^2 f(\rho)^2) - \rho f'(\rho)(5+\Omega^2 f(\rho)^2)]}{\rho^2(1+\Omega^2 f(\rho)^2)^3}$ (4.57)

$$- \frac{\lambda\Omega^2 f(\rho)^5 f''(\rho)}{\rho f'(\rho)(1+\Omega^2 f(\rho)^2)^2} + \frac{(\lambda+2\mu)\Omega^2 f(\rho)^6}{\rho^3 f'(\rho)(1+\Omega^2 f(\rho)^2)^4} + \rho S^{\phi\phi(0)} \frac{\Omega^2 f(\rho)^4(5+\Omega^2 f(\rho)^2)}{f'(\rho)(1+\Omega^2 f(\rho)^2)^3}$$

$$\mathcal{A}(\rho) = -\frac{(\lambda+\mu)f'(\rho)}{\rho(1+\Omega^2 f(\rho)^2)} \tag{4.58}$$

$$\mathcal{B}(\rho) = -\frac{f(\rho)(\lambda+2\mu) - 2\mu\Omega^2\rho^2 f(\rho) f'(\rho)^2(1+\Omega^2 f(\rho)^2)}{\rho^3(1+\Omega^2 f(\rho)^2)^3} \tag{4.59}$$

$$- \frac{\mu[-f'(\rho)+\rho f''(\rho)]}{\rho^2(1+\Omega^2 f(\rho)^2} - \frac{\mu f'(\rho)^2}{\rho f(\rho)(1+\Omega^2 f(\rho)^2)^2} + 2S^{\rho\rho(0)} \frac{\Omega^2\rho f'(\rho)}{f(\rho)(1+\Omega^2 f(\rho)^2)}$$

$$- 2S^{\phi\phi(0)} \frac{\rho}{f(\rho)(1+\Omega^2 f(\rho)^2)^2} - 2S^{\phi\phi(0)} \frac{\Omega^2\rho f(\rho)}{(1+\Omega^2 f(\rho)^2)^2}$$

$$\mathcal{C}(\rho) = \frac{\mu f(\rho)^2}{\rho(1+\Omega^2 f(\rho)^2)} + \rho S^{\rho\rho(0)} \tag{4.60}$$

$$\mathcal{D}(\rho) = -\frac{\mu f(\rho)[f(\rho)(1+\Omega^2 f(\rho)^2) - 2\rho f'(\rho)]}{\rho(1+\Omega^2 f(\rho)^2)^2} + 2\frac{\mu f'(\rho) f(\rho)}{\rho(1+\Omega^2 f(\rho)^2)^2}$$

$$+ \rho S^{\rho\rho(0)} \big[\frac{2f'(\rho)}{f(\rho)(1+\Omega^2 f(\rho)^2)} - \frac{f''(\rho)}{f'(\rho)}\big] + \rho S^{\phi\phi(0)} \frac{f(\rho)}{f'(\rho)(1+\Omega^2 f(\rho)^2)^2} \tag{4.61}$$

$$\mathcal{E}(\rho) = -\frac{(\lambda+2\mu)f(\rho)^2}{\rho^3(1+\Omega^2 f(\rho)^2)^3} - S^{\phi\phi(0)} \frac{\rho}{(1+\Omega^2 f(\rho)^2)^2} - S^{\phi\phi(0)} \frac{2\Omega^2\rho f(\rho)^2}{(1+\Omega^2 f(\rho)^2)^2} \tag{4.62}$$

$$\mathcal{F}(\rho) = -S^{\phi\phi(0)} \frac{\Omega\rho}{1+\Omega^2 f(\rho)^2} \tag{4.63}$$

 $(\rho) = \frac{(\lambda+2\mu)\Omega^2 f(\rho)^5}{\rho^3(1+\Omega^2 f(\rho)^2)^3} + \rho S^{\phi\phi(0)} \frac{\Omega^2 f(\rho)^3}{(1+\Omega^2 f(\rho)^2)^2}$ (4.64)

$$- 2\rho S^{\phi\phi(0)} \frac{\Omega^2 f(\rho)^3}{(1+\Omega^2 f(\rho)^2)^2}$$

and the bending contributions are

$$EL^{\parallel(1)}_{\text{bend}} = -\frac{K_{33}\Omega^3 f(\rho)\sin(\tilde{\phi})}{(1+\Omega^2 f(\rho)^2)^{7/2}}\left[(-1+\Omega^2 f(\rho)^2)\kappa_0 + 2\Omega^2\delta\tilde{\rho} + 2\Omega^2 f(\rho)\delta\tilde{\phi}\right] \tag{4.65}$$

$$\begin{aligned} EL^{\rho(1)}_{\text{bend}} = &-\frac{K_{33}\Omega^4\rho\cos(\tilde{\phi})}{(1+\Omega^2 f(\rho)^2)^4 f'(\rho)^2}\big[f(\rho)(1-\Omega^4 f(\rho)^4)\delta\tilde{\rho}' \\ &- f'(\rho)(8-5\Omega^2 f(\rho)^2-\Omega^4 f(\rho)^4)(\delta\tilde{\rho}+f(\rho)\delta\tilde{\phi}) \\ &+ \Omega f(\rho)f'(\rho)(1+\Omega^2 f(\rho)^2)^2\delta\tilde{s} - f(\rho)^2 f'(\rho)(15+3\Omega^2 f(\rho)^2)\kappa_0\big] \end{aligned} \tag{4.66}$$

$$\begin{aligned} EL^{\phi(1)}_{\text{bend}} = &-\frac{K_{33}\Omega^4\rho\sin(\tilde{\phi})}{f(\rho)f'(\rho)(1+\Omega^2 f(\rho)^2)^3}\big[(f(\rho)^2-\Omega^2 f(\rho)^4)\delta\tilde{\phi}' \\ &- f(\rho)f'(\rho)(7-3\Omega^2 f(\rho)^2)\delta\tilde{\phi} - 4f'(\rho)(2-\Omega^2 f(\rho)^2)\delta\tilde{\rho} \\ &+ 2\Omega f(\rho)f'(\rho)(1+\Omega^2 f(\rho)^2)\delta\tilde{s} - 10 f(\rho)^2 f'(\rho)\kappa_0. \end{aligned} \tag{4.67}$$

It's worth noting that the bending contributions don't meaningfully change the structure of the resulting ordinary differential equation (ODE), as they all contain lower order derivatives than accompanying columnar-elasticity driven contributions.

Now that we've worked out explicitly the linear force-balance equations for twisted-toroidal filament bundles, we can start to look at the structure of the resulting ODEs, and try to find solutions, either numerically, or in a series expansion around either boundary. First, however, we have some roadblocks which must be addressed.

4.4 Singular boundaries and bulk behavior

Now that we have reduced this problem to a system of linear ODEs, we would ideally try to take advantage of the numerous robust numerical algorithms for solving linear boundary value problems. Very quickly along the way, however, we run into some issues with singularities on the boundaries, and divergent behavior in the solutions. So, in order to find solutions with bounded and differentiable displacement fields, which we both expect and need in order to have a hope of describing experi-

mental systems, we have to pay pretty close attention to the behavior of the solutions of our differential equations at the singular boundaries.

If our bundles have force free boundary conditions and are (roughly) cylindrically symmetric, we can go ahead and learn some things about the behavior of our perturbative solutions on the outer boundary. Force free boundary conditions here are, as above, that $S^{\rho J} = 0$, with the additional condition that $\delta\tilde{x}_i|_{\rho=0} = 0$. There's nothing particularly unusual here, and this is basically identical to the sheet elasticity case.

4.4.1 Inner boundary

At the inner boundary, we have a singularity that arises because we dared to work in cylindrical coordinates. It's not really a problem if we're trying to solve an initial value problem starting at $\rho = 0$, but we run into some issues with the stability of shooting methods if we don't address it directly. In order to examine the behavior of the perturbative fields ($\delta\tilde{s}$, $\delta\tilde{\rho}$, and $\delta\tilde{\phi}$) near $\rho = 0$, both as an input into a possible numerical solution and to gain some intuition for the way that curvature couples to the various elastic modes.

Inspection of the $\rho \to 0$ behavior of the ODEs presented in Section 4.3 suggests that the singularities can be removed when $\delta\tilde{\rho} \sim \Omega^{k-1}\rho^k$, $\delta\tilde{\phi}$, $\Omega\delta\tilde{s} \sim \Omega^{k-1}\rho^{k-1}$, basically because $\delta\tilde{\phi}$ and $\delta\tilde{s}$ pick up a power of ρ from $f(\rho)$ in the displacement field (see Eq. (4.7)). Looking for solutions to the homogeneous (κ_0 terms vanish) case then demands that the resultant matrix of coefficients has a non-trivial kernel, and so the determinant of

$$\begin{pmatrix} k\mathfrak{A} + \mathfrak{B} & \mathfrak{C} & \mathfrak{D} \\ k(k-1)A + kB + C & (k-1)D + E & (k-1)F + G \\ k\mathcal{A} + \mathcal{B} & (k-1)(k-2)\mathcal{C} + (k-1)\mathcal{D} + \mathcal{E} & \mathcal{F} \end{pmatrix} |_{\rho=0} \tag{4.68}$$

should vanish, where $\mathfrak{A}$ is the coefficient of $\delta\tilde{\rho}'$, $\mathfrak{B}$ the coefficient of $\delta\tilde{\rho}$, $\mathfrak{C}$ the coefficient of $\delta\tilde{\phi}$, and $\mathfrak{D}$ the coefficient of $\delta\tilde{s}$ in the sum of Eqs. (4.49) and (4.66). Mathematica, thankfully, can do this for us, and we find here that there are three solutions: $k = 0$, with multiplicity 2, and $k = \pm 2$. Since the boundary conditions tell us that $\delta\tilde{x}_i|_{\rho=0}$, this means that we expect a scaling like $\delta\tilde{\rho} \sim \Omega\rho^2$, $\delta\tilde{\phi}$, $\Omega\delta\tilde{s} \sim \Omega\rho$. We can see why this is the case by looking at just the tangent component of the Euler-Lagrange equations[2]. As $\rho \to 0$, we can take $\delta\tilde{\rho}$, $\delta\tilde{\phi}$, and $\delta\tilde{s} \to 0$, by the inner boundary condition, and the κ_0 term goes to zero of its own accord. What's left is:

$$-\frac{2\Omega f'(\rho)\sin(\tilde{\phi})}{\sqrt{1+\Omega^2 f(\rho)^2}} S^{\rho\rho(0)}\delta\tilde{\rho}', \tag{4.69}$$

but neither $f'(\rho)$ nor $S^{\rho\rho(0)}$ vanish as $\rho \to 0$, so we're forced to take $\delta\tilde{\rho}'|_{\rho=0} = 0$.

We can push this power series solution to higher order, using the series solution to the helical case in Eq. (3.44) and with

$$\begin{aligned}
\delta\tilde{\rho} &= b_2\Omega\rho^2 + b_3\Omega^2\rho^3 + b_4\Omega^3\rho^4 + \cdots \\
\delta\tilde{\phi} &= c_1\Omega\rho + c_2\Omega^2\rho^2 + c_3\Omega^3\rho^3 + \cdots \\
\delta\tilde{s} &= d_1\rho + d_2\Omega\rho^2 + d_3\Omega^2\rho^3 + \cdots .
\end{aligned} \tag{4.70}$$

Doing so, we find at lowest order that:

$$\begin{aligned}
c_1 &= c_1 \\
d_1 &= -\frac{8c_1(a_1^2\lambda - \lambda + 2a_1^2\mu)}{3(a_1^2-1)(\lambda+\mu)} + \frac{K_{33}\Omega\kappa_0(7a_1^2\mu - 2\mu + 5a_1^2\lambda - 2\lambda}{12(\lambda+\mu)(a_1^2-1)} \\
b_2 &= -\frac{a_1 c_1}{3} + \frac{K_{33}\Omega\kappa_0}{12(\lambda+\mu)(a_1^2-1)},
\end{aligned} \tag{4.71}$$

[2]This will become something of a theme in this chapter, for reasons that I do not quite understand

where $a_1 = f'(0)$. Notably, the lowest order coupling between the curvature and twist is mediated by the bending elasticity. We then find that:

$$\begin{aligned} c_2 &= 0 \\ d_2 &= 0 \\ b_3 &= 0, \end{aligned} \tag{4.72}$$

which is nice and straightforward. As including bending-driven terms at higher orders is not particularly informative, and at the next highest order in ρ, things begin to get a bit hairy, we'll reproduce here just the $K_{33} \to 0$ contributions, for which this is the lowest order contribution:

$$c_3 = \frac{1}{288(a_1^2-1)\big[(a_1^2-1)\lambda + (2a_1^2-1)\mu\big]\big[(2a_1^2-1)\lambda + (3a_1^2-1)\mu\big]}$$

$$\Big\{ c_1\big[60\lambda^2 + 120\lambda\mu + 60\mu^2\big]a_1^2 + \tfrac{\kappa_0}{\Omega}\big[117\lambda^2 + 234\lambda\mu + 117\mu^2\big]a_1^3 \tag{4.73}$$

$$- c_1\big[234\lambda^2 + 448\lambda\mu + 214\mu^2\big]a_1^4 - \tfrac{\kappa_0}{\Omega}\big[468\lambda^2 + 1125\lambda\mu + 657\mu^2\big]a_1^5$$

$$+ c_1\big[228\lambda^2 + 702\lambda\mu + 334\mu^2\big]a_1^6 + \tfrac{\kappa_0}{\Omega}\big[585\lambda^2 + 1620\lambda\mu + 1107\mu^2\big]a_1^7$$

$$+ c_1\big[114\lambda^2 + 374\lambda\mu + 312\mu^2\big]a_1^8 + \tfrac{\kappa_0}{\Omega}\big[234\lambda^2 + 729\lambda\mu + 567\mu^2\big]a_1^9\Big\}, \tag{4.74}$$

and

$$d_3 = \frac{1}{12(a_1^2-1)^2(\lambda+\mu)\big[(2a_1^2-1)\lambda + (3a_1^2-1)\mu\big]}$$

$$\Big\{ - c_1\big[28\lambda^2 + 56\lambda\mu + 28\mu^2\big]a_1^2 - \tfrac{\kappa_0}{\Omega}\big[39\lambda^2 + 78\lambda\mu + 39\mu^2\big]a_1^3 \tag{4.75}$$

$$+ c_1\big[130\lambda^2 + 344\lambda\mu + 214\mu^2\big]a_1^4 + \tfrac{\kappa_0}{\Omega}\big[156\lambda^2 + 387\lambda\mu + 231\mu^2\big]a_1^5$$

$$- c_1\big[176\lambda^2 + 570\lambda\mu + 450\mu^2\big]a_1^6 - \tfrac{\kappa_0}{\Omega}\big[195\lambda^2 + 576\lambda\mu + 417\mu^2\big]a_1^7$$

$$+ c_1\big[74\lambda^2 + 294\lambda\mu + 288\mu^2\big]a_1^8 + \tfrac{\kappa_0}{\Omega}\big[78\lambda^2 + 267\lambda\mu + 225\mu^2\big]a_1^9\Big\},$$

and

$$
\begin{aligned}
b_4 = & \frac{1}{288(a_1^2-1)\big[(a_1^2-1)\lambda+(2a_1^2-1)\mu\big]\big[(2a_1^2-1)\lambda+(3a_1^2-1)\mu\big]} \\
& \Big\{ -c_1\big[84\lambda^2+168\lambda\mu_8 4\mu^2\big]a_1^3 - \tfrac{\kappa_0}{\Omega}\big[81\lambda^2+162\lambda\mu+81\mu^2\big]a_1^4 \\
& + c_1\big[342\lambda^2+824\lambda\mu+482\mu^2\big]a_1^5 + \tfrac{\kappa_0}{\Omega}\big[324\lambda^2+801\lambda\mu+477\mu^2\big]a_1^6 \\
& - c_1\big[432\lambda^2+1314\lambda\mu+938\mu^2\big]a_1^7 - \tfrac{\kappa_0}{\Omega}\big[405\lambda^2+1188\lambda\mu+855\mu^2\big]a_1^8 \\
& + c_1\big[174\lambda^2+658\lambda\mu+624\mu^2\big]a_1^9 + \tfrac{\kappa_0}{\Omega}\big[162\lambda^2+549\lambda\mu+459\mu^2\big]a_1^{10}\Big\}.
\end{aligned} \tag{4.76}
$$

Principally, this serves to illustrate that coupling between curvature κ_0 and the elasticity, in the form of the Lamé parameters λ and μ, quickly begins to play an oversized role in the behavior of twisted-toroidal bundles at larger radii.

4.4.2 Outer boundary

It turns out that there is also some singular behavior on the outer boundary. Notably, our Euler-Lagrange equations we have:

$$0 = S^{IJ}h_{IJ} \tag{4.77}$$

$$0 = D_I dV S^{IJ} - D_s dV S^{IJ} t_I. \tag{4.78}$$

So, at the free boundary, we have:

$$0 = S^{IJ}h_{IJ} \tag{4.79}$$

$$0 = \partial_I S^{IJ} - \partial_s t_I S^{IJ} + S^{IK}\Gamma^{\mathrm{mod}J}_{IK}, \tag{4.80}$$

all of which can be broken up into ρ and ϕ components, if we so please. The problem here comes when the leading order derivative for any of our displacements has a $S^{\rho J}$ coefficient out front. And, since the $\delta\tilde{s}$ terms only show up in the t_Is and Christoffel

symbols, this is basically guaranteed for them, as well as the $\delta\tilde{\rho}$ contribution from h_{IJ}, which has:

$$S^{\rho\rho(0)} f'(\rho)\delta\tilde{\rho}'(\rho) = S^{\phi\phi(0)} \frac{\Omega f(\rho)}{(1+\Omega^2 f(\rho)^2)^2}\left[\Omega^2\kappa_0 f(\rho)^4 - \delta\tilde{\rho} - f(\rho)\delta\tilde{\phi}\right]. \tag{4.81}$$

So if we try and put this in normal form, we wind up dividing by $S^{\rho\rho(0)}$, which is zero at the outer boundary, and so we have ourselves a Singularity. This is thankfully a removable singularity, cause it goes to zero like $(\rho/R - 1)$, which we can confirm by doing a right quick series expansion in Mathematica which I'm not going to reproduce here, but it does mean that we pretty quickly develop problems when we try to integrate numerically. A quick sketch of a matrix analysis of the ODEs tells us that, when all's said and done, we have:

$$\partial_\rho \delta\tilde{s} \propto \frac{1}{(S^{\rho\rho(0)})^2}\left[A\kappa_0 + B\partial_\rho\delta\tilde{\rho} + C\partial_\rho\delta\tilde{\phi} + D\delta\tilde{\rho} + E\delta\tilde{\phi}\right] \tag{4.82}$$

as our scaling as $\rho \mapsto 1$. This is fairly singular, and it should probably worry us that it doesn't change based on the power of the ρ derivative here.

On the inner boundary, we have another removable singularity at $\rho = 0$, but this (after fixing some mistakes), is basically just the usual removable singularity in cylindrical coordinates, and the Frobenius method gives us either a $1/\rho^2$ divergence or going to zero as ρ^2 for $\delta\tilde{\rho}$, with $\delta\tilde{s} \sim \delta\tilde{\phi} \sim \delta\tilde{\rho}/\rho$ near zero. Notably, this agrees pretty well with what we see numerically (citation needed).

We can also give the Frobenius method a shot on the outer boundary, but, for $\delta\tilde{\rho} \sim \rho^k$, $k \geq 0$, this fails to satisfy the boundary conditions. For $k > 0$, this is basically because the differential equation is inhomogeneous, and for the $\mathbf{t}$ component of the ODE, with $\delta\tilde{\rho} \sim a_0 x^k$, and $\delta\tilde{\phi} \sim b_0 x^k$ and $x = (\rho - R)$, we have that

$$\left[S^{\rho\rho(0)} f'(\rho)\right]'_R k a_0 x^k = S^{\phi\phi(0)}|_R \frac{\Omega f(R)}{(1+\Omega^2 f(R)^2)^2}\left[\Omega^2\kappa_0 f(R)^4 - a_0 x^k - f(R) b_0 x^k\right]. \tag{4.83}$$

And, since $\lim_{x\to 0} x^k = 0$, this would give us $S^{\phi\phi(0)}|_R \frac{\Omega f(R)}{(1+\Omega^2 f(R)^2)^2}\Omega^2\kappa_0 f(R)^4 = 0$, which is not true.

For $k = 0$, we have a little more work to do to show that this can't satisfy our boundary value problem. The leading (x^0) term of a series expansion gives that:

$$A\delta\tilde{\rho}|_{x=0} + B\delta\tilde{\phi}|_{x=0} + C\kappa_0 = 0, \tag{4.84}$$

providing a relationship between $\delta\tilde{\rho}|_{x=0}$ and $\delta\tilde{\phi}|_{x=0}$:

$$\begin{aligned}\delta\tilde{\rho}|_{x=0} = &\frac{-8f(R)^3(\Omega^2-1)\mu(\lambda+\mu) + 2f(R)(-4\mu(\lambda+\mu) + K_{33}\Omega^4(\lambda+2\mu))}{8(1+f(R)^2(\Omega^2-1))\mu(\lambda+\mu) - 2K_{33}\Omega^4(\lambda+2\mu)}\delta\tilde{\phi}|_{x=0} \\ &+ \frac{8f(R)^4\Omega^2\mu(\lambda+\mu) + 8f(R)^6\Omega^2(\Omega^2-1)\mu(\lambda+\mu)}{8(1+f(R)^2(\Omega^2-1))\mu(\lambda+\mu) - 2K_{33}\Omega^4(\lambda+2\mu)}\kappa_0 \\ &+ \frac{-K_{33}\Omega^2(\lambda+2\mu) + f(R)^2K_{33}\Omega^4(\lambda+2\mu)}{8(1+f(R)^2(\Omega^2-1))\mu(\lambda+\mu) - 2K_{33}\Omega^4(\lambda+2\mu)}\kappa_0,\end{aligned} \tag{4.85}$$

where here we've de-dimensionalized lengths by R for convenience, but can basically put it back in by matching units. If we then plug this into the second order equation along the $\mathbf{t}$ direction, and impose the boundary conditions on $\delta\tilde{\rho}'$ and $\delta\tilde{\phi}'$, we find that we're left with a non-zero term proportional to κ_0.

For $k < 0$, we again run into problems with the boundary conditions, which have:

$$\delta\tilde{\phi}'|_R = \frac{\delta\rho(R)f'(R)}{f(R)^2} \tag{4.86}$$

$$\delta\tilde{\rho}'|_R = \frac{\lambda(\Omega^2\kappa_0 f(R)^5 - f(R)\delta\tilde{\rho}(R) - f(R)^2\delta\tilde{\phi}(R))}{R^2(\lambda+2\mu)(1+\Omega^2 f(R)^2)^2 f'(R)}. \tag{4.87}$$

All of these coefficients are just numbers, so we wind up with two conditions that are basically $x^{k-1} = Ax^k$, and since this should still be true multiplying through by x^{-k}, we get that $0 = A$, which is not true, and so there are no removably singular solutions to the boundary value problem.

This is, fundamentally, a problem introduced by the inhomogeneous nature of the differential equations, and is relieved by taking κ_0 to zero. Unfortunately, this fails to address exactly the problem we are interested in, which is the coupling of the perturbative displacements to the bending of the central curve through the non-equidistance of the filament packing.

4.5 Discussion and future directions

The singularities in the linear force-balance equations described in the section above, unfortunately, make it difficult to present any concrete results about the structure of twisted toroidal bundles, which is ultimately the goal of this chapter. To try and get around this problem, we could instead introduce a pressure at the boundary in the helical bundle case, so that $S^{\rho\rho(0)}|_{\rho=R} = P$. While there are possible physical sources for such a pressure, including the possibility of surface energies and surface stresses [131], both implementing such approaches in the differential equations above and understanding the impact they may have on the helical bundles discussed in Ch. 3 remain works in progress.

4.5.1 Almost equidistant ansatzes, revisited

Barring a general solution to the linear force-balance equations, however, perhaps it's possible to at least find a stable configuration in one of the "almost equidistant" families introduced in Ch.. 2. It is easy to see that, in the general case, this impossible by considering again the tangent component of the Euler-Lagrange equations. Since (in the absence of bending, which covers a multitude of sins), $S^{IJ}h_{IJ} = 0$, and, since non-equidistant configurations like twisted-tori are neither equidistant ($h_{IJ} = 0$) nor isometric ($S^{IJ} = 0$), in the absence of specific symmetries, in general we expect a mix of both splay and biaxial splay in the bulk, in proportion determined by the Poisson ratio.

In the low curvature limit, we can see explicitly that neither are in mechanical equilibrium. First, note that both the trace free and determinant free ansatzes fall into the broader class of perturbative fields described in Section 4.3, with $\delta\tilde{\rho} = 0$ for both, and

$$\delta\tilde{\phi} = -\Omega^2\kappa_0 f(\rho)^3 \sin(\tilde{\phi}) \tag{4.88}$$

for the splay-free case, and

$$\delta\tilde{\phi} = 0 \tag{4.89}$$

for the determinant-free case. It is now easy to see that force balance fails in the determinant free bundle by considering the tangent component of the Euler-Lagrange equations, which is now equal to:

$$\frac{2\Omega f(\rho)\sin(\tilde{\phi})}{(1+\Omega^2 f(\rho)^2)^{5/2}} S^{\phi\phi(0)}\Omega^2\kappa_0 f(\rho)^4, \tag{4.90}$$

which fails to be zero. For splay free bundles, the situation is a little less obvious, but no less damning. Tangent force balance is satisfied, but substituting for $\delta\tilde{\phi}$ in the ρ and ϕ components of the Euler-Lagrange equations yields two incompatible equations for $\delta\tilde{s}$.

Since neither texture is in elastic equilibrium, we can in principle compare the two by evaluating their elastic energy directly. Taking exactly the form for the tangent field given in Ch. 2, we have left to solve for a radial deformation field, $f(\rho)$, as in the helical bundle case. Substituting this whole-cloth into a Hookean energy density functional, we once again expand in powers of the central curve's curvature, κ_0. Integrating over $\tilde{\phi}$, the Eulerian angular coordinate, provides a relatively simple variational problem in $f(\rho)$, with corrections to the helical field at $\mathcal{O}(\varepsilon^2)$. Integrating over the energy functional for both the $\det(h) = 0$ and $\mathrm{tr}(h) = 0$ ansatzes then allows us to compare them directly for a range of twists and curvatures. Preliminary results

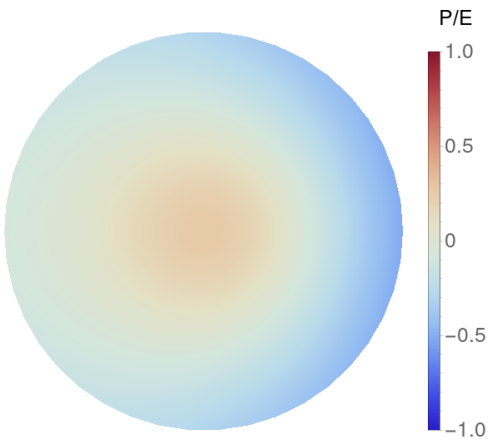

Figure 4.2: The pressure profile for a determinant free bundle with $\Omega R = 1$, $\kappa_0 R = .02$, and $K_{33} = 0$. Curvature induced modifications to the radial displacement field reduce the overall energy, while frustrated terms arising from twist-curvature coupling generate a $\tilde{\phi}$ dependent stress profile in the cross-section.

in this direction are shown in Fig. 4.2, which shows a pressure profile derived from the determinant free ansatz.

While we have shown here that the boundary value problem develops nasty singularities in the small curvature expansion around the helical bundles, we remain haunted by the prospect that these singularities may be phantoms, like many other specters which arise in Frenet-Serret frames with vanishing curvatures. To further explore this possibility, we can consider several slightly different perturbations, including expansion in twist around the isometric developable domain centered on a circle, and overtwisting an off-center helical bundle. Because twist appears only at second order in the developable domain case, however, and off-center helical domains lack the radial symmetry that makes solutions to the centered ones readily accessible, this too remains in its infancy.

There are also interesting questions raised by the non-manifold metric geometry we introduced in Ch. 3, and used in this chapter to describe the geometry of non-equidistant filament bundles. In this chapter, we derived one possible route to the force balance equations for twisted-toroidal filament bundles, based on linear pertur-

bations of the coordinates in the helical bundle case outlined above. In thin sheets, however, another, perhaps more common, approach would be to explicitly impose the geometric constraints on curvatures encoded in the Gauss-Codazzi-Mainardi equations as *Lagrange multipliers* in the variational problem [30]. While we hint in this following chapter at some possible generalizations for the non-integrable case, the constrained optimization problem solved by the writing of this dissertation has not yet allowed a complete exploration of the fundamental relationships between the "extrinsic" geometry encoded by the convective flow tensor, and the "intrinsic" geometry encoded by the derivatives in Eq. (4.16). We again note that, unlike surfaces, filament bundles can develop Gaussian curvature in the cross-section while remaining equidistant, by twisting without splay or biaxial splay [1]. We therefore anticipate that these geometric identities can be expressed in terms of twist-dependent corrections to the Gauss-Codazzi-Mainardi equations.

CHAPTER 5

OUTLOOK AND CONCLUSIONS

And for the first time in my life I think
that happiness may not be **having** *all*
the answers... it may be having time and
space to wonder.

EMILIE: La Marquise Du Châtelet
Defends Her Life Tonight
Lauren Gunderson

Frustrated filaments continue to fascinate and flummox, but we hope that the perspective presented above, focusing on the connections between stretching, symmetries, and shape, clarifies more than it confuses. A better understanding of the geometry of filament bundles, including recognition of the important role played by constant spacing in frustrating filament, follows from Ch. 2. While the role of geometric frustration in shaping materials' responses has long been recognized, we have now shown the importance of the previously unrecognized *longitudinal frustration*, which, notably, does not obviously fit into existing paradigms dependent on curvature [10], local misfit [19], and global topological constraints [132].

These geometric constraints on constant spacing also expose the weaknesses of prior two-dimensional treatments of the elasticity of columnar liquid-crystals. In Ch. 3, we explore this breakdown, and consider the geometric nonlinearities necessary to account for non-equidistant behavior. Perhaps most importantly, we have made substantial progress towards understanding the role of geometric nonlinearities in non-equidistant filament bundles by introducing a gauge-theoretic perspective on the elasticity theory for frustrated filament bundles in Ch. 3. With a tool fit for the

task, we then revisit the behavior of helical filament bundles, extending our analysis beyond the small twist limit, and incorporating the impact of bending elasticity.

We then once again turn our attention to non-equidistant configurations, in Ch. 4, deriving the force balance equations for twisted-toroidal filament bundles by perturbing around the helical state. While emergent singularities in the Euler-Lagrange equations interrupt our search for solutions, we gain important intuition about the behavior of small-curvature deformations. Not to be defeated, we also propose several possible workarounds to the problem of these singularities, and note some remarkable features of the non-manifold metric geometry which become apparent in the force-balance equations.

The theory of filament bundles looks very different than it did when we started, and we leave the field in possession of the elastic energy and geometrical framework necessary to study arbitrary fields of fibers. Unfortunately, non-linear partial differential equations will always be difficult to solve, but our hope is that we've made it so that the first step in future problems, from the specific shapes of slender bundles under loading to the instabilities that arise from untwisting—write down the energy—is now evident. The prospect of finding computational methods adapted to the elasticity of filament bundles also remains a challenge. While mesh-based partial differential equation solvers such as finite element methods, can be implemented for surfaces and volumes, there is not, to our knowledge, an obvious way to generalize the language of discrete differential geometry to the "continuous family of planes" setting of filament elasticity.

There are specific technical questions to be answered here as well. Beyond the obvious "find an equilibrium, twisted, non-equidistant configuration," it remains interesting to consider strictly minimally non-equidistant configurations under given constraints. Analogous to the relationship of fluid membranes to thin sheets, the minimizers of this "filament Willmore functional" (or, rather, of the Frank-Oseen

free energy when $K_{22} - K_{24} = K_{33} = 0$), may not have obvious, direct material relevance, but could provide insight into close packings of slender filaments of very stiff materials. We also encourage further consideration of filament assemblies with programmed uniform negative metric curvature, as yet another opportunity to probe the difference between the (relatively symmetric) response of thin-elastic sheets and the (highly asymmetric) response of filaments [47]. Further questions are raised by effective renormalization of the bending elasticity by internal twist degrees of freedom, which suggests that a suitable slender-bundle limit could provide a generic correspondence between the microscopic twist of a hierarchical filament assembly and its macroscopic elastic moduli.

Of course, there are applications beyond filaments as well. The gauge-theoretic perspective on filament elasticity presented in Ch. 3 generalizes naturally to other soft-elastic liquid crystals, but there is reason to believe it can be extended to other materials with continuous zero modes, like conformal mechanical metamaterials [107]. Here, the relevant symmetries are *conformal maps*, rather than reptations, but the idea is the same: by projecting out the zero modes from the deformation gradient in a way compatible with the metric of the embedding space, we hope that we can derive a strain measure which accounts explicitly for the non-linear behavior of large deformations.

BIBLIOGRAPHY

[1] Daria W. Atkinson, Christian D. Santangelo, and Gregory M. Grason. Constant spacing in filament bundles. *New Journal of Physics*, 21(6):062001, June 2019. ISSN 1367-2630. doi: 10.1088/1367-2630/ab1c2d. URL https://doi.org/10.1088%2F1367-2630%2Fab1c2d.

[43] Isaac R. Bruss and Gregory M. Grason. Non-Euclidean geometry of twisted filament bundle packing. *Proceedings of the National Academy of Sciences*, 109 (27):10781–10786, 2012.

[38] Y. Bouligand. Geometry of (non smectic) hexagonal mesophases. *Journal de Physique*, 41(11):1297–1306, 1980. doi: 10.1051/jphys:0198000410110129700. URL https://hal.archives-ouvertes.fr/jpa-00208957.

[39] M. Kléman. Developable domains in hexagonal liquid crystals. *Journal de Physique*, 41(7):737–745, 1980. doi: 10.1051/jphys:01980004107073700. URL https://hal.archives-ouvertes.fr/jpa-00209299.

[42] Jonathan V. Selinger and Robijn F. Bruinsma. Hexagonal and nematic phases of chains. I. Correlation functions. *Physical Review A*, 43(6):2910–2921, March 1991. doi: 10.1103/PhysRevA.43.2910. URL https://link.aps.org/doi/10.1103/PhysRevA.43.2910.

[46] Gregory M. Grason. Defects in crystalline packings of twisted filament bundles. I. Continuum theory of disclinations. *Physical Review E*, 85(3), March 2012. ISSN 1539-3755, 1550-2376. doi: 10.1103/PhysRevE.85.031603. URL https://link.aps.org/doi/10.1103/PhysRevE.85.031603.

[2] P. M. Chaikin and T. C. Lubensky. *Principles of Condensed Matter Physics*. Cambridge University Press, Cambridge, 1995. ISBN 978-0-521-79450-3. doi: 10.1017/CBO9780511813467. URL https://www.cambridge.org/core/books/principles-of-condensed-matter-physics/70C3D677A9B5BEC4A77CBBD0A8A23E64.

[3] Nakul Prabhakar Bende, Arthur A. Evans, Sarah Innes-Gold, Luis A. Marin, Itai Cohen, Ryan C. Hayward, and Christian D. Santangelo. Geometrically controlled snapping transitions in shells with curved creases. *Proceedings of the National Academy of Sciences*, 112(36):11175–11180, September 2015. ISSN 0027-8424, 1091-6490. doi: 10.1073/pnas.1509228112. URL https://www.pnas.org/content/112/36/11175. Publisher: National Academy of Sciences Section: Physical Sciences.

[4] H. S. Seung and David R. Nelson. Defects in flexible membranes with crystalline order. *Physical Review A*, 38(2):1005, 1988.

[5] Amir Azadi and Gregory M. Grason. Defects in crystalline packings of twisted filament bundles. II. Dislocations and grain boundaries. *Physical Review E*, 85(3), March 2012. ISSN 1539-3755, 1550-2376. doi: 10.1103/PhysRevE.85.031604. URL https://link.aps.org/doi/10.1103/PhysRevE.85.031604.

[6] Guangnan Meng, Jayson Paulose, David R. Nelson, and Vinothan N. Manoharan. Elastic Instability of a Crystal Growing on a Curved Surface. *Science*, 343(6171):634–637, February 2014. ISSN 0036-8075, 1095-9203. doi: 10.1126/science.1244827. URL http://science.sciencemag.org/content/343/6171/634.

[7] James P. Sethna, David C. Wright, and N. D. Mermin. Relieving cholesteric frustration: the blue phase in a curved space. *Physical Review Letters*, 51(6): 467, 1983.

[8] David C. Wright and N. David Mermin. Crystalline liquids: the blue phases. *Reviews of Modern Physics*, 61(2):385, 1989.

[9] M. Kléman. Frustration in polymers. *Journal de Physique Lettres*, 46(16):723–732, 1985. doi: 10.1051/jphyslet:019850046016072300. URL https://hal.archives-ouvertes.fr/jpa-00232890.

[10] Jean-François Sadoc and Rémy Mosseri. *Geometrical Frustration*. Collection Alea-Saclay: Monographs and Texts in Statistical Physics. Cambridge University Press, 1999. doi: 10.1017/CBO9780511599934.

[11] Douglas M. Hall, Isaac R. Bruss, Justin R. Barone, and Gregory M. Grason. Morphology selection via geometric frustration in chiral filament bundles. *Nature Materials*, 15(7):727–732, July 2016. ISSN 1476-1122, 1476-4660. doi: 10.1038/nmat4598. URL http://www.nature.com/articles/nmat4598.

[12] Idan Niv and Efi Efrati. Geometric frustration and compatibility conditions for two-dimensional director fields. *Soft Matter*, 14(3):424–431, January 2018. ISSN 1744-6848. doi: 10.1039/C7SM01672G. URL http://pubs.rsc.org/en/content/articlelanding/2018/sm/c7sm01672g.

[13] Yael Klein, Efi Efrati, and Eran Sharon. Shaping of Elastic Sheets by Prescription of Non-Euclidean Metrics. *Science*, 315(5815):1116–1120, February 2007. ISSN 0036-8075, 1095-9203. doi: 10.1126/science.1135994. URL https://science.sciencemag.org/content/315/5815/1116.

[14] Jungwook Kim, James A. Hanna, Myunghwan Byun, Christian D. Santangelo, and Ryan C. Hayward. Designing Responsive Buckled Surfaces by Halftone Gel Lithography. *Science*, 335(6073):1201–1205, March 2012. ISSN 0036-8075, 1095-9203. doi: 10.1126/science.1215309. URL https://science.sciencemag.org/content/335/6073/1201.

[15] A. R. Bausch, M. J. Bowick, A. Cacciuto, A. D. Dinsmore, M. F. Hsu, D. R. Nelson, M. G. Nikolaides, A. Travesset, and D. A. Weitz. Grain Boundary Scars and Spherical Crystallography. *Science*, 299(5613):1716, March 2003. doi: 10.1126/science.1081160. URL `http://science.sciencemag.org/content/299/5613/1716.abstract`.

[16] Gregory M. Grason. Chiral and achiral mechanisms of self-limiting, twisted bundle assembly. *arXiv:1909.05208 [cond-mat]*, September 2019. URL `http://arxiv.org/abs/1909.05208`. arXiv: 1909.05208.

[17] Richard S Millman and George D. Parker. *Elements of Differential Geometry*. Englewood Cliffs, N.J. : Prentice-Hall, 1977. ISBN 0132641437.

[18] Joseph D. Paulsen, Evan Hohlfeld, Hunter King, Jiangshui Huang, Zhanlong Qiu, Thomas P. Russell, Narayanan Menon, Dominic Vella, and Benny Davidovitch. Curvature-induced stiffness and the spatial variation of wavelength in wrinkled sheets. *Proceedings of the National Academy of Sciences*, 113(5): 1144–1149, February 2016. ISSN 0027-8424, 1091-6490. doi: 10.1073/pnas.1521520113. URL `https://www.pnas.org/content/113/5/1144`.

[19] Gregory M. Grason. Misfits unite. *Nature Physics*, 13(12):1149–1150, December 2017. ISSN 1745-2481. doi: 10.1038/nphys4201. URL `http://www.nature.com/articles/nphys4201`. Number: 12 Publisher: Nature Publishing Group.

[20] José Bico, Benoît Roman, Loïc Moulin, and Arezki Boudaoud. Adhesion: Elastocapillary coalescence in wet hair. *Nature*, 432(7018):690, December 2004. ISSN 1476-4687. doi: 10.1038/432690a. URL `https://www.nature.com/articles/432690a`.

[21] Mei Zhang, Ken R. Atkinson, and Ray H. Baughman. Multifunctional Carbon Nanotube Yarns by Downsizing an Ancient Technology. *Science*, 306(5700): 1358–1361, November 2004. ISSN 0036-8075, 1095-9203. doi: 10.1126/science.1104276. URL `http://science.sciencemag.org/content/306/5700/1358`.

[22] Andreas Thess, Roland Lee, Pavel Nikolaev, Hongjie Dai, Pierre Petit, Jerome Robert, Chunhui Xu, Young Hee Lee, Seong Gon Kim, Andrew G. Rinzler, Daniel T. Colbert, Gustavo E. Scuseria, David Tománek, John E. Fischer, and Richard E. Smalley. Crystalline Ropes of Metallic Carbon Nanotubes. *Science*, 273(5274):483–487, July 1996. ISSN 0036-8075, 1095-9203. doi: 10.1126/science.273.5274.483. URL `http://science.sciencemag.org.silk.library.umass.edu/content/273/5274/483`.

[23] F. Livolant, A. M. Levelut, J. Doucet, and J. P. Benoit. The highly concentrated liquid-crystalline phase of DNA is columnar hexagonal. *Nature*, 339:724, June 1989. URL `http://dx.doi.org/10.1038/339724a0`.

[24] Y. Bouligand. Defects and textures of hexagonal discotics. *Journal de Physique*, 41(11):1307–1315, 1980. doi: 10.1051/jphys:0198000410110130700. URL https://hal.archives-ouvertes.fr/jpa-00208958.

[25] George A. Costello. *Theory of Wire Rope*. Mechanical Engineering Series. Springer-Verlag, New York, 1990. ISBN 978-0-387-97189-6. doi: 10.1007/978-1-4684-0350-3. URL https://mathscinet.ams.org/mathscinet-getitem?mr=1101811.

[26] E. N. Gilbert. The packing problem for twisted pairs. *The Bell System Technical Journal*, 58(10):2143–2162, December 1979. ISSN 0005-8580. doi: 10.1002/j.1538-7305.1979.tb02960.x.

[27] Th V Kármán. Festigkeitsprobleme im maschinenbau. In *Mechanik*, pages 311–385. Springer, 1907.

[28] August Föppl. *Vorlesungen über technische Mechanik*, volume 6. BG Teubner, 1909.

[29] Philippe G. Ciarlet. An Introduction to Differential Geometry with Applications to Elasticity. *Journal of Elasticity*, 78(1):1–215, January 2005. ISSN 1573-2681. doi: 10.1007/s10659-005-4738-8. URL https://doi.org/10.1007/s10659-005-4738-8.

[30] E. Efrati, E. Sharon, and R. Kupferman. Elastic theory of unconstrained non-Euclidean plates. *Journal of the Mechanics and Physics of Solids*, 57(4):762–775, April 2009. ISSN 0022-5096. doi: 10.1016/j.jmps.2008.12.004. URL http://www.sciencedirect.com/science/article/pii/S0022509608002160.

[31] Efi Efrati, Eran Sharon, and Raz Kupferman. The metric description of elasticity in residually stressed soft materials. *Soft Matter*, 9(34):8187–8197, August 2013. ISSN 1744-6848. doi: 10.1039/C3SM50660F. URL http://pubs.rsc.org/en/content/articlelanding/2013/sm/c3sm50660f.

[32] W. T. Koiter. On the nonlinear theory of thin elastic shells. *Proc. Koninkl. Ned. Akad. van Wetenschappen, Series B*, 69:1–54, 1966. URL https://ci.nii.ac.jp/naid/10003111993/en/.

[33] Salem Al Mosleh and Christian Santangelo. Nonlinear mechanics of rigidifying curves. *Physical Review E*, 96(1):013003, July 2017. doi: 10.1103/PhysRevE.96.013003. URL https://link.aps.org/doi/10.1103/PhysRevE.96.013003.

[34] F. C. Frank. I. Liquid crystals. On the theory of liquid crystals. *Discussions of the Faraday Society*, 25:19, 1958. ISSN 0366-9033. doi: 10.1039/df9582500019. URL http://xlink.rsc.org/?DOI=df9582500019.

[35] Thomas Machon and Gareth P. Alexander. Umbilic Lines in Orientational Order. *Physical Review X*, 6(1):011033, March 2016. doi: 10.1103/PhysRevX.6.011033. URL https://link.aps.org/doi/10.1103/PhysRevX.6.011033.

[36] Jonathan V. Selinger. Interpretation of saddle-splay and the Oseen-Frank free energy in liquid crystals. *Liquid Crystals Reviews*, 6(2):129–142, July 2018. ISSN 2168-0396. doi: 10.1080/21680396.2019.1581103. URL https://doi.org/10.1080/21680396.2019.1581103.

[37] Epifanio G. Virga. Uniform distortions and generalized elasticity of liquid crystals. *Physical Review E*, 100(5):052701, November 2019. doi: 10.1103/PhysRevE.100.052701. URL https://link.aps.org/doi/10.1103/PhysRevE.100.052701. Publisher: American Physical Society.

[40] Randall D. Kamien and David R. Nelson. Iterated Moiré Maps and Braiding of Chiral Polymer Crystals. *Physical Review Letters*, 74(13):2499–2502, March 1995. doi: 10.1103/PhysRevLett.74.2499. URL https://link.aps.org/doi/10.1103/PhysRevLett.74.2499.

[41] Randall D. Kamien and David R. Nelson. Defects in chiral columnar phases: tilt-grain boundaries and iterated moiré maps. *Physical Review E*, 53(1):650, 1996.

[44] Gregory M. Grason and Robijn F. Bruinsma. Chirality and Equilibrium Biopolymer Bundles. *Physical Review Letters*, 99(9), August 2007. ISSN 0031-9007, 1079-7114. doi: 10.1103/PhysRevLett.99.098101. URL https://link.aps.org/doi/10.1103/PhysRevLett.99.098101.

[45] Gregory M. Grason. Braided bundles and compact coils: The structure and thermodynamics of hexagonally packed chiral filament assemblies. *Physical Review E*, 79(4), April 2009. ISSN 1539-3755, 1550-2376. doi: 10.1103/PhysRevE.79.041919. URL https://link.aps.org/doi/10.1103/PhysRevE.79.041919.

[47] Isaac R. Bruss and Gregory M. Grason. Defect-Driven Shape Instabilities of Bundles. *Physical Review X*, 8(3):031046, August 2018. doi: 10.1103/PhysRevX.8.031046. URL https://link.aps.org/doi/10.1103/PhysRevX.8.031046.

[48] Randall D. Kamien. Liquids with Chiral Bond Order. *Journal de Physique II*, 6 (4):461–475, April 1996. ISSN 1155-4312, 1286-4870. doi: 10.1051/jp2:1996192. URL http://dx.doi.org/10.1051/jp2:1996192.

[49] J. Swift and B.S. Andereck. Statics and dynamics near the nematic-columnar phase transition in liquid crystals. *Journal de Physique Lettres*, 43(12):437–440, 1982. doi: 10.1051/jphyslet:019820043012043700. URL https://hal.archives-ouvertes.fr/jpa-00232073. Publisher: Edp sciences.

[50] Barrett O'Neill. The fundamental equations of a submersion. *The Michigan Mathematical Journal*, 13(4):459–469, December 1966. ISSN 0026-2285, 1945-2365. doi: 10.1307/mmj/1028999604. URL https://projecteuclid.org/euclid.mmj/1028999604.

[51] Gregory M. Grason. *Colloquium* : Geometry and optimal packing of twisted columns and filaments. *Reviews of Modern Physics*, 87(2):401–419, May 2015. ISSN 0034-6861, 1539-0756. doi: 10.1103/RevModPhys.87.401. URL https://link.aps.org/doi/10.1103/RevModPhys.87.401.

[52] Andreea Panaitescu, Gregory M. Grason, and Arshad Kudrolli. Measuring geometric frustration in twisted inextensible filament bundles. *Physical Review E*, 95(5), May 2017. ISSN 2470-0045, 2470-0053. doi: 10.1103/PhysRevE.95.052503. URL http://link.aps.org/doi/10.1103/PhysRevE.95.052503.

[53] Andreea Panaitescu, Gregory M. Grason, and Arshad Kudrolli. Persistence of Perfect Packing in Twisted Bundles of Elastic Filaments. *Physical Review Letters*, 120(24):248002, June 2018. doi: 10.1103/PhysRevLett.120.248002. URL https://link.aps.org/doi/10.1103/PhysRevLett.120.248002.

[54] Tomaso Aste and D. L Weaire. *The Pursuit of Perfect Packing*. Taylor & Francis, New York, 2008. ISBN 978-1-4200-6817-7 978-1-4200-6818-4. URL http://www.crcnetbase.com/isbn/9781420068184.

[55] John Conway and Neil J. A. Sloane. *Sphere Packings, Lattices and Groups*. Springer Science & Business Media, December 1998. ISBN 978-0-387-98585-5.

[56] Maurice Kléman. *Points, lines, and walls: in liquid crystals, magnetic systems, and various ordered media*. J. Wiley, Chichester; New York, 1983. ISBN 978-0-471-10194-9.

[57] Jayanth R. Banavar and Amos Maritan. Colloquium: Geometrical approach to protein folding: a tube picture. *Reviews of Modern Physics*, 75(1):23–34, January 2003. doi: 10.1103/RevModPhys.75.23. URL https://link.aps.org/doi/10.1103/RevModPhys.75.23.

[58] Jayanth R. Banavar, Oscar Gonzalez, John H. Maddocks, and Amos Maritan. Self-Interactions of Strands and Sheets. *Journal of Statistical Physics*, 110(1):35–50, January 2003. ISSN 1572-9613. doi: 10.1023/A:1021010526495. URL https://doi.org/10.1023/A:1021010526495.

[59] S. Neukirch and G.H.M. van der Heijden. Geometry and Mechanics of Uniform n-Plies: from Engineering Ropes to Biological Filaments. *Journal of Elasticity*, 69(1):41–72, November 2002. ISSN 1573-2681. doi: 10.1023/A:1027390700610. URL https://doi.org/10.1023/A:1027390700610.

[60] Laurent Bozec, Gert van der Heijden, and Michael Horton. Collagen Fibrils: Nanoscale Ropes. *Biophysical Journal*, 92(1):70–75, January 2007. ISSN 0006-3495. doi: 10.1529/biophysj.106.085704. URL http://www.sciencedirect.com/science/article/pii/S0006349507708056.

[61] Jakob Bohr and Kasper Olsen. The close-packed triple helix as a possible new structural motif for collagen. *Theoretical Chemistry Accounts*, 130(4):1095–1103, December 2011. ISSN 1432-2234. doi: 10.1007/s00214-010-0761-3. URL https://doi.org/10.1007/s00214-010-0761-3.

[62] Yehuda Snir and Randall D. Kamien. Entropically Driven Helix Formation. *Science*, 307(5712):1067–1067, February 2005. ISSN 0036-8075, 1095-9203. doi: 10.1126/science.1106243. URL http://science.sciencemag.org.silk.library.umass.edu/content/307/5712/1067.

[63] Christian D. Santangelo, Vincenzo Vitelli, Randall D. Kamien, and David R. Nelson. Geometric Theory of Columnar Phases on Curved Substrates. *Physical Review Letters*, 99(1), July 2007. ISSN 0031-9007, 1079-7114. doi: 10.1103/PhysRevLett.99.017801. URL https://link.aps.org/doi/10.1103/PhysRevLett.99.017801.

[64] Felix Knöppel, Keenan Crane, Ulrich Pinkall, and Peter Schröder. Stripe Patterns on Surfaces. *ACM Trans. Graph.*, 34(4):39:1–39:11, July 2015. ISSN 0730-0301. doi: 10.1145/2767000. URL http://doi.acm.org/10.1145/2767000.

[65] E L Starostin. On the perfect hexagonal packing of rods. *Journal of Physics: Condensed Matter*, 18(14):S187–S204, April 2006. ISSN 0953-8984, 1361-648X. doi: 10.1088/0953-8984/18/14/S04. URL http://stacks.iop.org/0953-8984/18/i=14/a=S04?key=crossref.50f3869b7f0c190bef52a888387c16b0.

[66] Nicholas V. Hud and Kenneth H. Downing. Cryoelectron microscopy of λ phage DNA condensates in vitreous ice: the fine structure of DNA toroids. *Proceedings of the National Academy of Sciences*, 98(26):14925–14930, 2001.

[67] Amélie Leforestier and Françoise Livolant. Structure of toroidal DNA collapsed inside the phage capsid. *Proceedings of the National Academy of Sciences*, 106 (23):9157–9162, June 2009. ISSN 0027-8424, 1091-6490. doi: 10.1073/pnas.0901240106. URL http://www.pnas.org/content/106/23/9157.

[68] Alan Cooper. The precipitation of toroidal collagen fibrils. *Biochemical Journal*, 112(4):515–519, May 1969. ISSN 0264-6021. URL https://www.ncbi.nlm.nih.gov/pmc/articles/PMC1187741/.

[69] Bryan Gin-ge Chen, Paul J. Ackerman, Gareth P. Alexander, Randall D. Kamien, and Ivan I. Smalyukh. Generating the Hopf Fibration Experimentally in Nematic Liquid Crystals. *Physical Review Letters*, 110(23):237801, June 2013. doi: 10.1103/PhysRevLett.110.237801. URL https://link.aps.org/doi/10.1103/PhysRevLett.110.237801.

[70] Paul J. Ackerman and Ivan I. Smalyukh. Diversity of Knot Solitons in Liquid Crystals Manifested by Linking of Preimages in Torons and Hopfions. *Physical Review X*, 7(1):011006, January 2017. doi: 10.1103/PhysRevX.7.011006. URL https://link.aps.org/doi/10.1103/PhysRevX.7.011006.

[71] Paul J. Ackerman and Ivan I. Smalyukh. Static three-dimensional topological solitons in fluid chiral ferromagnets and colloids. *Nature Materials*, 16(4):426–432, April 2017. ISSN 1476-1122, 1476-4660. doi: 10.1038/nmat4826. URL http://www.nature.com/articles/nmat4826.

[72] Paul Sutcliffe. Skyrmion Knots in Frustrated Magnets. *Physical Review Letters*, 118(24), June 2017. ISSN 0031-9007, 1079-7114. doi: 10.1103/PhysRevLett.118.247203. URL http://link.aps.org/doi/10.1103/PhysRevLett.118.247203.

[73] Paul Sutcliffe. Hopfions in chiral magnets. *Journal of Physics A: Mathematical and Theoretical*, 51(37):375401, September 2018. ISSN 1751-8113, 1751-8121. doi: 10.1088/1751-8121/aad521. URL http://stacks.iop.org/1751-8121/51/i=37/a=375401?key=crossref.81dd37b5db435cd0f1e6fc069fa140bd.

[74] Yizhou Liu, Roger K. Lake, and Jiadong Zang. Binding a hopfion in a chiral magnet nanodisk. *Physical Review B*, 98(17), November 2018. ISSN 2469-9950, 2469-9969. doi: 10.1103/PhysRevB.98.174437. URL https://link.aps.org/doi/10.1103/PhysRevB.98.174437.

[75] J F Sadoc and J Charvolin. 3-sphere fibrations: a tool for analyzing twisted materials in condensed matter. *Journal of Physics A: Mathematical and Theoretical*, 42(46):465209, November 2009. ISSN 1751-8113, 1751-8121. doi: 10.1088/1751-8113/42/46/465209. URL http://stacks.iop.org/1751-8121/42/i=46/a=465209?

[76] I. M Kulić, D Andrienko, and M Deserno. Twist-bend instability for toroidal DNA condensates. *Europhysics Letters*, 67(3):418–424, August 2004. ISSN 0295-5075, 1286-4854. doi: 10.1209/epl/i2004-10076-x. URL https://iopscience.iop.org/article/10.1209/epl/i2004-10076-x/meta.

[77] Isaac R. Bruss and Gregory M. Grason. Topological defects, surface geometry and cohesive energy of twisted filament bundles. *Soft Matter*, 9(34):8327, 2013. ISSN 1744-683X, 1744-6848. doi: 10.1039/c3sm50672j. URL http://xlink.rsc.org/?DOI=c3sm50672j.

[78] Luis Cajamarca and Gregory M. Grason. Geometry of flexible filament cohesion: Better contact through twist? *The Journal of Chemical Physics*, 141(17):174904, November 2014. ISSN 0021-9606. doi: 10.1063/1.4900983. URL https://aip.scitation.org/doi/10.1063/1.4900983.

[79] Yuezhou Wang, Igor Ostanin, Cristian Gaidău, and Traian Dumitrică. Twisting Carbon Nanotube Ropes with the Mesoscopic Distinct Element Method: Geometry, Packing, and Nanomechanics. *Langmuir*, 31(45):12323–12327, November 2015. ISSN 0743-7463, 1520-5827. doi: 10.1021/acs.langmuir.5b03208. URL http://pubs.acs.org/doi/10.1021/acs.langmuir.5b03208.

[80] O. Gonzalez, J. H. Maddocks, F. Schuricht, and H. von der Mosel. Global curvature and self-contact of nonlinearly elastic curves and rods. *Calculus of Variations and Partial Differential Equations*, 14(1):29–68, January 2002. ISSN 0944-2669, 1432-0835. doi: 10.1007/s005260100089. URL https://link.springer.com/article/10.1007/s005260100089.

[81] Jason Cantarella, Robert B. Kusner, and John M. Sullivan. On the minimum ropelength of knots and links. *Inventiones mathematicae*, 150(2):257–286, November 2002. ISSN 0020-9910, 1432-1297. doi: 10.1007/s00222-002-0234-y. URL https://link.springer.com/article/10.1007/s00222-002-0234-y.

[82] Oscar Gonzalez and John H. Maddocks. Global curvature, thickness, and the ideal shapes of knots. *Proceedings of the National Academy of Sciences*, 96(9):4769–4773, April 1999. ISSN 0027-8424, 1091-6490. doi: 10.1073/pnas.96.9.4769. URL http://www.pnas.org/content/96/9/4769.

[83] M.-F. Achard, M. Kléman, Yu. A. Nastishin, and H.-T. Nguyen. Liquid crystal helical ribbons as isometric textures. *The European Physical Journal E*, 16(1):37–47, January 2005. ISSN 1292-8941, 1292-895X. doi: 10.1140/epje/e2005-00005-2. URL http://link.springer.com/10.1140/epje/e2005-00005-2.

[84] D. A. Coleman, J. Fernsler, N. Chattham, M. Nakata, Y. Takanishi, E. Körblova, D. R. Link, R.-F. Shao, W. G. Jang, and J. E. Maclennan. Polarization-modulated smectic liquid crystal phases. *Science*, 301(5637):1204–1211, 2003.

[85] Detlef Gromoll and Gerard Walschap. *Submersions, Foliations, and Metrics*, pages 1–44. Birkhäuser Basel, Basel, 2009. ISBN 978-3-7643-8715-0. doi: 10.1007/978-3-7643-8715-0. URL https://doi.org/10.1007/978-3-7643-8715-0.

[86] Alejandro D. Rey. Liquid crystal models of biological materials and processes. *Soft Matter*, 6(15):3402–3429, July 2010. ISSN 1744-6848. doi: 10.1039/B921576J. URL https://pubs.rsc.org/en/content/articlelanding/2010/sm/b921576j.

[87] H. Shin and G. M. Grason. Filling the void in confined polymer nematics: Phase transitions in a minimal model of dsDNA packing. *Europhysics Letters*, 96(3):36007, November 2011. ISSN 0295-5075, 1286-4854. doi: 10.1209/0295-5075/96/36007. URL https://epljournal.edpsciences.org/articles/epl/abs/2011/21/epl13948/epl13948.html.

[88] Aidan I. Brown, Laurent Kreplak, and Andrew D. Rutenberg. An equilibrium double-twist model for the radial structure of collagen fibrils. *Soft Matter*, 10(42):8500–8511, October 2014. ISSN 1744-6848. doi: 10.1039/C4SM01359J. URL https://pubs.rsc.org/en/content/articlelanding/2014/sm/c4sm01359j.

[89] P. G. de Gennes and J. Prost. *The Physics of Liquid Crystals*. International Series of Monographs on Physics. Oxford University Press, Oxford, New York, second edition edition, August 1995. ISBN 978-0-19-851785-6.

[90] Anthony Charles Neville. *Biology of Fibrous Composites: Development beyond the Cell Membrane*. Cambridge University Press, 1993. doi: 10.1017/CBO9780511601101.

[91] Yves Bouligand. Liquid crystals and biological morphogenesis: Ancient and new questions. *Comptes Rendus Chimie*, 11(3):281–296, March 2008. ISSN 1631-0748. doi: 10.1016/j.crci.2007.10.001. URL http://www.sciencedirect.com/science/article/pii/S1631074807002615.

[92] Douglas M. Hall and Gregory M. Grason. How geometric frustration shapes twisted fibres, inside and out: competing morphologies of chiral filament assembly. *Interface Focus*, 7(4):20160140, August 2017. doi: 10.1098/rsfs.2016.0140. URL https://royalsocietypublishing.org/doi/full/10.1098/rsfs.2016.0140.

[93] Vinzenz Koning, Benjamin C. van Zuiden, Randall D. Kamien, and Vincenzo Vitelli. Saddle-splay screening and chiral symmetry breaking in toroidal nematics. *Soft Matter*, 10(23):4192–4198, May 2014. ISSN 1744-6848. doi: 10.1039/C4SM00076E. URL https://pubs.rsc.org/en/content/articlelanding/2014/sm/c4sm00076e.

[94] J. Charvolin and J. F. Sadoc. A geometrical template for toroidal aggregates of chiral macromolecules. *The European Physical Journal E*, 25(3):335–341, March 2008. ISSN 1292-8941, 1292-895X. doi: 10.1140/epje/i2008-10313-8. URL http://link.springer.com/10.1140/epje/i2008-10313-8.

[95] Rémy Mosseri and Jean-François Sadoc. Hopf fibrations and frustrated matter. *Structural Chemistry*, 23(4):1071–1078, aug 2012. ISSN 1040-0400, 1572-9001. doi: 10.1007/s11224-012-0010-6. URL http://link.springer.com/10.1007/s11224-012-0010-6.

[96] P. G. de Gennes. Polymeric liquid crystals: Frank elasticity and light scattering. *Molecular Crystals and Liquid Crystals*, 34(8):177–182, August 1976. ISSN 0026-8941. doi: 10.1080/15421407708083702. URL https://www.tandfonline.com/doi/full/10.1080/15421407708083702.

[97] Barbara Brodsky and Anton V. Persikov. Molecular Structure of the Collagen Triple Helix. In *Advances in Protein Chemistry*, volume 70 of *Fibrous Proteins: Coiled-Coils, Collagen and Elastomers*, pages 301–339. Academic Press, January 2005. doi: 10.1016/S0065-3233(05)70009-7. URL http://www.sciencedirect.com/science/article/pii/S0065323305700097.

[98] Vsevolod Katritch, Jan Bednar, Didier Michoud, Robert G. Scharein, Jacques Dubochet, and Andrzej Stasiak. Geometry and physics of knots. *Nature*, 384 (6605):142–145, November 1996. ISSN 1476-4687. doi: 10.1038/384142a0. URL https://www.nature.com/articles/384142a0.

[99] M. Carlen, B. Laurie, J. H. Maddocks, and J. Smutny. BIARCS, GLOBAL RADIUS OF CURVATURE, AND THE COMPUTATION OF IDEAL KNOT SHAPES. In *Physical and Numerical Models in Knot Theory*, volume 36 of *Series on Knots and Everything*, chapter 5, pages 75–108. WORLD SCIENTIFIC, September 2005. ISBN 978-981-256-187-9 978-981-270-346-0. doi: 10.1142/9789812703460_0005.

[100] Ted Ashton, Jason Cantarella, Michael Piatek, and Eric J. Rawdon. Knot Tightening by Constrained Gradient Descent. *Experimental Mathematics*, 20(1):57–90, March 2011. ISSN 1058-6458, 1944-950X. doi: 10.1080/10586458.2011.544581. URL http://www.tandfonline.com/doi/abs/10.1080/10586458.2011.544581.

[101] Jorge A Calvo, Kenneth C Millett, Eric J Rawdon, and Andrzej Stasiak. *Physical and Numerical Models in Knot Theory*, volume 36 of *Series on Knots and Everything*. WORLD SCIENTIFIC, 2005. doi: 10.1142/5766.

[102] E. J. Janse van Rensburg. A tutorial on knot energies. In *Physical and Numerical Models in Knot Theory*, volume 36 of *Series on Knots and Everything*, chapter 2, pages 19–44. WORLD SCIENTIFIC, September 2005. ISBN 978-981-256-187-9. doi: 10.1142/9789812703460_0002.

[103] L. Faddeev and Antti J. Niemi. Stable knot-like structures in classical field theory. *Nature*, 387(6628):58, May 1997. ISSN 1476-4687. doi: 10.1038/387058a0. URL https://www.nature.com/articles/387058a0.

[104] Richard A. Battye and P. M. Sutcliffe. Knots as Stable Soliton Solutions in a Three-Dimensional Classical Field Theory. *Physical Review Letters*, 81(22):4798–4801, November 1998. ISSN 0031-9007, 1079-7114. doi: 10.1103/PhysRevLett.81.4798. URL https://link.aps.org/doi/10.1103/PhysRevLett.81.4798.

[105] Jane Austen. *Pride and Prejudice*. T. Egerton, 1813.

[106] Xiaoming Mao, Ning Xu, and T. C. Lubensky. Soft Modes and Elasticity of Nearly Isostatic Lattices: Randomness and Dissipation. *Physical Review Letters*, 104(8):085504, February 2010. doi: 10.1103/PhysRevLett.104.085504. URL https://link.aps.org/doi/10.1103/PhysRevLett.104.085504.

[107] K. Sun, A. Souslov, X. Mao, and T. C. Lubensky. Surface phonons, elastic response, and conformal invariance in twisted kagome lattices. *Proceedings of the National Academy of Sciences*, 109(31):12369–12374, July 2012. ISSN 0027-8424, 1091-6490. doi: 10.1073/pnas.1119941109. URL http://www.pnas.org/cgi/doi/10.1073/pnas.1119941109.

[108] M. Warner, P. Bladon, and E. M. Terentjev. "Soft elasticity" — deformation without resistance in liquid crystal elastomers. *Journal de Physique II*, 4(1): 93–102, January 1994. ISSN 1155-4312, 1286-4870. doi: 10.1051/jp2:1994116. URL http://jp2.journaldephysique.org/10.1051/jp2:1994116.

[109] Patrick Oswald and Pawel Pieranski. *Smectic and Columnar Liquid Crystals*. Taylor & Francis, 2006.

[110] Amélie Leforestier, Antonio Šiber, Françoise Livolant, and Rudolf Podgornik. Protein-DNA Interactions Determine the Shapes of DNA Toroids Condensed in Virus Capsids. *Biophysical Journal*, 100(9):2209–2216, May 2011. ISSN 0006-3495. doi: 10.1016/j.bpj.2011.03.012. URL http://www.sciencedirect.com/science/article/pii/S0006349511003225.

[111] Serban L. Ilca, Xiaoyu Sun, Kamel El Omari, Abhay Kotecha, Felix de Haas, Frank DiMaio, Jonathan M. Grimes, David I. Stuart, Minna M. Poranen, and Juha T. Huiskonen. Multiple liquid crystalline geometries of highly compacted nucleic acid in a dsRNA virus. *Nature*, 570(7760):252–256, June 2019. ISSN 1476-4687. doi: 10.1038/s41586-019-1229-9. URL http://www.nature.com/articles/s41586-019-1229-9. Number: 7760 Publisher: Nature Publishing Group.

[112] Noa Rubin, Emanuel Perugia, Michal Goldschmidt, Mati Fridkin, and Lia Addadi. Chirality of Amyloid Suprastructures. *Journal of the American Chemical Society*, 130(14):4602–4603, April 2008. ISSN 0002-7863. doi: 10.1021/ja800328y. URL https://doi.org/10.1021/ja800328y.

[113] Jean-Christophe P. Gabriel, Franck Camerel, Bruno J. Lemaire, Hervé Desvaux, Patrick Davidson, and Patrick Batail. Swollen liquid-crystalline lamellar phase based on extended solid-like sheets. *Nature*, 413(6855):504–508, October 2001. ISSN 1476-4687. doi: 10.1038/35097046. URL http://www.nature.com/articles/35097046. Number: 6855 Publisher: Nature Publishing Group.

[114] D. G. Phillips, Canh-Dung Tran, W. B. Fraser, and G. H. M. van der Heijden. Torsional properties of staple fibre plied yarns. *The Journal of The Textile Institute*, 101(7):595–612, June 2010. ISSN 0040-5000. doi: 10.1080/00405000802632886. URL https://doi.org/10.1080/00405000802632886.

[115] Samuel Poincloux, Tian Chen, Basile Audoly, and Pedro Reis. What is the bending rigidity of a book? stacked plates as a dissipative structured beam. *Bulletin of the American Physical Society*, 2020.

[116] G. Grinstein and Robert A. Pelcovits. Nonlinear elastic theory of smectic liquid crystals. *Physical Review A*, 26(2):915–925, August 1982. doi: 10.1103/PhysRevA.26.915. URL https://link.aps.org/doi/10.1103/PhysRevA.26.915.

[117] C. N. Yang and R. L. Mills. Conservation of Isotopic Spin and Isotopic Gauge Invariance. *Physical Review*, 96(1):191–195, October 1954. doi: 10.1103/PhysRev.96.191. URL https://link.aps.org/doi/10.1103/PhysRev.96.191. Publisher: American Physical Society.

[118] Glen E. Bredon. *Topology and Geometry*. Graduate Texts in Mathematics. Springer-Verlag, New York, 1993. ISBN 978-0-387-97926-7. URL https://www.springer.com/gp/book/9780387979267.

[119] R. W. Sharpe. *Differential Geometry: Cartan's Generalization of Klein's Erlangen Program*. Graduate Texts in Mathematics. Springer-Verlag, New York, 1997. ISBN 978-0-387-94732-7. URL https://www.springer.com/gp/book/9780387947327.

[120] P. G. de Gennes. An analogy between superconductors and smectics A. *Solid State Communications*, 10(9):753–756, May 1972. ISSN 0038-1098. doi: 10.1016/0038-1098(72)90186-X. URL http://www.sciencedirect.com/science/article/pii/003810987290186X.

[121] T. C. Lubensky, G. Grinstein, and Robert A Pelcovits. Gauge transformations and anharmonic effects in smectic liquid crystals. *Physical Review B*, 25(9):6022–6025, May 1982. doi: 10.1103/PhysRevB.25.6022. URL https://link.aps.org/doi/10.1103/PhysRevB.25.6022.

[122] Claudio Giannessi. Frank energy for a discotic liquid crystal. *Physical Review A*, 34(1):705–706, July 1986. doi: 10.1103/PhysRevA.34.705. URL https://link.aps.org/doi/10.1103/PhysRevA.34.705.

[123] Olaf Stenull and T. C Lubensky. Phase Elasticity. *private communication*, 2009.

[124] C. D. Santangelo and Randall D. Kamien. Bogomol'nyi, Prasad, and Sommerfield Configurations in Smectics. *Physical Review Letters*, 91(4):045506, July 2003. doi: 10.1103/PhysRevLett.91.045506. URL https://link.aps.org/doi/10.1103/PhysRevLett.91.045506.

[125] Carl Friedrich Gauss. *Principia generalia Theoriae Figurae Fluidorum in statu Aequilibrii*. Dietrichs, 1834.

[126] Xin Cao and Weiguo Wu. The establishment of a mechanics model of multi-strand wire rope subjected to bending load with finite element simulation and experimental verification. *International Journal of Mechanical Sciences*, 142-143:289–303, July 2018. ISSN 0020-7403. doi: 10.1016/j.ijmecsci.2018.04.051. URL http://www.sciencedirect.com/science/article/pii/S0020740318309111.

[127] Nicholas Hud and Igor Vilfan. Toroidal DNA Condensates: Unraveling the Fine Structure and the Role of Nucleation in Determining Size. *Annual Review of Biophysics and Biomolecular Structure*, 34(1), February 2005. doi: 10.1146/annurev.biophys.34.040204.144500.

[128] A. Cardou and C. Jolicoeur. Mechanical Models of Helical Strands. *Applied Mechanics Reviews*, 50(1):1–14, January 1997. ISSN 0003-6900. doi: 10.1115/1.3101684. URL `http://dx.doi.org/10.1115/1.3101684`.

[129] J. M. T. Thompson, G. H. M. van der Heijden, and S. Neukirch. Supercoiling of DNA plasmids: mechanics of the generalized ply. *Proceedings of the Royal Society of London A: Mathematical, Physical and Engineering Sciences*, 458 (2020):959–985, April 2002. ISSN 1364-5021, 1471-2946. doi: 10.1098/rspa.2001.0901. URL `http://rspa.royalsocietypublishing.org/content/458/2020/959`.

[130] George B. Arfken and Hans J. Weber. *Mathematical Methods for Physicists*. Elsevier Academic Press, 6 edition, 2005. Ch. 9.

[131] Pierre Müller and Andrés Saúl. Elastic effects on surface physics. *Surface Science Reports*, 54(5):157–258, August 2004. ISSN 0167-5729. doi: 10.1016/j.surfrep.2004.05.001. URL `http://www.sciencedirect.com/science/article/pii/S0167572904000408`.

[132] Subir Sachdev and David R. Nelson. Statistical mechanics of pentagonal and icosahedral order in dense liquids. *Physical Review B*, 32(3):1480, 1985.